Structural Mechanics Characterization of Steel Intermeshed Connections

A Dissertation
SUBMITTED TO THE FACULTY OF
UNIVERSITY OF MINNESOTA
BY

Mohammad Ebrahim Shemshadian

IN PARTIAL FULFILLMENT OF THE REQUIREMENTS
FOR THE DEGREE OF
Doctor of Philosophy

Advisor: Arturo E. Schultz
Co-advisor: Jia-Liang Le

July 2020

Acknowledgments

I would like to acknowledge all who made this research possible. First and foremost, I would like to express my extreme gratitude to my advisor, Professor Arturo E. Schultz for his guidance, support, and technical expertise during the course of my research. He is not only an inspiring mentor, but also a wonderful person. A special thanks goes to my co-advisor Professor Jia-Liang Le for his input and feedback, which were offered whenever I needed them. I would also like to thank fellow graduate student, Ramzi Labbane and the Galambos Laboratory manager, Paul Bergson for their contributions and hard work during the experimental phase of the project.

I express my gratitude towards my fellow researchers on the AMASS[1] research group, especially Professor Debra Laefer at New York University, Dr. Salam Al-Sabah at University College Dublin, and Professor Patrick McGetrick at Queens University Belfast for their contributions and collaboration. I would also like to acknowledge Professor Lauren Linderman and Professor Ryan Elliott for serving on my doctoral scientific committee and for their helpful feedback. I am deeply grateful for the financial support provided by National Science Foundation (NSF) through the grant CMMI-1563115 and by Department of Civil, Environmental, and Geo- Engineering at University of Minnesota, Twin Cities.

Special thanks go to my family and the love of my life for their unending support, patience, and encouragement.

[1] Advanced Manufacturing for the Assembly of Structural Steel

Abstract

This thesis presents the efforts to develop a new class of steel connection named the “Intermeshed Connection” for gravity load resistance in frame structures. The thesis investigates the performance of the connection system using physical testing and numerical simulation, as well as methods for its design. The project herein lays the groundwork to transform the steel building construction industry by advancing the underlying science and engineering precepts for intermeshed connections created from precise, volumetric cutting. Advanced manufacturing techniques, such as high-definition plasma, water jet, and laser cutting, are powerful tools that offer fast operation and precise finish in the process of steel fabrication. To date, this class of advanced manufacturing equipment has only been used to accelerate traditional processes for cutting sheet metal or other conventional fabrication activities (e.g. cutting instead of drilling holes). Such approaches have not capitalized on the equipment’s full potential. The intermeshed connection is intended to exploit this potential by harnessing advanced cutting technologies for volumetric cutting open steel sections, which results in precise steel pieces that can intermesh (i.e. interlock) with each other and form a connection. In such connections, loads transfer mainly through direct contact of the connection components rather than by traditional means through welds or bolts, which facilitates fast assembly and disassembly of steel structures and material reuse. The intermeshed system, if fully automated, can enhance the integration between design, fabrication, and installation.

Although the intermeshed connection has multiple interesting features to offer, the idea of cutting of open steel sections poses challenges regarding the load-transfer

mechanisms and failure modes for intermeshed connections. For instance, implementation of the cuts would cause discontinuity in the beam or formation of sharp corners in the specimen. The former could interrupt load paths, and the latter could increase stress concentrations. Therefore, to introduce the intermeshed connection system to engineering practice, the structural behavior of these connections needs to be fully understood and adequate performance under gravity loads needs to be demonstrated.

The aim of the present study is to provide insight on the structural performance of the intermeshed connection at both global and local levels, and to investigate appropriate design methods. To reach this goal, numerous details of the intermeshed connection were considered, a design procedure was developed, physical specimens were designed and tested, and beams with intermeshed connections were analyzed using sophisticated numerical procedures. This investigation was conducted in a step-by-step state assessment of the intermeshed connection subjected to multiple scenarios of gravity loading and various support conditions. Load resistance and design of these connections were explored to evaluate the mechanics of intermeshed connections including stress and strain concentrations, effective material utilization, failure modes, and connection geometry optimization.

Relying on the interaction of individual components, the intermeshed connection demonstrates ample load carrying capacity, stiffness, and ductility, which fulfilled the design requirements. This connection promises to be robust, secure, dismountable and offers the ability to be manufactured within current industrial tolerances and be erected quickly.

Table of Contents

List of Tables

List of Figures

1

Introduction

Similar to other building practices, common techniques in the steel industry have not been updated in years. Specifically, alternatives for steel connections have failed to gain traction in the construction sector during the past 50 years. Arguably, one reason for this underperformance is the extensive regulations in this field. As a result, as a major economic sector, the construction industry is plagued with inefficiencies and low productivity [1].

Robotics and automated systems have the potential to reduce labor costs while improving productivity and quality. Developing new construction methodologies such as prefabricated, volumetric construction and digital technologies supported by robotics can further facilitate off-site fabrication [1,2]. To achieve improved construction efficiency and heightened material reuse, computer controlled, advanced manufacturing techniques such

as high-definition plasma, laser, and water jet cutting (Fig. 1-1) could be harnessed to construct steel connections.

(a) Plasma cutting performed by an industrial robot [3]

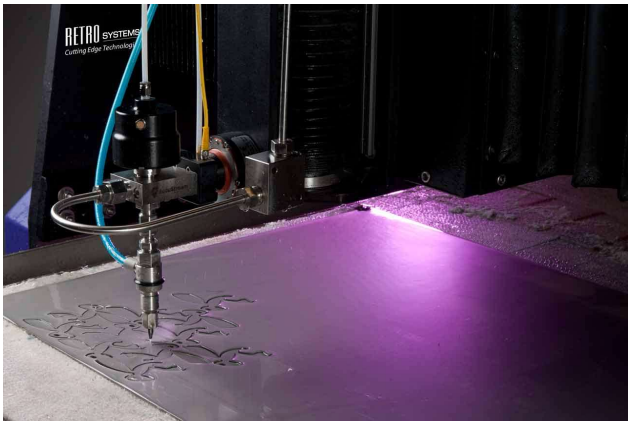

(b) Waterjet computer numerical control cutting machine [4]

Fig. 1-1 Advanced cutting techniques

The adoption rate of automation is still fairly low in the steel construction industry. Thus, there are not many instances of successful implementation of advanced cutting techniques in the technical literature. In a recent study, laser cutting technology was used to solve the problem of the joint fabrication of tubular structures being complex and costly. The LASTEICON [5] solution was proposed to achieve this objective by developing joints with passing-through beams, obtained by using laser cutting technology. Results of this research showed that computer-programmed automation could help reduce the welding quantity and fabrication time of such tubular connections, while the quality of the joint assembly has improved [6].

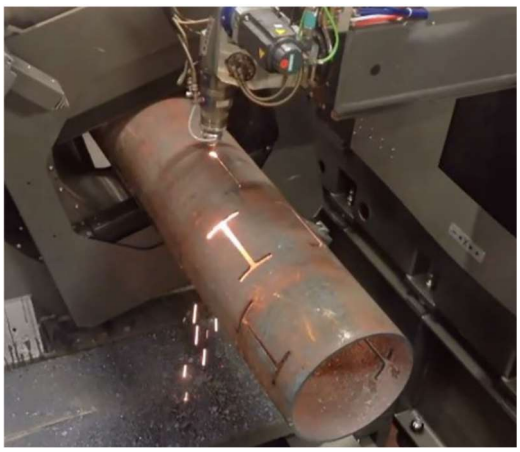

(a) Laser cutting process on a tubular profile

(b) Assembled prototype joint

Fig. 1-2: Laser cut solution in the tubular joints [7]

1.1. Background

During recent decades, alternatives to traditional steel connections have been proposed. Some of these innovative connections focused on ease of fabrication and erection [6,8], some prioritized sustainability and reducing construction waste through enabling the disassembly [9,10], and a few had their emphasis on seismic applications [11,12].

The first attempt to achieve ease of constructability by using interlocking connection was reported in 1991 by researchers at Lehigh University in the ATLSS project [13]. The goal was a new connection that was quicker, safer, and less expensive for erecting steel structures. The main concept of the ATLSS connection (Fig. 1-3) is to make use of a tapered male piece on the beam which slips into a steel casting that serves as a female guide mounted on the column to allow the initial placement of members with reduced human assistance. This concept was extended to other connection configurations including those for Shear Connections, Partial-Moment Connections, and Full-Moment Connections. While the connections performed well in laboratory tests, reliance on steel castings, which

are seldom produced by steel fabricators, added extra cost and construction complexity both which limited their use.

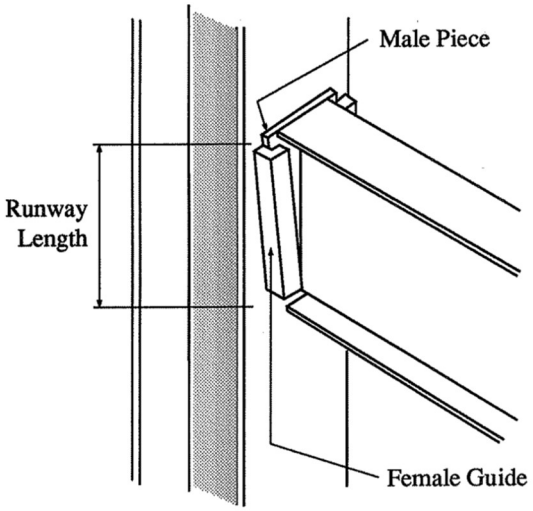

Fig. 1-3 ATLSS connection

In the early 2000s, Quicon® connection was developed with the goal to make site operations faster and safer. This system provides T-brackets and shoulder bolts for steel beam connections; the T-brackets include a series of keyhole-shaped notches that the shoulder bolts securely slide into on site. The applications of Quicon® are limited to simple geometries like warehouses and parking garages [9].

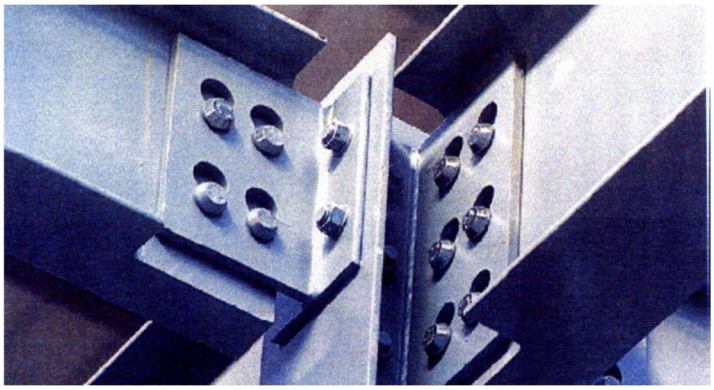
Fig. 1-4 Quicon® connection detail [9]

The Pin-Fuse Joint is an all-field-bolted connection. Columns are prefabricated with short beam stubs and a circular plated end connection. Beams are prefabricated with the matching circular connection at each end and are hoisted and pinned to the beam stub [14]. The joint incorporates a curved plated end connection using slip-critical bolts and a steel pin or hollow pipe adjacent to the beam column joint as it shown in Fig. 1-5. After severe damage and by loosening the bolts, the beam can be disassembled easily and reused later. However, the pin fuse connection can only resist beam shear and axial load and has no moment capacity. Also, there still exist concerns among the steel industry experts regarding the tight tolerances and high price point of this connection [14].

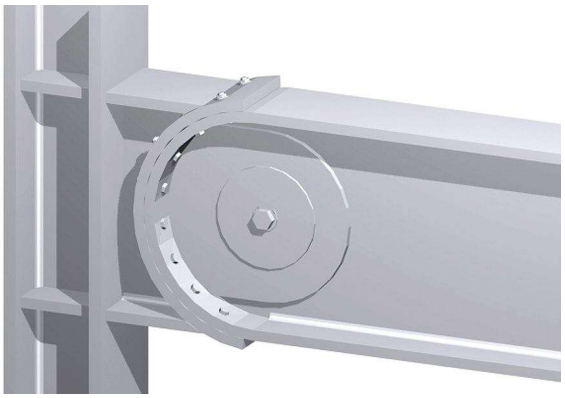

Fig. 1-5 Pin fuse connection [15]

The SidePlate® connection (Fig. 1-6) is a laboratory-tested and field-proven steel frame connection technology that reinforces the beam-column interface using extra plates to allow for fast construction. This connection is developed to carry moment, so it requires many connecting parts and a heavy-duty installation [9]. SidePlate® currently has four distinct connection types which require either field bolting (in most cases) or welding. Given the reliance on extensive field bolting this connection system does not alleviate many of the current limitations with connections in steel frame structures.

Fig. 1-6 SidePlate® connection implemented in a steel frame [16]

1.2. Research significance

The aforementioned connections are intended for moment frame connections, so their performance requirements are higher. Therefore, they involve multiple connecting parts, welding, and/or bolting which make the erection process relatively slow. Also, disassemble of the connection is not going to be an option. Many of these studies remained in the research phase and could not find commercial application, while a limited number of them resulted in connection solutions that reached the steel building construction market sector [15]. Thus, there is a need for a general class of connections for speedy and economical erection of steel frames by elimination of field welding and minimization of bolting. In this case, the connection would transfer loads from one connected part to the other by bearing and friction of contact faces between connected parts (aka intermeshed components). High-definition plasma and waterjet cutting afford the opportunity to meet this goal by providing the tools to cut the contact faces quickly and precisely.

At the connection level, there is a need to investigate the mechanics of intermeshed connections including stress-strain states, component interaction, and failure modes. In order to advance the intermeshing concept, appropriate connection details should be developed, investigated and validated. The goal is to design a connection that is able to meet the design requirements for strength, stiffness, and ductility; while simultaneously maintaining characteristics that make them practical for erection purposes and easily manufactured without requiring major changes in current fabrication routines. The designed specimens, then, need to be evaluated for expected load resistance and deformation demands by means of physical tests and finite element modeling.

At the frame level, on the other hand, the effects of implementing the intermeshed connections can be evaluated by investigating the response of steel frames equipped with intermeshed connections. Evaluation of system performance is needed because, due to the absence of welds or bolts in the connection detail, intermeshed connections are unlikely to behave as fully rigid connections. For adoption by design codes and standards, a detailed step-by-step design procedure for design should be developed that is based on fundamentals of structural mechanics and that can provide the sizes of the intermeshed components.

The current thesis pursues numerical and experimental analysis methods to provide the essential information for the development of the intermeshed system. A summary of these methods is outlined in the next section.

1.3. Thesis organization

The dissertation covers the following contents, divided into six chapters:

Chapter 1 introduces the research problem and the thesis objectives.

Chapter 2 proposes the first variation of the intermeshed connection called the 'front-intermeshed connection' that requires no external connector elements. A numerical study is conducted on the ultimate load capacity and failure modes of this intermeshed connection under mixed-mode loading. The experimental behavior of the connection component is also investigated through a series of tests. The numerical simulations are performed by using a commercially available 3D finite element software package. By considering different types of mixed mode loading, interaction diagrams of axial, shear, and moment capacities of the intermeshed connection are obtained. For each interaction diagram, the corresponding failure mechanism was analyzed. Finally, the simulated interaction between axial, shear, and moment capacities were further compared with the provision of the current design codes.

Chapter 3 introduces the second alternative of the intermeshed connection that employs shear plates and angles for conveying load between the beam parts. These external connectors are attached to the specimen from the side, thus giving rise to the label 'side-intermeshed'. An experimental investigation was performed to elucidate the mechanics of

intermeshed steel connections manufactured by high-definition plasma and waterjet cutting. Four full-scale specimens with intermeshed connections are designed to resist gravity loading in steel frames. The experimental testing program focuses on the behavior of intermeshed connections under vertical loads including pure flexural and combined flexural-shear loading. Both global load-deflection response and local deformation are measured to provide insights into the complex load transfer mechanisms.

Chapter 4 focuses on the challenges for introducing the intermeshed systems to the steel construction industry. Implementation of the intermeshed connection would cause a discontinuity in the beam, therefore, the effects of implementing such connections is evaluated by investigating the response of steel frames equipped with intermeshed connections. A detailed step-by-step design procedure is developed for the intermeshed systems, that is based on the fundamentals of structural mechanics and current code requirements. For the fabrication of the intermeshed connection, different accessible manufacturing options are explored to find the suitable cutting technique that could meet the high precision due to tight tolerances of these connection.

Chapter 5 provides insight on structural performance the intermeshed connection through comprehensive and detailed nonlinear finite element analyses. This investigation is conducted by an extensive state assessment of the connection subjected to multiple scenarios of gravity loading. Implementation of the intermeshed connection would cause a discontinuity in the beam, so this chapter addresses concerns regarding the load-transfer

mechanisms and failure modes for these connections. In order to verify the accuracy of these simulations, the numerical results are compared with experimental data from the four physical tests discussed in Chapter 3. Finally, some important factors of influence such as connection segment sizes, lateral constraint, support conditions, and failure modes are also explored via finite element modeling.

Chapter 6 presents a brief conclusion of the main observations and findings and discusses recommendations for future research.

The introduction sections of Chapters 2, 3, 4, and 5, provide a review on the literature relevant to the topic discussed in each chapter. These chapters are adopted from papers that are either published in or being reviewed by scientific journals in the field. To maintain the integrity of those papers, only minor modifications are incorporated in the corresponding chapter; thus, some overlapping information may be noticeable.

2

Numerical Study of the Behavior of Intermeshed Steel Connections under Mixed-Mode Loading[1]

In recent years, advanced manufacturing techniques, such as high-definition plasma, water jet, and laser cutting, have opened up an opportunity to create a new class of steel connections that rely on intermeshed (i.e. interlocked) components. The main advantage of this type of connection is that they do not require either welding or bolting, which allows faster construction. Although the interest in intermeshed connections has increased in recent years, the mechanical behavior of these connections has not been fully understood. This chapter presents a numerical study on the ultimate load capacity failure

[1] This chapter is adopted from the following manuscript:
M.E. Shemshadian, J.-L. Le, A.E. Schultz, P. McGetrick, S. Al-Sabah, D.F. Laefer, A. Martin, L.T. Hong, M.P. Huynh, Numerical study of the behavior of intermeshed steel connections under mixed-mode loading, J. Constr. Steel Res. 160 (2019) 89–100. doi:10.1016/J.JCSR.2019.04.024.

modes of intermeshed connections under mixed-mode loading. The experimental behavior of the connection components is also investigated through a series of tests. The study considers a recently developed intermeshed connection for beams and columns. The numerical simulations were performed by using a commercially available 3D finite element software package. By considering different types of mixed mode loading, interaction diagrams of axial, shear, and moment capacities of the intermeshed connection were obtained. The results indicated that there exists an intricate interaction among axial, shear, and moment capacities, which arises from the intermeshed configuration of the flanges and web. For each interaction diagram, the corresponding failure mechanism was analyzed. The simulated interaction between axial, shear, and moment capacities were further compared with the provision of the current design codes. While the intermeshed connection studied here showed promise for gravity loading, further study is needed to ensure alignment of the flanges so as to avoid axial and/or flexural failures.

2.1. Introduction

Field welding and bolting have played dominant roles in the construction of steel structural connections since the post-World War II era, despite considerable material and labor costs. With significant advances in manufacturing and building information modeling (BIM), there has been an increasing interest in developing new connection systems to facilitate more cost-effective construction [11]. Another motivation for developing new connection systems is to improve the ease of deconstructing steel structures, which would maximize the reusability of the components.

To achieve improved construction efficiency and heightened material reuse, computer controlled, advanced manufacturing techniques such as high-definition plasma, laser, and water jet cutting could be harnessed to create an entirely new class of "intermeshed" steel connections that rely on neither welding nor bolting [17,18]. Fully automated, precise, volumetric cutting of open steel sections, coupled with BIM-supported design and specification of building components, could radically transform how structural steel is fabricated, assembled, deconstructed, and reused [8]. To date, this class of manufacturing equipment has only been used to accelerate traditional processes, such as cutting sheet metal and making holes, and has not capitalized on the full potential of the equipment.

In the early 1990s, researchers developed a new type of steel connection, namely the ATLSS connection, which allows for quicker, safer, and less expensive erection of structural members [13]. The underlying concept of the ATLSS connection is a tapered end plate on the beam which slides into a fixture with a grooved guide mounted on the column. Through a series of experimental studies, this concept was used to develop shear connections, partial moment connections, and full moment connections. The experimental results indicated that the load carrying capacity of the ATLSS connection is predominantly governed by the capability for shear force transfer.

The Quicon® connection was developed in the early 2000s to make site operations faster and safer. This system provides T-brackets and shoulder bolts for steel beam connections; the T-brackets include a series of keyhole-shaped notches into which the shoulder bolts slide securely on site. To further speed assembly, both the T-brackets and the shoulder bolts can be attached to members off-site. The applications of the Quicon®

system are limited to simple geometries like warehouses and parking garages, thus it has not received widespread attention [9].

Another recent innovation is the ConX® moment connection, which requires no field welding [19]. For this connection, a collar corner assembly is shop-welded to the column at the proper floor framing locations. On site, beams are simply dropped into the column collar corner assemblies from above. A major challenge with the ConX® connection relates to the allowable tolerances in the foundations where the columns are connected [20]. All beams connecting to a ConX® node (the connecting parts of the beams and column) must be of the same nominal depth. There are also limitations on the beam flange thickness and width, the clear span-to-depth ratio of the beam, and the column wall thickness.

Another frame connection technology is the SidePlate® connection, which uses extra plates to reinforce the beam-column interface and to allow for speedy construction [9]. This connection is typically used to carry moment, thus requiring multiple connecting parts and a heavy duty installation process. All four variants require field bolting (in most cases) or field welding.

The aforementioned connections are intended for moment frame connections. Among these, only the SidePlate® and ConX® connections have found significant commercial use. Thus, there is a need for a general class of connections for speedy and economical erection of steel frames for gravity loads.

Motivated by the increasing interest in developing more cost-effective steel connections, recent research has focused on a relatively simple intermeshed connection

[21–23], in which the top and bottom flanges of the beam are connected with dovetails, and the webs are connected by means of a stepped web pattern (Fig. 2-1). The dovetail connection is intended to resist the axial tension and compression forces in the flanges under bending and/or axial loading, while the stepped web connection is intended to resist primarily shear forces in a single direction.

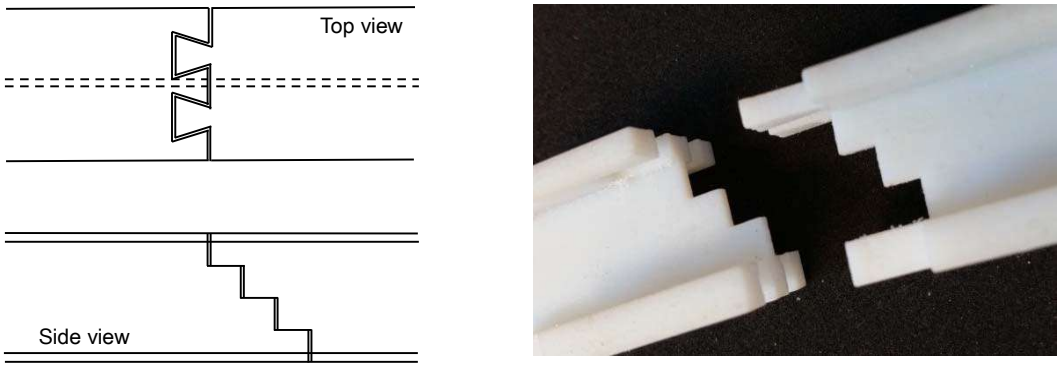

(a) Schematics (b) Model printed in resin

Fig. 2-1: Proposed intermeshed connection

The intermeshed connection (Fig. 2-1) can be easily adopted in structural frames, as long as pre-specified tolerances are met. In the application, beam stubs (Fig. 2-2) need to be welded to the column, which should be done at the fabrication shop. The central portion of the beam interlocks directly with the beam stubs in the field by gravity without further welding or bolting. Compared to traditional bolted or welded connections, this type of intermeshed connection requires little experience on the part of site workers for its assembly. Moreover, much of the shop effort for manufacturing the connections can be performed using computer-controlled equipment, which would significantly reduce the labor cost. In addition, the intermeshed connection also allows easy disassembly, which improves the reusability of structural components.

While the aforementioned intermeshed connection has several attractive features in terms of constructability, its mechanical behavior is not yet well understood. The expectation is that the three-dimensional interlocking mechanism would affect the load transfer capability of the connection. For engineering design practice, understanding this effect on the flexural, axial and shear capacities is essential for classification of this new type of connection. Notably, in contrast to traditional moment connections, where the moment and shear force are transferred separately through different connection components, the intermeshed connection is an integrated system. Therefore, there could exist intricate interactions between flexural, axial, and shear transfer behaviors, which cannot be captured by existing design codes.

In this study, the behavior of the intermeshed connection shown in Fig. 2-1 is investigated through a series of nonlinear finite element simulations. The simulations reveal the different failure modes of the connection under various mixed-mode loading conditions. This chapter is organized as follows: Section 2.2 describes the concept and geometry of the intermeshed connection considered in this study; Section 2.3 presents the mechanical behavior of the individual flange and web components of the intermeshed connection; Section 2.4 presents the nonlinear finite element simulation procedure; and Sections 2.5 to 2.7 discuss the simulation results and their implications for design practice.

2.2. Intermeshed Connection Concept and Configuration

As with conventional connection design, the intermeshed connection is designed to transfer bending moment through its flanges and shear force through its web. However, the

detailed load transfer mechanisms differ. In the intermeshed connection, the transfer of web shear and flange compression is facilitated through direct contact bearing of multiple, precisely shaped faces, while the transfer of tension through the flange relies on flange interlocking.

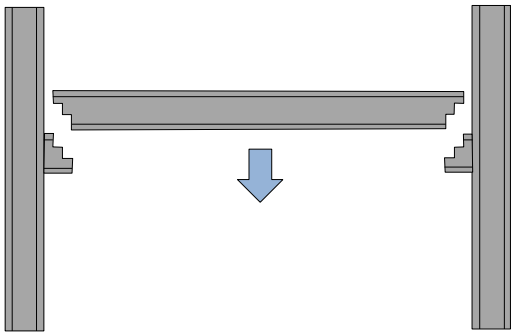

Fig. 2-2: Gravity assembly of the intermeshed connection in a structural frame

The simplicity of the flange intermeshing requires no additional interlocking components for transferring the axial loading into the flange. However, the interlocking of the tensile flange induces stress concentrations, which affect the efficiency of load transfer. The inclined stepped web connection allows for easy site assembly as the beam can be slotted in from above (Fig. 2-2), a method similar to current practice, but without relying on welding or bolting. Furthermore, no web locks are needed for gravity frames, which is the focus of this study. Fig. 2-2 shows the assembly of a beam in a structural frame using the intermeshed connections. The ideal location for placing this type of connection is at or near points of contraflexure, where shear demand may be high but moment and axial force demands are low.

The intermeshed connection transfers loads from one part to the other by bearing and friction on the connection contact faces, but contact will not be perfect due to industry

defined manufacturing and erection tolerances. As a result, localized contact is expected to occur in multiple small zones, which in turn create local stress concentrations that can cause local yielding [24]. The material yielding at the local contact zones would further lead to stress redistribution in the intermeshed connection and eventually a spread of the local contact area. This stress redistribution mechanism influences the shear and moment transfer capacity.

In traditional welded or bolted connections, the flanges and web are connected through different components, such as flange and web splice plates. In such instances, the transfer of shear and moment can be considered independent of each other. This is not the case for intermeshed connections which rely on the interlocking and bearing of the teeth and steps on both the flanges and web. Therefore, the flexural and shear behaviors of the connection are expected to interact with each other. As will be shown later, such interactions can have important consequences for the moment and shear capacities of the connection under general mixed-mode loading.

2.3. Mechanical Behavior of the Connection Components

To ensure that the dovetail and step cuts can facilitate the load transfer in the flanges and web, respectively, a series of experimental studies was performed on the individual flange and web [25]. The series consisted of six replicas of flange samples tested under tension and six replicas of web samples tested under shear. Flange and web samples were cut from a S275JR steel plate of 6 mm thickness by using waterjet cutting for the flange samples and laser cutting for the web samples.

The results showed that the performance of the samples was satisfactory, and that the mechanisms of tensile load transfer in the flange and shear load transfer in the web occurred as assumed in the connection concept presented in the previous section. Fig. 2-3(b) presents the measured load-displacement response under tension, which displayed a softening behavior in the post-peak regime. In the experiments, the failure mechanism could be characterized as slippage of the intermeshing flanges due to excessive in-plane deformation between the dovetail sections of the flanges, as illustrated in Fig. 2-3 (a). No rupture was observed during any of the tests.

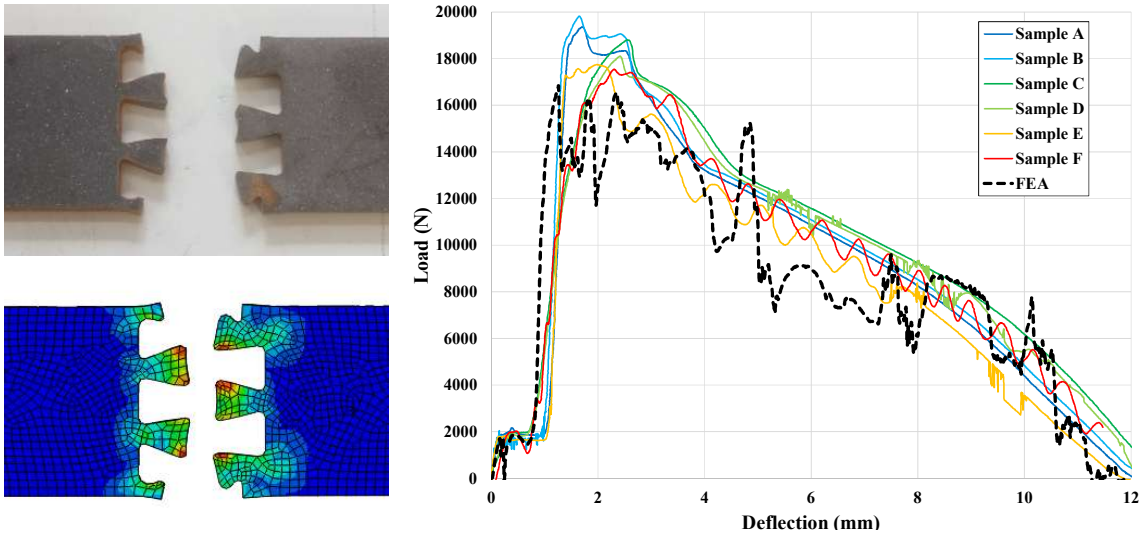

(a) Failure mode (b) Load-deflection relation

Fig. 2-3: Comparison of the test and FEA results of the dovetail flange under tension

For the tests of the web specimens under shear, slippage between the left and right sides of the specimens resulted in out-of-plane movements within the connection, leading to global buckling, (Fig. 2-4(a)). Finite element analysis (FEA), which will be discussed in the next section, also captured the fundamental trends in the tests (Fig. 2-3(b) and Fig. 2-4(b)).

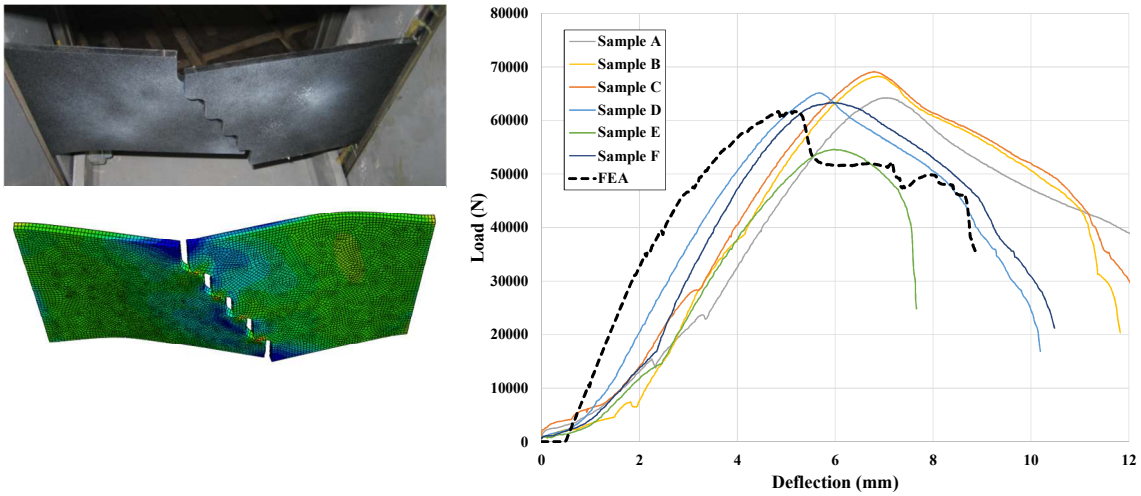

(a) Failure mode (b) Load-deflection relation

Fig. 2-4: Comparison of the test and FEA results of the step-shape web under shear

2.4. Finite Element Simulations — Methodology and Assumptions

The aforementioned results indicate that the intermeshed connection tended to exhibit complex mechanical behavior arising primarily from the nonlinear material response at the contact surfaces. In this study, FEA was used to investigate the nonlinear behavior of the connection under different loading situations [26]. The FEA simulations were performed in Abaqus, which is capable of handling material and geometrical nonlinearity, as well as contact between individual surfaces [27]. The structure was discretized by eight-node 3D solid elements with linear displacement interpolation [28]. The contact between the intermeshed cuts of the flanges and between the web steps were modeled by contact elements, in which a hard contact law was used in the normal direction to minimize overclosure, and a friction contact law was used in the tangential direction.

2.4.1. Simulation of the Experiments of the Connection Components

Nonlinear FEA was conducted in Abaqus to validate the results of the experimental studies on the flange under tension and web under compression that were reported in the preceding section. Fig. 2-5(a) shows the plan view of the flange and side view of the web used in the experiments and their dimensions. In order to take the practical tolerances into consideration, a 0.5-millimeter gap was left between the different parts of each specimen. Fig. 2-5(b) presents the experimentally derived material properties used as input parameter in the Abaqus model. This curve was generated based on tensile tests of dogbone samples with a 'Yun-Gardner' material model, which considers bilinear behavior plus nonlinear hardening [29]. A mesh size of 2.5 mm was utilized in all the FEA models. Mesh patterns can be seen in Fig. 2-3(a) and Fig. 2-4(a).

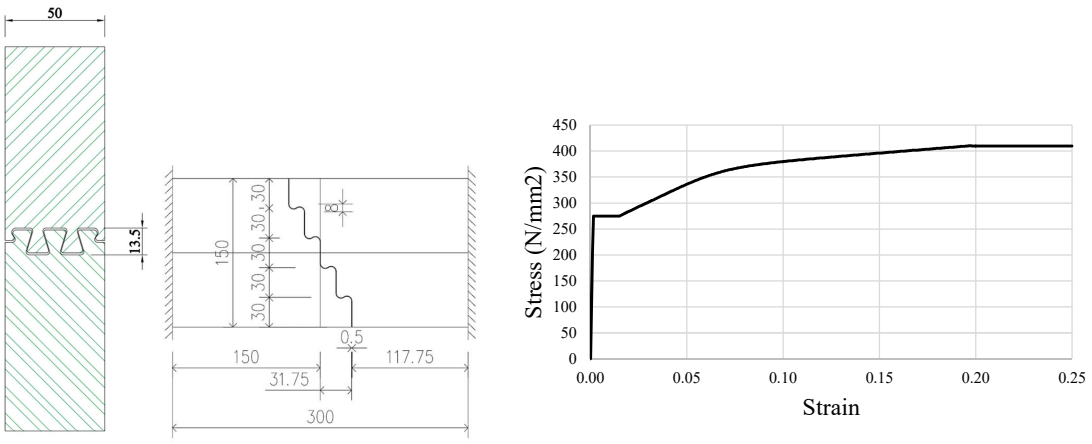

(a) Geometry of the samples in millimeters

(b) Material model

Fig. 2-5: Characteristics of the test specimens

In both the tension and shear tests, the results of the nonlinear FEA showed good agreement with the experimental tests (Fig. 2-3(b) and Fig. 2-4(b)). The plateau at the beginning of the FEA curves was the initial settlement when the gaps were closing. Failure

modes were also correctly predicted. Fig. 2-3(a) shows that under tension, the dovetail cuts slipped out due to the distortion of the teeth, without rupturing. In the shear test, out of plane buckling was the major failure mechanism (Fig. 2-4(a)).

2.4.2. Simulation of the Intermeshed Connection

In this study, two sets of nonlinear FEA were performed on the intermeshed connection as a whole. In the first set, 13 finite element analyses were conducted to investigate the general behavior and failure modes of the connection under different load combinations. In the second set, over 200 analyses were performed under a variety of load conditions to determine the load capacity of the connection. The results of the latter then served as the basis for the development of an axial force-shear force-moment interaction (*P*-*M*-*V*) diagram.

The connection was assumed to be cut from a UB 254×102×28 beam section. The cut geometry was designed to maximize the load bearing capacity of both the flange and web, while simplifying the connection arrangement as much as possible. To this end, various tooth widths and inclination angles for the intermeshed cuts, and different heights and widths for the steps were considered. The flange teeth and web steps were designed with round corners to reduce large stress concentrations. Meanwhile, multiple curves were used at the step corners to minimize the potential horizontal slip of the parts on either side of the step-shape cuts. Based on these considerations, trial geometries were developed and the performance of the connected parts was evaluated through nonlinear FEA. The final details of the connected parts and the cuts are shown in Fig. 2-6.

(a) Top flange view (b) Web side view

Fig. 2-6: Detailed design of the cuts in the intermeshed connection (dimensions in millimeters)

In the FEA, all of the structural components were modeled based on the European steel grade S355, which is similar to ASTM A992 Grade 50 steel used in the USA [30]. The constitutive behavior of the steel was assumed to follow the Von Mises yield criterion coupled with an isotropic kinematic hardening flow rule [26]. Fig. 2-7 shows the uniaxial stress-strain response of the material with the following material parameters: E = 210 GPa, σ_{prop} = 320 MPa, σ_y = 357 MPa, σ_{y2} = 366.1 MPa, σ_{ult} = 541.6 MPa, E_{p1} = 0.21 GPa, E_{p2} = 0.86 GPa, ε_{p_y1} = 0.4%, ε_{p_y2} = 2%, ε_{p_ult} = 14% [31].

To explore the behavior of the intermeshed connection, the independent loading cases were investigated first, followed by the combined cases. In the simulation, the member length was considered to be sufficiently short (155 mm) to minimize the bending moment induced by the applied shear force (Fig. 2-8). By doing so, lateral torsional buckling was also suppressed, which was ideal for studying the behavior of the connection alone. The present model was able to capture the local buckling of the compressive flange, which could affect the load transfer capacity of the connection.

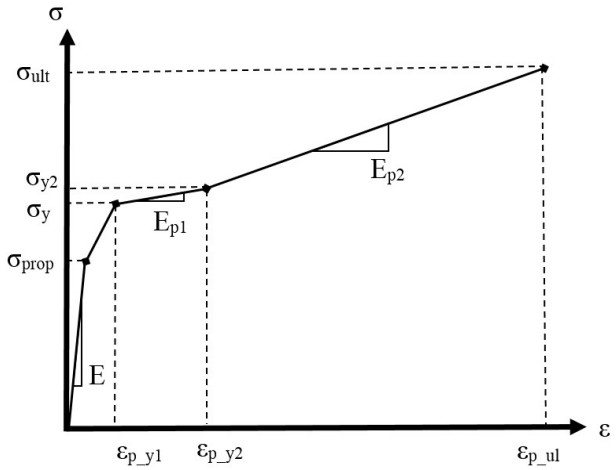

Fig. 2-7: The uniaxial stress-strain curve of steel [31]

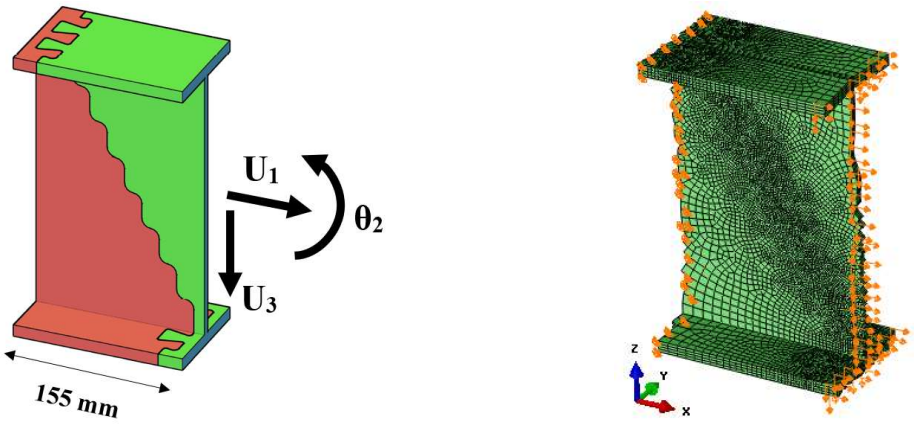

(a) Loading and boundary conditions (b) Abaqus model

Fig. 2-8: Numerical simulation of the intermeshed connection

In the model, the left side of the connection was connected rigidly to its support (e.g. the column flange), i.e. $U_1=U_2=U_3= 0$, where U_1, U_2, and U_3 were the displacement in X, Y, and Z direction, respectively. The right side of the connection was subjected to different displacement conditions to simulate different load cases (Fig. 2-8).

The first round of analysis involved four basic loading cases: (1) pure tension, (2) pure shear, (3) pure compression, and (4) pure flexure. In each case, the corresponding deformation pattern was prescribed to the right side of the member (e.g. uniform

deformation U_1 for pure tension and compression, uniform deformation U_3 for pure shear, and rotational deformation θ_2 for pure flexure).

In the second part of the analysis, the aforementioned basic loading cases were combined to create mixed-mode loading, in which the relative dominance was described by the ratio of the corresponding displacements. For example, in the case of combined tension-shear loading, the ratio of $U_3/U_1 = 2$ represented a shear-dominant case, $U_3/U_1 = 0.5$ represented a tension-dominant case, and $U_3/U_1 = 1$ represented a balanced case. The present analysis considered combined tension-shear, compression-shear, and flexure-shear loading. These loading cases are highly relevant to the actual loading scenario for building frames. In all analyses, the reaction forces at the left support were extracted from the simulation, and the complete force-displacement and moment-rotation curves were determined. For design purposes, the primary interest was the overall load carrying capacity of the connection.

2.5. Failure modes

2.5.1. Basic loading cases

Fig. 2-9 presents the simulated load-deformation curve of the connection under tension. The simulation results showed that the tensile capacity of the connection was dominated by the interlocking of the flange plates. From Fig. 2-9, the post-peak regime of the overall load-deformation response can be seen to exhibit a gradual softening behavior (i.e. reduction of load-carrying capacity), which signified the loss of interlocking action of the flange teeth. The simulated failure mode can be characterized by the slippage of the

dovetail flanges without any rupturing. This was consistent with the flange tensile test shown in Fig. 2-3(a).

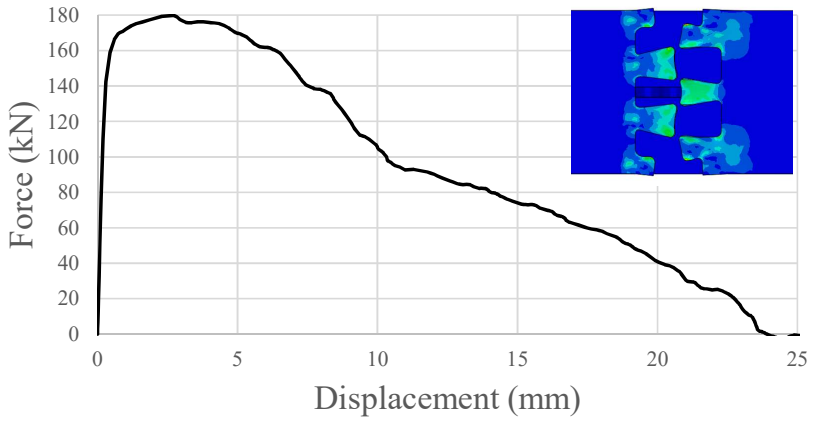

Fig. 2-9: Simulated tensile behavior of the intermeshed connection

The simulation predicted the maximum tensile capacity of the intermeshed connection to be 180 kN, which refers to when the intermeshed flange was fully engaged. The tensile capacity can be estimated using a simple hand calculation [32], in which the load carrying capacity of the flange is governed by its effective net area, A_e. Based on the connection geometry shown in the Fig. 2-6(a), the right side of the connection has the minimum net area, and therefore the peak tensile load of the connection can be calculated as per Equation 2-1:

$$T_u = 2F_y A_e = 2F_y(t * \sum(w_i U_i)) \qquad \text{Equation 2-1}$$

where F_y is the material yield strength, t is the flange thickness, w_i is the width of each tooth, and U is the shear lag factor. According to the AISC Specification (2016), shear lag occurs when the tension load is not transmitted to all the elements of the cross-section simultaneously [33]. This leads to a non-uniform stress distribution and, consequently, a

reduction in the tensile strength, because the flange section is not fully employed at the critical location. This effect is captured by the shear lag factor U in AISC specification [34]. Based on Equation 2-1, a peak tensile capacity of 186 kN was obtained, which is in good agreement with the simulation results (180 kN).

Fig. 2-10 shows the load-displacement response of the connection under pure compression. Unlike the case of uniaxial tension, the compressive load-displacement curve exhibited a gentle softening behavior in the post-peak regime due to continuous contact being maintained through the flange teeth and web steps during the compressive loading. When the prescribed displacement became large (14 mm), the load carrying capacity was lost due to the onset of local compressive buckling.

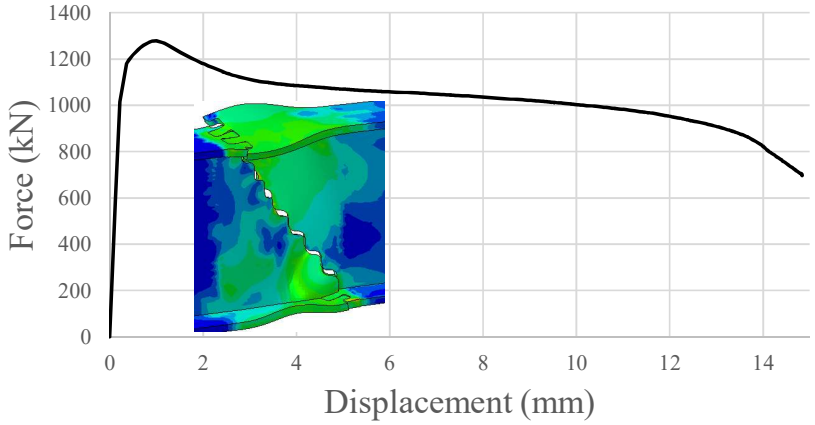

Fig. 2-10: Simulated compressive behavior of the intermeshed connection

The simulation predicted that the peak compression capacity of the connection was 1279 kN (see Fig. 2-10), which is fairly close to the plastic capacity of the beam section in axial compression (1321 kN). This indicates that the intermeshing mechanism did not undermine the peak axial compression capacity of the beam. In addition, the present simulation showed that the peak compressive capacity was much larger than the tensile

capacity. This difference is explained by the tensile capacity being governed by the effective area of the flange teeth whereas, for the compression case, the entire cross section contributes to the load carrying capacity.

Fig. 2-11 presents the simulated load-displacement response of the intermeshed connection under shear loading, which largely relied on the web steps. Similar to the tension case, the load-displacement response under shear loading also exhibited a general post-peak softening behavior. The reduction in load carrying capacity was primarily due to the loss of contact of some web steps. Meanwhile, the load-displacement curve for the shear loading case showed a fair amount of ductility near the peak load. This can be attributed to the fact that the flanges provided a certain degree of web restraint. The other salient feature is that, at the final stage of analysis, the connection still possessed some amount of load carrying capacity, because there was still some contact between the pieces at the bottom part of the web (Fig. 2-11). The simulation predicted a peak shear resistance of 286 kN, which was close to the nominal shear capacity of the beam (i.e. $V_u = 0.6F_yA_w$ where A_w was the web area of the beam). This indicates that the intermeshed connection was able to develop about 90% the full plastic shear capacity of the beam.

The separation along the stepped web interface of the connection can be seen in Fig. 2-11. A closer look at the abutting surfaces showed that the shear deformation (U_3) is almost constant over the section height (Fig. 2-12(a)), while the axial deformation (U_1) caused by the secondary moment is almost linear (Fig. 2-12(b)). The latter movement (U_1) completely opens the top half of the connection interface with a peak deformation of 19 mm, therefore the contact forces vanish in that area (Fig. 2-13).

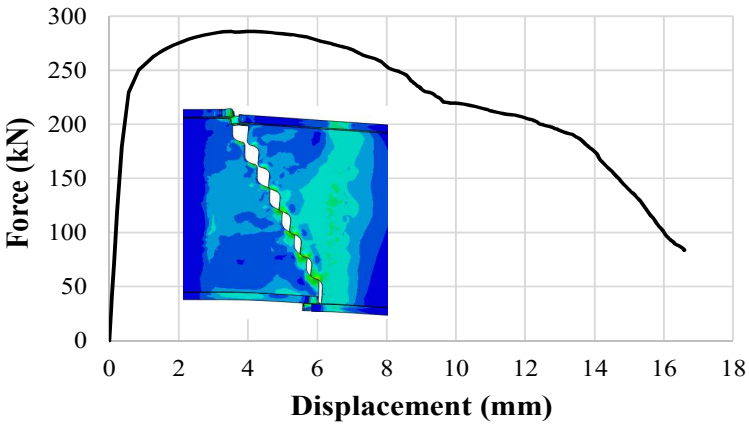

Fig. 2-11: Simulated shear behavior of the intermeshed connection

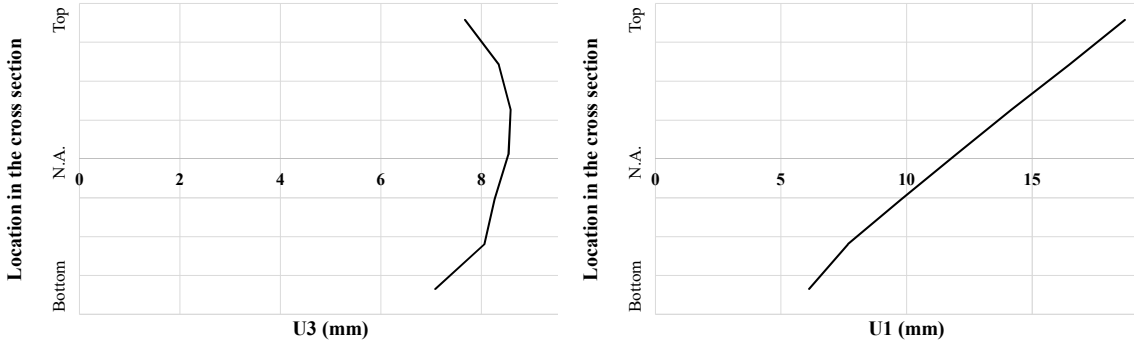

(a) Shear deformation (b) Axial deformation

Fig. 2-12: Final relative movement at the abutting surfaces of the connection under shear load

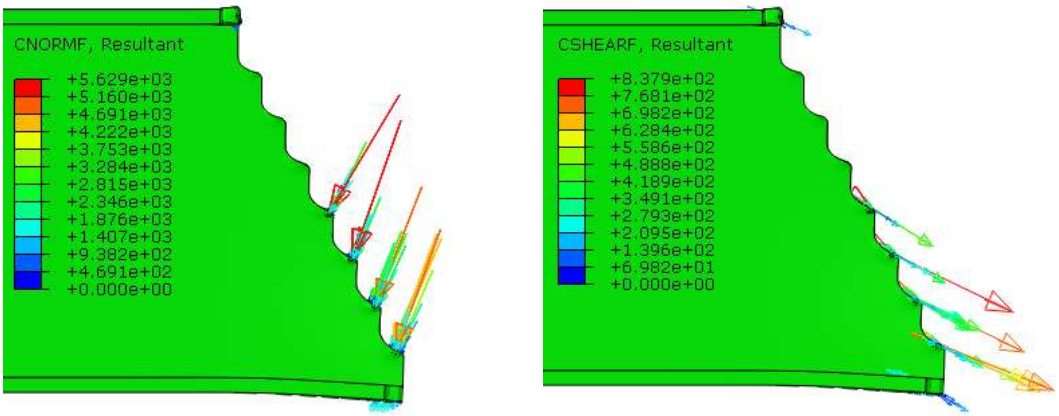

(a) Normal forces (b) Tangential forces

Fig. 2-13: Contact forces on the connection under shear load

For flexural loading, the connection showed a peak moment capacity of 23 kN-m. Based on the foregoing analysis of pure tension and compression cases, one may estimate the peak flexural capacity via Equation 2-2:

$$M_u = \frac{1}{2} T_u d \qquad \text{Equation 2-2}$$

where d is the depth of connection, and T_u is the tensile capacity of the entire connection, thereby implying that the force in the tension flange is $0.5T_u$. Equation 2-2 predicts a moment capacity of 22.5 kN-m, which is slightly lower than that predicted by the FEA partly because the frictional contribution of the web is neglected.

Fig. 2-14 shows the simulated moment-rotation curve of the connection under negative bending. Once the peak moment was reached, the connection experienced a significant loss of its moment carrying capacity due to slippage of the intermeshed connection at the top flange. Once the top flange disengaged, the entire connection lost its moment capacity completely.

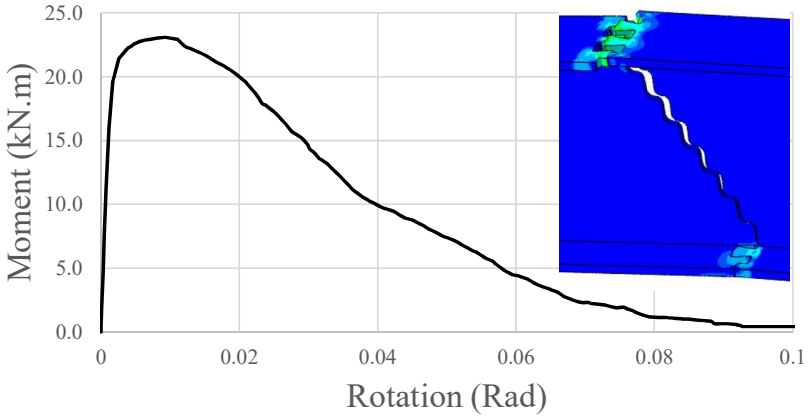

Fig. 2-14: Simulated moment-rotation relationship of the intermeshed connection in pure bending

2.5.2. Combined loading cases

The aforementioned analysis indicated that the connection was able to develop almost full plastic capacity under some single-mode loading cases. However, in real world applications, the connections will likely experience combinations of these loading modes. This section discusses the performance of the connection under mixed-mode loading.

Tension-Shear: For combined tension-shear loading, the relative dominance between tension and shear is described by the ratio of the applied displacements (U_3/U_1). The simulation showed that, when $U_3/U_1 = 1$, the peak tensile capacity reduced by 20% compared to that without shear loading. This reduction increased to 40% when shear loading became more dominant (e.g. $U_3/U_1 = 2$). Under combined shear and tensile loading, the connection exhibited a complicated behavior. Fig. 2-15(a) and (b) show the simulated load-deformation responses in the normal and tangential directions, respectively, for the case of $U_3/U_1 = 1$. When compared to the pure tension (Fig. 2-9) and pure shear (Fig. 2-11) cases, the connection had less force and deformation capacities. Under shear loading, the connection manifested ductile behavior until reaching the point of failure, whereas a pronounced softening behavior was seen in the tensile loading direction. This indicates that the failure of the connection was primarily governed by tension. The observed reduction in tensile capacity can be attributed to the relative vertical movement between the two sides of the connection that was mobilized by the shear force and, consequently, made the flanges slip out of their intermeshed positions. When this phenomenon occurred (Fig. 2-15(c)), there was no component to resist tension, and the connection lost all load capacity.

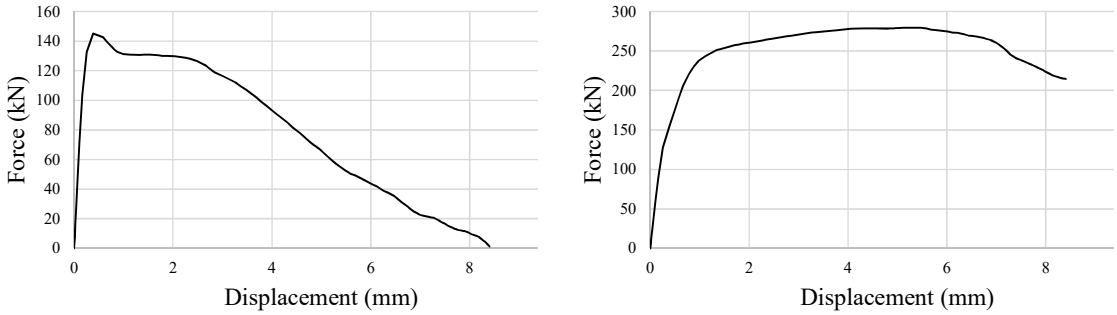

(a) Response in the normal direction (b) Response in the tangential direction

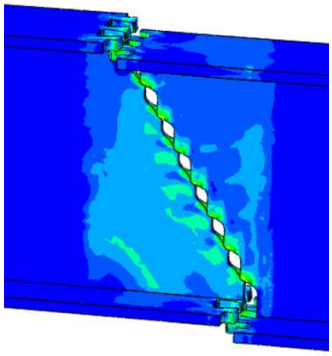

(c) Deformation pattern

Fig. 2-15: Simulated behavior of the intermeshed connection under tension-shear loading

Compression-Shear: Similar to the foregoing analysis, the compression-shear loading was investigated by considering three different ratios of U_3/U_1. It was found that, in all three cases, the presence of shear loading had little influence on the compressive behavior of the connection and the maximum compression capacity was essentially unaffected. However, mixed-mode loading had a significant effect on the shear behavior. The simulation showed that, when compared to the load capacity under pure shear (Fig. 2-11), the maximum shear capacity of the connection was reduced by 20%, 40%, and 60%, respectively, as the U_3/U_1 ratio decreased from 2 to 1 to 0.5. The reduction of the shear capacity can be attributed to the misalignment of the web steps when the applied compression became sufficiently large, and thus reduced the ability to transfer shear.

Fig. 2-16(a) and (b) show the simulated load-deformation responses in the normal and tangential directions for the case of $U_3/U_1 = 1$. In the tangential direction (U_3), the load-deformation response in Fig. 2-16(b) exhibited a non-monotonic response. There was a local peak right after the elastic regime, after which the connection started to lose its load capacity. After a small increment in displacement, the connection regained its load capacity exhibiting a hardening behavior and reached a second peak load, after which the connection experienced a softening behavior leading to ultimate failure.

The simulation indicated that the first drop signified local buckling of the web under shear loading. In fact, the buckling began as soon as the connection elements began to exhibit nonlinear behavior under combined stresses. Consequently, the overall stiffness decreased, and buckling occurred in the web. With continued loading, the shear resistance started to increase again when U_3 reached a displacement of 2 mm. This was the same displacement at which the buckling of flanges began due to compression. The increase in the shear strength at this point was a result of the formation of tension field action in the web (Fig. 2-16(c)). The results showed that tension fields began to form in the web when the flanges started to buckle. The vertical component of these fields provided extra load transfer capacity, which enhanced the shear resistance.

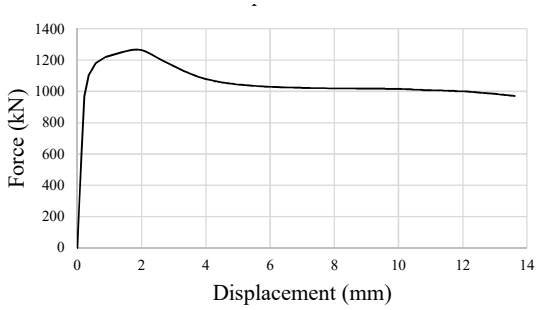

(a) Response in the normal direction

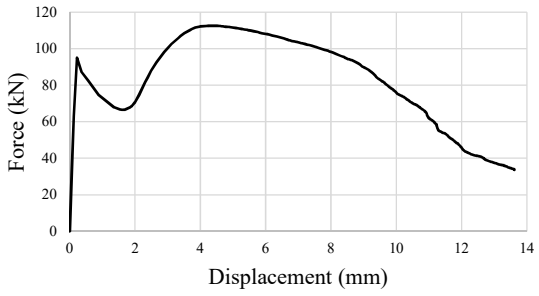

(b) Response in the tangential direction

(c) Deformation pattern

Fig. 2-16: Simulated behavior of the intermeshed connection under compression-shear loading

Flexure-Shear: For combined flexure-shear loading, rotation θ_2 and displacement U_3 were applied simultaneously to the connection. Three loading cases were considered: flexure-dominant case, flexure-shear balanced case, and shear-dominant case. In all three cases, negative flexural loading was used. In the balanced case, the ratio of applied rotation and tangential deformation (θ_2/U_3) was set equal to the ratio of the maximum rotation under pure flexure (Fig. 2-14) and maximum tangential deformation under pure shear (Fig. 2-11). In the flexural dominant case, the ratio of applied rotation and tangential deformation was twice that of the balanced case, whereas in the shear dominant case, this ratio was one-half of that of the balanced case. The simulation showed that for the balanced and shear dominant cases, the presence of significant shear loading caused a drastic decrease in moment capacity. While for the flexure dominant case (Fig. 2-17), the moment capacity was about 80% of the original moment capacity under pure flexural loading.

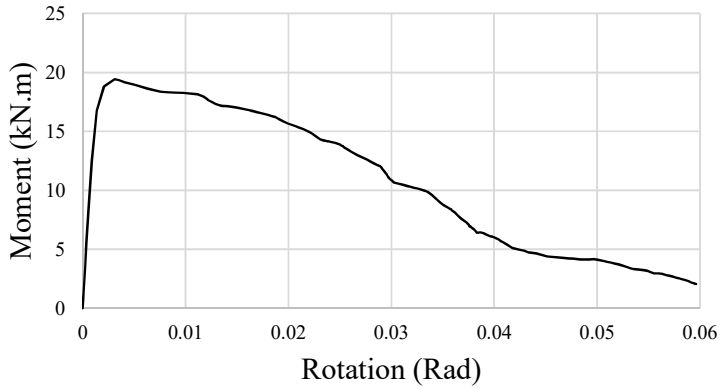

Fig. 2-17: Simulated moment-rotation response of the intermeshed connection under flexure-shear loading (flexure dominant case)

To better understand this observation, the deformation mechanism of the connection under flexure-shear loading was investigated, as shown in Fig. 2-18. As it was discussed earlier, under pure flexure, the connection failed when slippage occurred at the top flange (Fig. 2-18(a)). However, when a small shear was applied along with the flexural loading (Fig. 2-18(b)), the shear force helped to maintain the top flange level and prevented the vertical slip. But when the shear load was large (Fig. 2-18(c)), it moved the right-hand side of the connection downward until the right flange slipped out from the bottom this time. Thus, the effect of shear on flexural behavior could be either beneficial or detrimental depending on the amount of shear force applied.

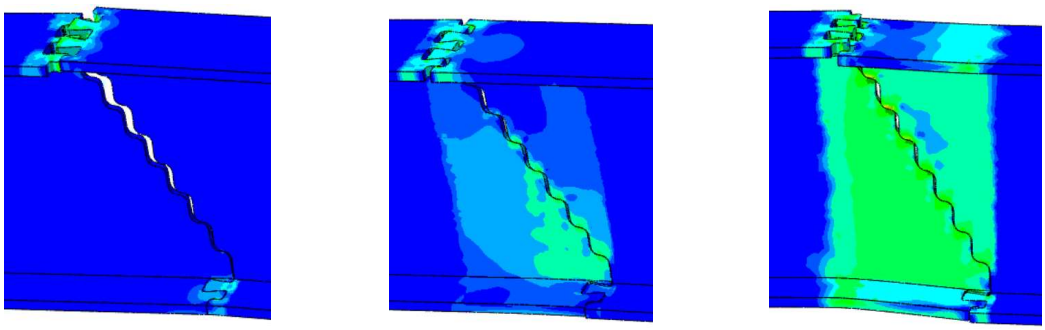

(a) With no shear (pure flexure case)

(b) When shear is small (flexure dominant case)

(c) When shear is large (shear dominant case)

Fig. 2-18: Deformation mechanism of connection under flexure-shear loading

2.6. *P-M-V* interaction diagram

The prior discussion of FEA of the intermeshed connection indicated that, under mixed mode loading, there were intricate interactions among different failure mechanisms. For design purposes, the key consideration was the peak load carrying capacity. The capacity interaction diagram was constructed by considering more than 200 combinations of axial force (P), moment (M), and shear (V). These were compared with the *P-M-V* interaction proposed in the AISC Specification (2016) and in Eurocode 3 [33,35].

Fig. 2-19 (a) and (b) show the simulated *P-M-V* interaction diagram plotted in both 3D and 2D. For a given applied axial force, the *M-V* interaction curve appears asymmetrical in terms of the moment capacity, which is largely caused by the deformation generated by shear loading. As mentioned earlier, the geometry of the intermeshed connection only allows the application of shear force in one direction. As shown in Fig. 2-11, the applied shear loading would cause slippage of the web step, while the connection experiences a certain level of rotation due to the existence of a small bending moment. As a consequence, the applied shear force improves the positive moment capacity, in which the bottom flange is in tension. Fig. 2-19(b) shows that shear loading could enhance the positive moment capacity by up to 50%. The opposite effect occurs for negative moment capacity, where the applied shear force would lead to a significant reduction of moment capacity.

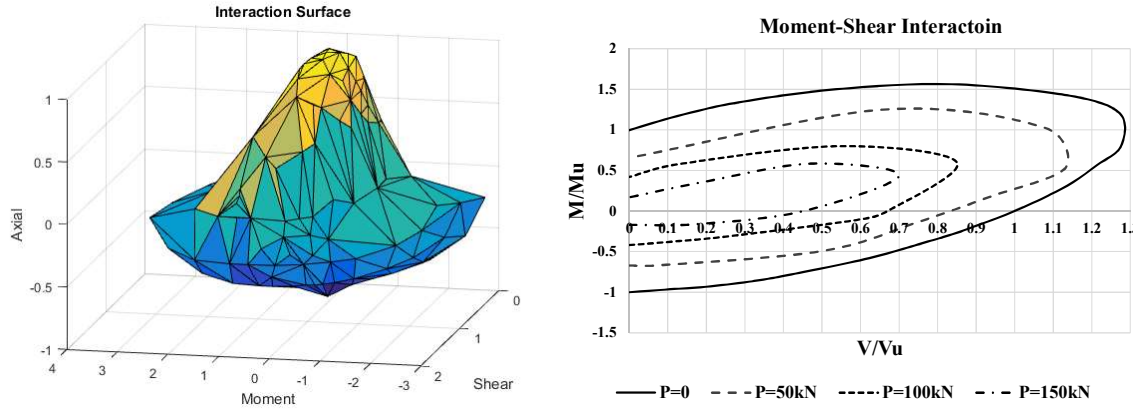

(a) Plotted in 3D (b) Plotted in 2D with various axial loads

Fig. 2-19: Simulated P-M-V interaction diagram

Current code specifications have provisions for interaction diagrams. For example, Eurocode indicates that when the applied shear force, V, exceeds 50% of plastic design shear resistance V_p, then the moment and axial resistances of the section can be determined using a reduced yield strength $(1-\rho)f_y$ [35], where ρ is calculated as

$$\rho = \left(2V/V_p - 1\right)^2 \qquad \text{Equation 2-3}$$

When the applied shear force is less than 50% of V_p, no reduction in yield strength is required. The resulting *M-V-P* interaction diagram is shown in Fig. 2-20(a).

The AISC specification considers interaction among moment, shear, axial load and torsion. Specifically, in the absence of torsion, the *M-V-P* interaction can be expressed as per Equation 2-4:

$$\frac{P}{P_u} + \frac{M}{M_u} + \left(\frac{V_r}{V_c}\right)^2 \leq 1 \qquad \text{Equation 2-4}$$

where M_u, V_u, and P_u are the peak capacities of the connection under pure moment, shear, and axial loading. Fig. 2-20(b) presents the interaction diagram described by Equation 2-4.

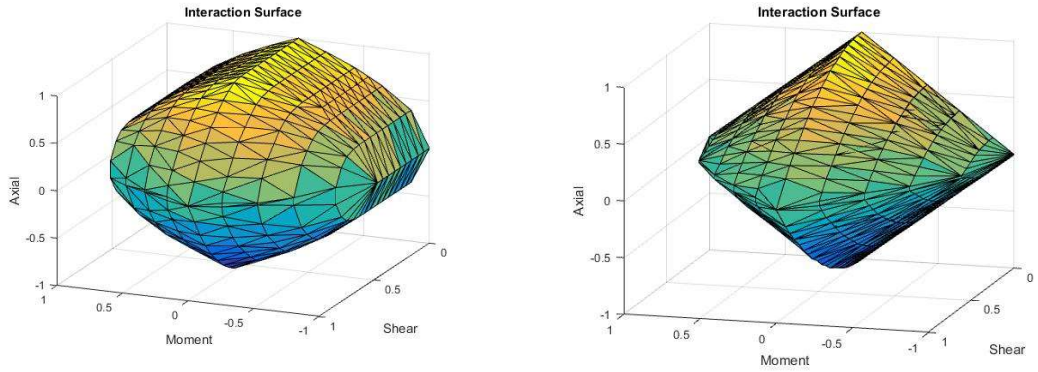

(a) Eurocode (b) AISC

Fig. 2-20: *P-M-V* interaction diagrams according to codes specifications

The aforementioned code recommendations are compared with the present simulation results. Fig. 2-21 shows the comparison for the moment-shear interaction in the absence of axial loading. In the negative moment regime for the intermeshed connection, the AISC specification represented the *M-V* interaction accurately, while the Eurocode overestimated the moment capacity for all shear loading levels. In the positive moment regime, both the AISC specification and the Eurocode grossly underestimated the moment capacity. This discussion reveals that the interactions included in current design codes may not accurately describe the behavior of the intermeshed connection under general mixed-mode loading. In this regard, high-fidelity FEA simulations are essential for investigating the structural behavior of such a connection.

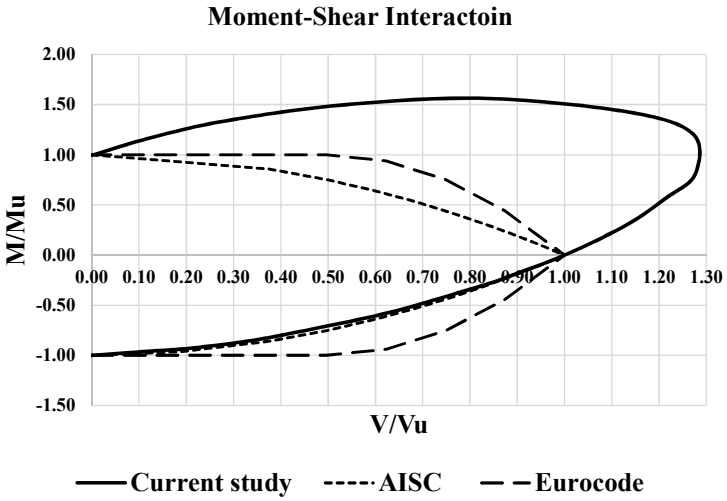

Fig. 2-21: M-V interaction diagrams of the connection simulated by the current study and prescribed by the AISC specification and Eurocode.

2.7. Classification of the intermeshed connection

Following current code standards (e.g. AISC specification and Eurocode), the intermeshed connection can be classified in terms of its stiffness, strength, and ductility. Based on the simulated moment-rotation curve of the connection, the stiffness can be defined as the initial slope of the curve, the strength as the peak moment capacity, and the ductility as the rotation at which the moment capacity drops by 20% in the post-peak regime. Based on these definitions, the initial stiffness, strength and ductility of the present connection were estimated to be about 17,400 kN·m/rad, 23 kN·m and 0.02 rad, respectively.

The AISC specification classifies connection types based on stiffness and strength. In terms of a stiffness criterion, the AISC uses the ratio between the flexural stiffness of the beam (EI/L) and the connection stiffness. Consider a typical beam length of 6 meters (about 20 feet). For the intermeshed connection studied here, the bending stiffness ratio

between the connection and the beam is about 13. According to the AISC specification [33], one would classify the connection as partially restrained.

In terms of the strength criterion, the AISC specification classifies connections that transmit less than 20% of the fully plastic moment of the beam at a rotation of 0.02 as simple connections. The intermeshed connection considered here transmits only 18% of the beam moment capacity due to the reduced load carrying capacity of the intermeshed flange. Therefore, the intermeshed connection would be classified as a simple connection.

Notably, the AISC specification also requires a rotation capacity of 0.03 rad for a connection to be considered as ductile. But the maximum rotation of the intermeshed connection, captured in the FEA, is about 0.02 rad. Therefore, the intermeshed connection is not recommended for cases in which large plastic deformations are required. This implies that the connection could be used in frames that resist gravity loads only.

In the Eurocode, there are different limits for connection classifications. For the stiffness-based classification, the connection can be considered as semi-rigid, if the stiffness of the connection is in the range between $0.5EI/L$ and $25EI/L$, where EI/L is the flexural stiffness of the beam. Therefore, the intermeshed connection would be considered semi-rigid ($13EI/L$) according to the Eurocode. In terms of the moment strength, the Eurocode considers a connection as nominally pinned, if its peak moment resistance is not greater than 25% of the plastic moment resistance of the beam. Therefore, based on the Eurocode, the intermeshed connection would be classified as a simple connection.

Connection classification is essential for proper modeling of a frame, as well as for determining the applicability of a system and the appropriate design specifications that

must be considered. Both the AISC Specification and the Eurocode would treat the connection studied here as a simple connection in terms of force transfer and partially-restrained (semi-rigid) in terms of the stiffness.

2.8. Conclusions

This study analyzed the behavior of a new type of steel connection that uses multi-degree of freedom, volumetric cutting with the aim of reducing fabrication costs and simplifying the erection process. Nonlinear finite element simulations were performed to investigate the complex behavior and failure modes of the intermeshed connection under mixed-mode loading. The simulation results showed that the connection exhibited excellent shear resistance, even in the presence of flexural and axial loading. However, the axial or flexural behavior was greatly affected by the alignment of the intermeshed flange connection. The presence of shear loading could have a significant influence on the deformation pattern of the flange and, consequently, the axial and moment capacity of the connection.

The *P-M-V* interaction diagram of the connection, simulated by nonlinear FEA simulations, showed that existing code recommendations of *P-M-V* interaction were not applicable to the intermeshed connection considered herein. In some cases, the code recommendation would grossly underestimate the load capacity of the connection, while in other cases an overestimation could occur. Therefore, detailed numerical analysis plays an essential role in determining the load capacity of the intermeshed connection under general mixed-mode loading until further code-based guidance can be developed.

Based on the classification requirement by both the AISC specification and the Eurocode, the intermeshed connection should be considered as a type of simple connection. This finding implies that the intermeshed connection can be used in gravity bearing structural systems, which is consistent with the intended design philosophy for this type of connection. However, the connection performance could be unsatisfactory if flange alignment is not maintained. Further research is needed to determine strategies to minimize such outcomes.

The intermeshed connection considered here can be used for a gravity load frame, because it exhibits good shear resistance, even in the presence of flexure and axial loading. However, the ability of a gravity load frame to undergo lateral drift would have to be evaluated separately, if it was part of a larger system that included an independent lateral load system (e.g. shear wall or braced frame). Notably, the connection is intended for placement at locations near beam inflection points where the bending moment is low and axial loading is negligible. For the purpose of modeling, the intermeshed connection can be represented as a pin connection, but a small amount of additional flexural stiffness may be needed for a fully accurate numerical representation.

3

Experimental Study of Intermeshed Steel Connections Manufactured Using Advanced Cutting Techniques[1]

Advanced manufacturing techniques, such as plasma, waterjet, and laser can facilitate field assembly and disassembly of steel structural components, and therefore potentially transform how steel structures are designed and constructed. These techniques have opened up an opportunity to create a new class of steel connections that rely on intermeshed (i.e. interlocked) components in lieu of traditional connectors such as weld and bolt. This paper presents an experimental investigation on the mechanics of such intermeshed steel connections manufactured by high-definition plasma and waterjet

[1] This chapter is adopted from the following manuscript:
M.E. Shemshadian, R. Labbane, A.E. Schultz, J.-L. Le, D.F. Laefer, S. Al-Sabah, P. McGetrick, Experimental study of intermeshed steel connections manufactured using advanced cutting techniques, J. Constr. Steel Res. 172 (2020) 106169. doi:10.1016/j.jcsr.2020.106169.

cutting. Four full-scale specimens with an intermeshed connection were designed to resist gravity loading in steel frames. The experimental testing program focused on the behavior of intermeshed connections under vertical loads including pure flexural and combined flexural-shear loading. Both global load-deflection response and local deformation were measured to provide insights into the complex load transfer mechanisms. The experiments demonstrated ample load carrying capacity, approaching the beam plastic moment, and ample ductility, approaching a deflection over span length ratio of 1/60 to 1/40, through the interaction of individual components. Analysis of the test data also raises important questions that must be addressed for the practical design of these connections.

3.1. Introduction

Presently, steel connections are almost exclusively made with bolts and welds. Both bolted and welded connections are labor intensive and contribute to a significant portion of the total cost of a steel structure [36]. Recent development of high definition plasma, laser, and waterjet cutting, when combined with fully automated computer-controlled techniques, could facilitate fast fabrication with high precision [17,18] that may allow for the development of an entirely new class of steel connections to improve both erection efficiency and material reuse. This equipment is currently employed to accelerate some conventional fabrication activities, such as the cutting of holes in lieu of drilling. However, to date, the steel construction industry has not capitalized on the full potential of advanced manufacturing equipment.

Over the past three decades, some alternatives to traditional steel connections have been introduced [6,9,12,20]. Some of these connections include components, such as castings or special/complex fixtures, that must be fabricated by a specialty manufacturer other than the steel fabricator, and thus add cost, time and complexity to the fabrication process. Arguably, large-scale adoption of a new connection system would have a greater opportunity for market penetration, if all components can be manufactured by a steel fabricator. Additionally, some of the connections previously developed were intended to carry moment, thus requiring heavier connecting parts and a more complex installation process than is needed for gravity load framing. For these reasons, only a couple of these connection systems have found significant commercial adoption [11,19].

A recent study on the cost and construction productivity between alternative and conventional methods for steel connections showed that buildings relying on quick connection systems could offer significantly lower labor hours for erection [20,37]. Quick connection systems can be fabricated using interlocking elements to create “intermeshed connections”, yet none of the alternative connections that have been previously developed have utilized advanced cutting techniques in their fabrication process. Thus, there is an untapped potential to harness these techniques to develop a class of connections that eliminates field welding and minimizes bolting. This type of connection would rely on advanced manufacturing techniques such as waterjet and plasma cutting during fabrication to create the interlocking elements. The fabrication costs associated with the intermeshed steel connections could be reduced by relying on automation, and the simpler and faster field erection could also offset labor costs relative to conventional connections systems.

An intermeshed connection system has been proposed to help transform how structural steel is fabricated, assembled, deconstructed, and reused [22,38]. In this class of connection, the transfer of forces is facilitated through direct contact of multiple, precisely shaped surfaces of the interlocking elements. In a system with intermeshed connections, beam stubs would be shop-welded to the column, and the central portion of the beam would interlock directly with the beam stubs when placed in the field (Fig. 3-1). This assembly process is fast and requires minimal worker training, while allowing for future disassembly of steel frames and potential material reuse. Most importantly, the majority of fabrication efforts can be performed using computer-controlled, high-precision cutting equipment, which would significantly reduce manual labor.

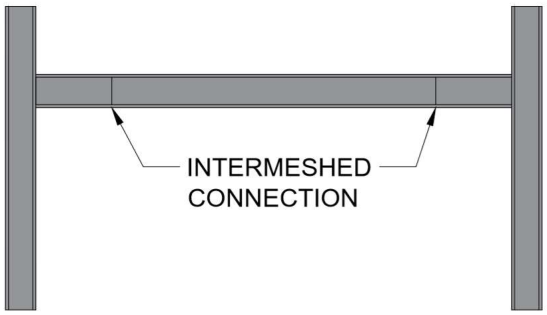

Fig. 3-1: Intermeshed connection locations in a steel frame

The aforementioned class of intermeshed connections has several attractive features in terms of constructability and reuse, but several questions and uncertainties need to be addressed. For instance, the tolerance level could affect the selection of cutting technique in the manufacturing process, therefore, pre-specifying the permissible tolerance level is crucial. Furthermore, there should exist an appropriate load path through the

connection detail for transferring loads, since the three-dimensional (3D) cuts will likely affect the load transfer capability of the connection. Thus, the behavior and performance of intermeshed connections requires experimental and analytical investigation.

3.2. Scope and objectives

This chapter focuses on full-scale experimental testing conducted on an innovative intermeshed steel connection. The behavior of load resisting mechanisms of this connection system is quantified, and a design procedure is developed for the intermeshed connection when it is implemented in a steel frame.

Based on the concept of direct contact between connected parts, a connection detail was proposed for connecting beam parts, and a design procedure was developed to create a realistic and practical connection. The connection was proportioned to resist forces that may exist in a typical gravity load systems, and the ductility and strength of the connection were considered in the design procedure. High-definition plasma and waterjet cutting were adopted for the fabrication of all intermeshed pieces.

The experimental work involved four major-axis beam tests with the intermeshed connections located along the beam span. Two pure bending moment tests were conducted, as well as two tests with single point loads. In one of the tests, the connection was placed in the pure moment region, whereas in the other three tests, the connection was subjected to a combination of bending moment and shear forces. The specimens were instrumented to enable a comparison between experimental results and the expectations from the design procedure.

3.3. Intermeshed concept and design procedure

In a regular I-shaped steel section, moment is transferred in the top and bottom flanges and can be idealized as a force couple comprised of tension and compression resultants located at opposite (i.e. top and bottom) flanges. Therefore, discrete elements could be used to carry tension and compression resultants, even though the compressive resultant can be resisted through direct bearing contact between the connected steel sections. Shear forces are resisted primarily in the beam web, so a connecting element in the web could also be considered.

Implementing the intermeshed concept and based on the detail described above, an alternative steel connection was proposed and called 'intermeshed connection' [23,39] (see Fig. 3-2). In this connection, the flange forces are transferred through side elements in the form of angles. This connection is envisioned with teeth cut into the sides of the beam flanges and rectangular holes (sockets) cut into the angles. The flanges and side angles intermesh into each other via corresponding teeth and sockets; and consequently, forces are transferred between the flanges and angles through direct bearing [21,23]. The angles not only connect different parts of the beam, but also keeps the flanges level and therefore prevents them from undesirable slippage. Once the beam flanges are connected, the section is expected to transfer moments via the connector angles. To transfer shear force, a pair of steel shear plates are bolted to the beam webs on both sides of the joint.

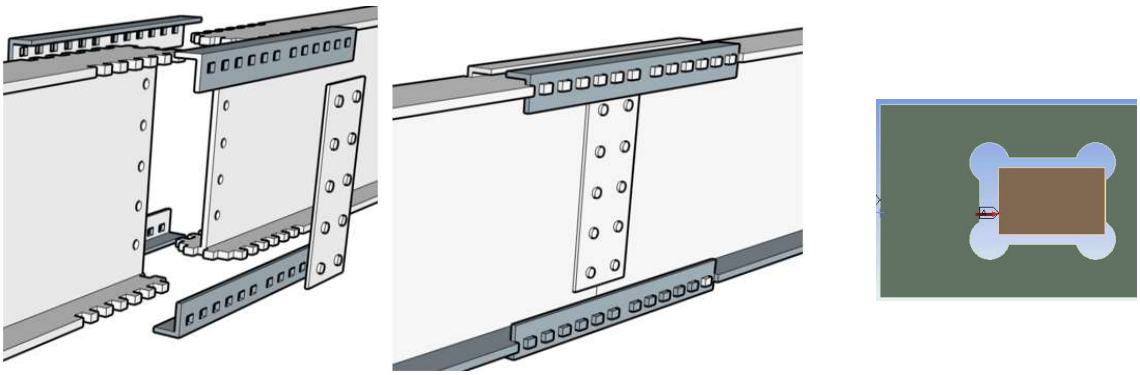

(a) 3D Exploded view (b) 3D View of assembled connection (c) Sockets with round corners (not in scale)

Fig. 3-2 Final version of the intermeshed connection

The sockets in the angles and the teeth in the flanges can both be fabricated using a variety of advanced manufacturing techniques. The hole tolerance controls the adjustability of the connection, with larger tolerances aiding in the connecting elements being placed more easily, as it better accommodates imperfections in the connected members. As the angles could be replaced after an overloading event, they are considered sacrificial elements. With this design philosophy, the side elements (i.e. angles) should be the weakest component of the frame and the teeth be the strongest. This concept helps achieve the goals of the intermeshed steel connection project for greater reuse of materials and at the same time satisfies the safety and ductility goals of the structure.

The configuration of the intermeshed connection was decided upon for practical purposes without consideration of the dimensions of the various connection elements. Although the depths of teeth and sockets correspond to flange thickness, many other geometric dimensions must be determined based upon the fundamental mechanics, engineering judgment, and design criteria. The tooth length, number of teeth, and tolerances must be selected for the connecting angle elements to meet the expected

connection performance. In addition, the plate at the web must also be designed to resist the shear force safely.

Intermeshed connections are intended for use in gravity frames, therefore the main loads come from dead and live loads. Since lateral loads are assumed to be resisted by structural core walls or braced frames, using lateral loading as a controlling factor for connection design is not necessary. However, gravity frames made using intermeshed connections must be able to resist the effects of lateral drifts imposed by the lateral load resisting system with no loss of vertical load capacity.

The intermeshed connection considered in this study consists of multiple intermeshed components. Due to interruption in load and stress paths, such a connection is not expected to achieve the full load carrying capacity of the steel section [22]. Therefore, the intermeshed steel connection would be most efficient when located near the inflection point and away from the support. This can be achieved by executing the connections on-site to beam stubs that are shop welded to the columns prior to erection (Fig. 3-1). Though locating a connection away from the supports leads to a reduction in both shear and moment demand from gravity loads, the forces at the connection may still be significant.

The procedure used to design the intermeshed connection considers the design of the angles and web shear plates as independent elements. In this procedure, the angles are assumed to take the bending moment and the plates take the shear force. The requirements of the current American steel design standard [33] were used to design angles as well as teeth number, size, and spacing. To ensure that the failure occurs in the angles rather than the teeth, the concept of 'capacity design' was exploited. In this approach, the angles were designed to resist the axial forces from applied loads (obtained from elastic analysis). The

teeth were subsequently designed for the maximum expected forces based on connector angle capacity. Given the number of variables needed to define connection resistance, an iterative approach for the proportioning of the elements was needed.

The sockets in the angles included tolerances for manufacturing imperfections since structural members are expected to have small imperfections. Therefore, an extra 1.5 mm of space was provided on each side of the teeth to accommodate imperfections. One potential concern related to the sockets is the stress concentration at sharp corners. Depending on the length-to-width ratio of the angle sockets, previous studies have shown that the stress concentration factor can be as large as five [40], which can result in a premature failure of the angle connector. To alleviate this issue, circular holes were added to the corners of the sockets in the angles to create stress-reducing radii (Fig. 3-2(c)). A finite element model was developed to investigate the effectiveness of such a change. Results showed that the stress concentration factor was reduced to 1.7 at the corners [22].

3.4. Test setup and specimens

The experimental program consisted of four tests, as shown in Fig. 3-3 and Table 3-1. In Test 1 the connection was located in a pure bending moment region along the span of the beam. In the other three tests, the connection was placed in locations, where both bending moment and shear are present. A pure flexural loading test was important since the angle connectors and flange teeth were designed for the sole purpose of resisting a pre-selected value of bending moment.

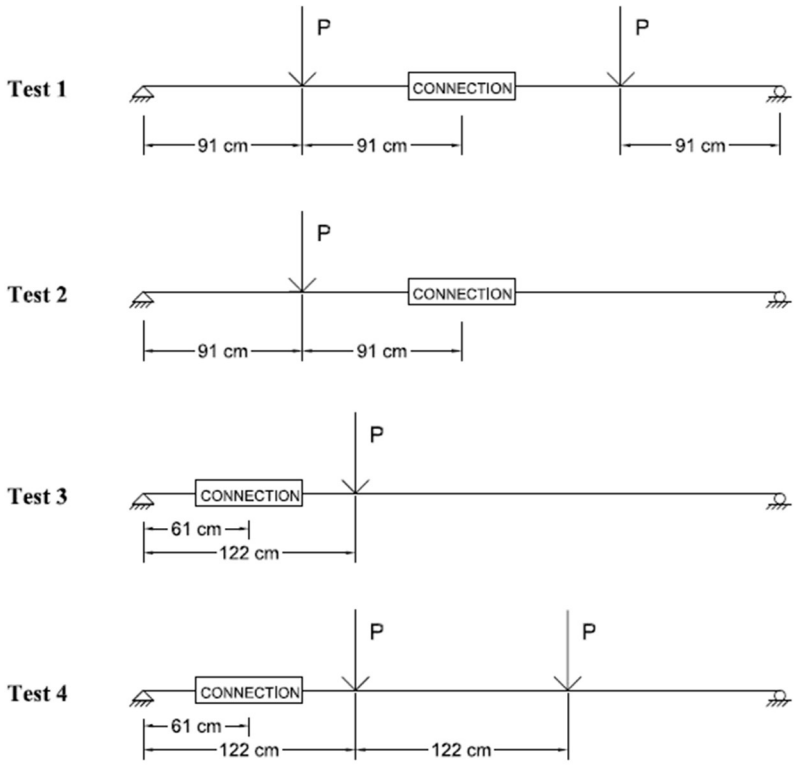

Fig. 3-3: Experiment configuration for Tests 1-4; P indicates loading location

Tests with combined flexural and shear loading were also imperative since these connections are intended to be placed in moment frames, while shear force is present. Test 2 was designed to demonstrate how the presence of shear force in the connection region of Test 1 will affect the bending behavior of the specimen. Test 3 and 4 were designed to simulate the probable scenarios in practice when connection is located near an inflection point.

Table 3-1: Intermeshed Connection Test Specimens

Test	Loading Description	$M_{C,\ design}$ (kN-m)	$V_{C,\ design}$ (kN)	$M_{C,\ design} / V_{C,\ design}$	Beam Section*	Angle*	Shear Plate (mm)
1	Pure bending	171	N.A.	N.A.	W18×46	L2½×2×3/8	PL368×152×6
2	Bending & shear	171	93	1.84	W18×46	L2½×2×3/8	PL368×152×6
3	Bending & shear	243	396	0.61	W21×57	L3×2×3/8	PL368×152×6
4	Bending & shear	243	396	0.61	W21×57	L3×2×3/8	PL368×152×6

* US designations for hot rolled steel shapes

Wide flange Grade 50 steel beams were used in the tests, since this is the most commonly used steel grade for structural framing [41]. The beam sizes, W18×46 and W21×57, were selected from commonly employed members based upon engineering judgment. Span lengths of 3.7 m were chosen for the testing program due to testing limitations. The W18×46 and W21×57 intermeshed connections were designed according to the procedure described in the previous section, and detailed sketches were sent for fabrication using robotically-controlled plasma cutting equipment for the beam sections and a waterjet cutting table for the angles (Fig. 3-4(a)). The higher accuracy and precision of the waterjet cutting operation (less than 1 mm precision) were needed for the radii in the sockets, whereas the accuracy of the high-definition plasma cutting operation (about 1.5 mm precision) was sufficient to cut the teeth in the beams flanges.

(a) Cutting process (b) Final product

Fig. 3-4: Manufacturing the intermeshed connection

To determine the material properties in tension, coupon tests were conducted on samples of the beams and angles in accordance with ASTM E8/E8M [42]. Results are presented in Table 3-2 and Fig. 3-5.

Table 3-2: Tensile properties of specimen components

Item	σ_y (MPa)	σ_u (MPa)	ε_u (%)
W18×46 flange	379	490	40
W18×46 web	414	503	33
W21×57 flange	379	490	35
W21×57 web	421	496	28
L2½ × 2 × 3/8	400	531	36
L3 × 2 × 3/8	359	517	36

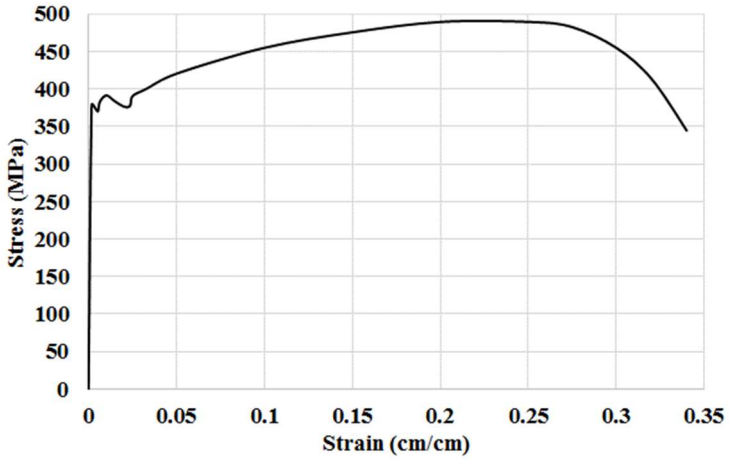

Fig. 3-5: Stress-Strain behavior of a coupon from a W21×57 flange

The experimental program was conducted using an MTS 600-kip load frame (with capacity of 2700 kN) located in the Galambos Laboratory of the Department of Civil, Environmental and Geo-Engineering at the University of Minnesota (Fig. 3-6(a)). The beams were simply supported with various loading schemes. To avoid unwanted lateral deflections in the beams, bracing was added to the sides of the test specimen. However, the bracing design was modified as the program progressed from one test to the next due to the need for additional lateral restraint. Slippage of angles out of their positions would cause premature failure, therefore, a locking mechanism was used for the testing that would also serve to provide indications of the forces needed for restraint of the angles (Fig. 3-6(b)).

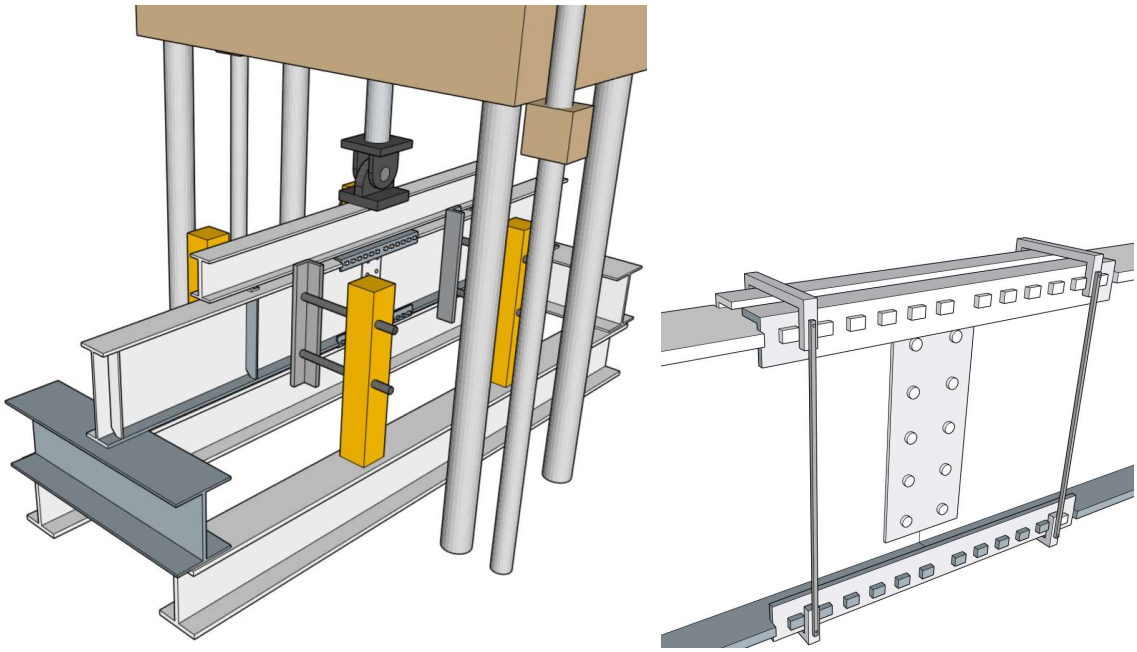

(a) Test setup for the first experiment (b) Channel restraints

Fig. 3-6: Experimental program in Galambos laboratory

Instrumentation locations for Test 1 were determined based on stress distribution results of a preliminary finite element model of the first specimen [26,27]. However, the instrumentation was slightly modified as testing progressed.

An initial finite element model showed the stresses radiating out from the teeth towards the center of the flange, resulting in different stress levels along the flange center (see Fig. 3-7). Because of this result, the strain gages on the flange were placed in the center, as shown in Fig. 3-9. To sample the stress state in the beam, strain gages were also located outside of the connection region on the top and bottom flanges, and a rosette was located at the center of the web as well.

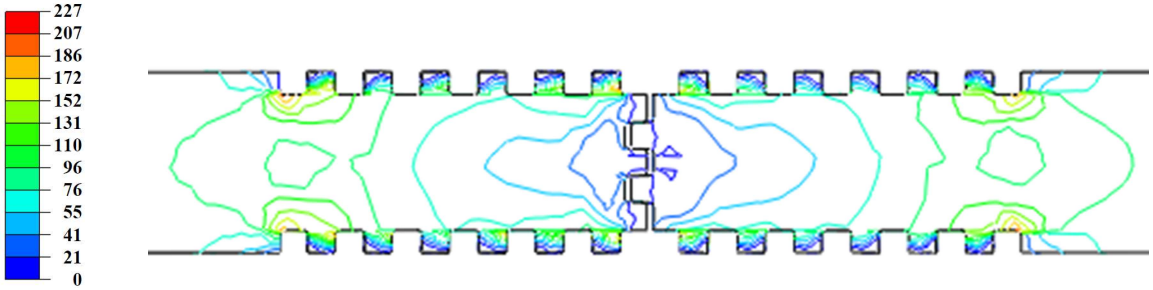

Fig. 3-7: Von Mises stress contours of beam flange (unit is MPa)

The same finite element model demonstrated the distribution of angle stresses. Starting from the outside ends of an angle, the stresses built up from each additional tooth, until the center of the angle was reached. Therefore, stresses were always highest around the center two sockets in the angle (Fig. 3-8).

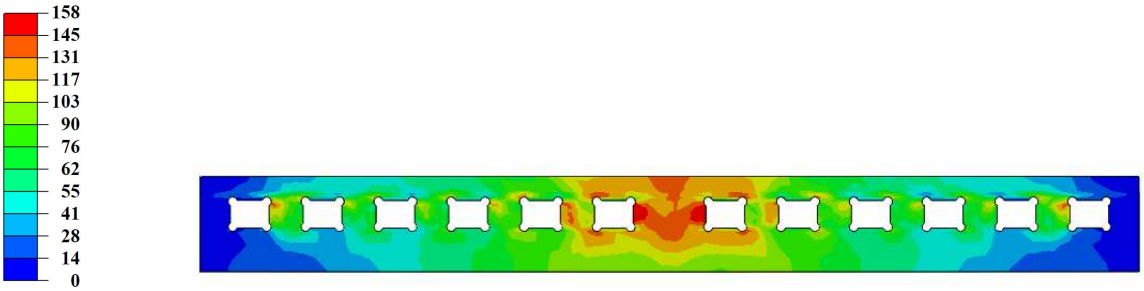

Fig. 3-8: Von Mises stress contours of angle (unit is MPa)

Since the maximum stresses and strains that occurred in the angle were towards the center, as indicated by the finite element model results, all instrumentation was placed at the center of the angle. Similarly, strain gages were placed on the inside and outside of each leg of the angles. Images of the instrumentation for angles, shear plates, and beams are shown in Fig. 3-9. Squares denote strain gages, circles denote rosettes, and rectangles denote LVDTs.

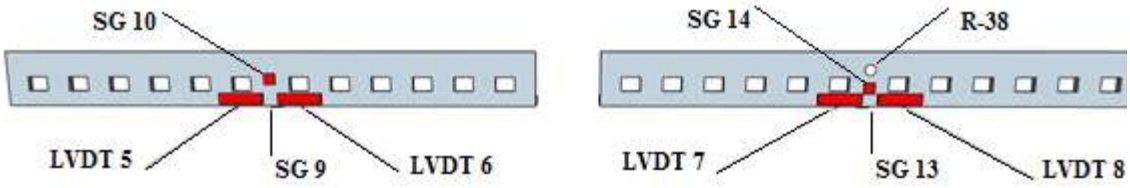

Tension angles instrumentation (left: back angle, right: front angle)

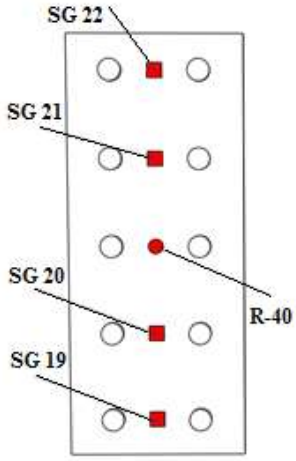

Shear plate instrumentation

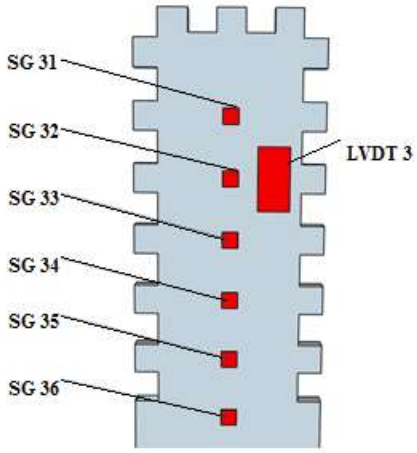

Beam bottom flange instrumentation

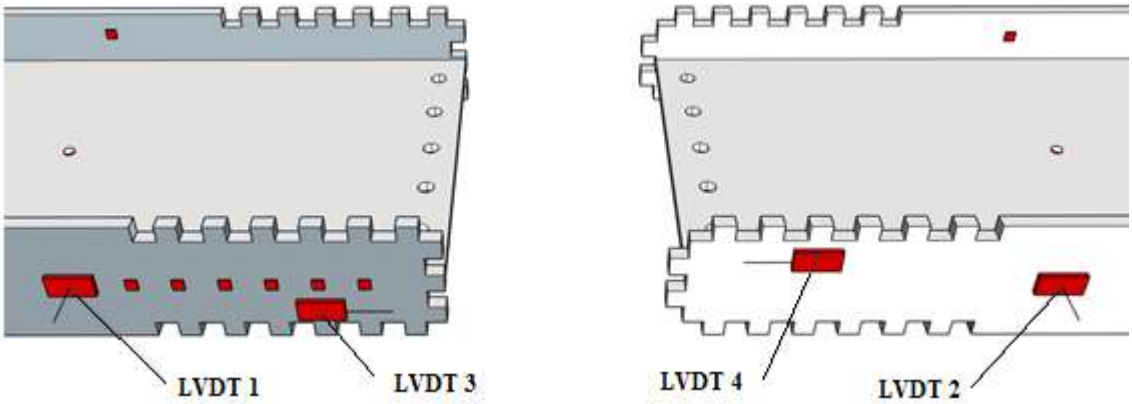

LVDTs on bottom flange

Fig. 3-9 Instrumentation the specimen of Test 1

3.5. Experimental results and observations

3.5.1. Intermeshed connection under pure bending

The first beam test was a pure bending moment test of a W18×46 steel wide-flange beam, and it was conducted in four separate stages using a displacement-controlled

protocol. Fig. 3-10 presents the data recorded from the LVDTs. Increasing displacements were measured at relatively low loads due to the shear plate bolts slipping into place and engaging with the plate. This is labeled as 'initial settlement' in Fig. 3-10, and the displacement of about 2 cm in the LVDT data was due to the closing of tolerance gaps at bolt holes and angle sockets. The bolts were slipping into contact with the beam web and shear plates while making audible sounds; at the same time, the teeth were visibly moving into bearing contact with the angle sockets. During this stage, the beam flanges at the top moved closer together, and the flanges at the bottom moved farther apart. The specimen started to yield around a displacement of 3.8 cm, one-half of which belongs to initial settlement stage. However, strength degradation did not start until later (at a displacement of 7.5 cm) which shows a significant amount of specimen ductility.

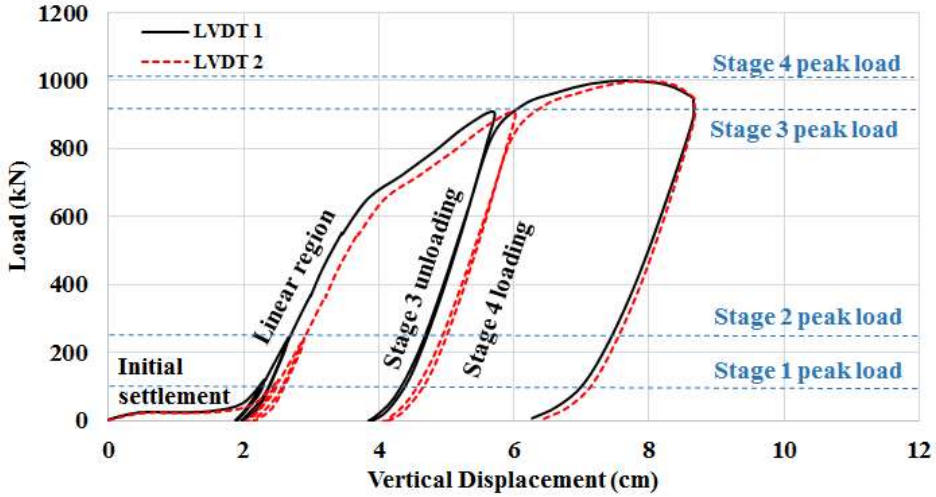

Fig. 3-10: Test 1 total load vs. vertical LVDT displacement

During the test, a maximum load of 1001 kN was recorded, and lateral torsional buckling of the specimen was observed. The angles in compression bent out-of-plane due to lateral torsional buckling of the beam (Fig. 3-13(a)). Onset of this behavior was recorded

near the peak load, and the various connection elements continued to deform inelastically after the peak load was reached. The test was stopped after 7% of the peak load capacity was lost.

The LVDT data from the angle recorded one brief period in which the angles were carrying load asymmetrically (Fig. 3-11(a)). LVDT 5 measured a reduction in displacement near its yield point, and at this point the parallel LVDT 7 recorded an increase in displacement (see Fig. 3-9). This phenomenon coincided with the onset of lateral buckling. In fact, yielding of the angles led to a significant stiffness reduction in the beam which caused the initiation of lateral buckling in the specimen and consequently asymmetric displacements in LVDTs 5 and 7. Two strain gages on the beam top flange recorded inelastic behavior, as did three gages at the center of the bottom flange. The gages located farthest from the connection centerline recorded the highest strains (Fig. 3-11(b)). A comparison between curves provided in Fig. 3-11 shows that initiation of plasticity in all angles occurred at a load of approximately 489 kN. At this load level, all beam strain gages indicated the intended linear elastic behavior, which proves the effectiveness of the design procedure that was employed.

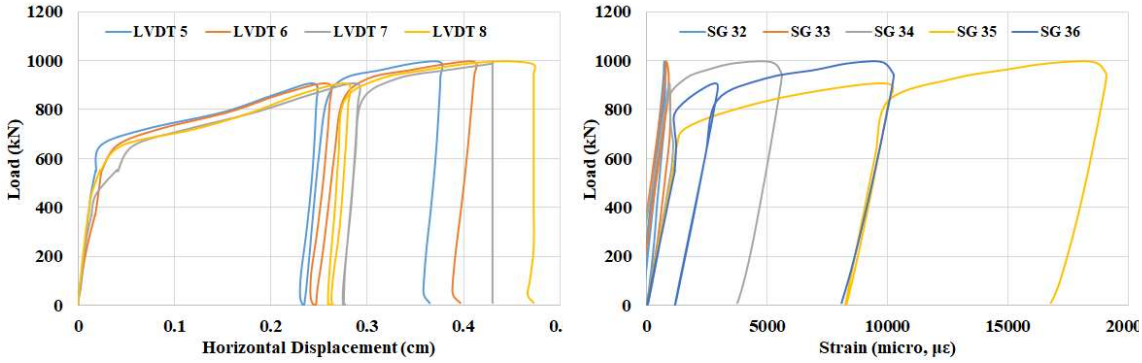

(a) Horizontal displacement from tension angle LVDTs

(b) Beam bottom flange strain

Fig. 3-11: Test 1 total vertical load versus different displacements and strains

Inspection of the specimen during and after the test was performed to spot any smaller-scale phenomena in the connection region. In the post-loading image, the teeth in compression flange had moved closer together, and the teeth in tension flange had moved farther apart (Fig. 3-12(a)). Fig. 3-12(b) shows that the centermost sockets in tensile angles elongated the most in comparison to the other sockets. Necking also began directly above the centermost sockets. On the basis of measured socket lengths after the test, the permanent deformation of the tension angles at this location was approximately 5 mm.

(a) Elongation of the sockets in the left half of the tension angle center sockets (b) Necking above the

Fig. 3-12: Test 1 deformation in tension angles

The angles in compression experienced relatively high measured strains of as much as 0.015. However, once the angles became plastic due to the large axial strains, connection resistance to lateral-torsional buckling of the beam was reduced. This effect, combined with insufficient stiffness from the lateral bracing system, allowed the beam to undergo lateral-torsional buckling before the beam section reached its plastic moment capacity. The curvature of the angle, shown in Fig. 3-13(a), was due to the lateral pressure being applied by the beam as it deflected laterally and twisted. The same angle was also bent vertically around centerline (Fig. 3-13(b)). While the angles underwent large plastic deformations, the teeth did not experience any major damage (Fig. 3-13(c)). Therefore, the capacity

design method was effective in ensuring that the beam remain functional during the test until the angles failed due to large plastic deformations.

(a) Kinking of compression angle due to lateral-torsional buckling of the specimen

(b) Bending of compression angle due to the applied vertical load

(c) Small deformations in the teeth

Fig. 3-13: Test 1 compression flange and angles post-testing

The first test was stopped when the vertical load capacity of the beam decreased to about 93% of the peak value due to lateral torsional buckling of the beam. In Tests 1 and 2, EFCO members (lightweight built-up steel sections made using perforated steel channels) were used for lateral bracing. To avoid the same undesired failure mode, the lateral bracing for the second test was enhanced by providing additional braced locations.

For Tests 3 and 4, stiffer braces made of stiffened W12×35 steel sections were used (Fig. 3-14).

(a) EFCO members for Test 1 and Test 2

(b) W12×35 for Test 3 and Test 4

Fig. 3-14: Modifications to bracing

To simplify the displacement measurements for the following tests, the LVDTs were replaced with string potentiometers (aka 'string pots' are cable actuated position sensor). The string pots had a range of 25 cm, and they were attached to each beam flange approximately 2.5 cm. from the connection centerline (Fig. 3-15(a)).

3.5.2. Intermeshed connection under combined bending and shear

Tests 2-4 were run under combined bending and shear loads. To further investigate the performance of intermeshed connection under this load case, a variety of details were examined. Three different moment to shear ratios ($M_{C,\ design}$ / $V_{C,\ design}$) were tested on two different beams, W18×46 and W21×57 (Table 3-1). The location of the intermeshed connection was also altered between center and side of the beams as illustrated in Fig. 3-3.

The second beam, another W18×46, was tested with a single point load over a stiffener, and with the connection under both shear force and bending moment, as noted in Table 3-1. The beam and connection responded in a manner that was expected to the vertical loading that produced a constant ratio of shear to moment. Similar to Test 1, the magnitude of deflection needed to fully engage the connection was relatively large, but this deflection was smaller than in Test 1 (1.3 cm in Test 2 versus 2 cm in Test 1), which suggests that the presence of shear helps close the gaps in the intermeshed connection. Once the flange teeth and the shear plate bolts made contact with the corresponding surface in the angles and the beam webs, the connection generated internal resistance to offset the applied loads. A peak load of 810 kN was reached, and the beam section failed when the moment at the loading point was equal to its calculated plastic moment capacity (Fig. 3-15(b)).

The maximum vertical deflection measured was 8.9 cm. String Pot 2 measured slightly more displacement than String Pot 1 since it was located on the side of the connection adjacent to the point load. The beam flanges on either side of the connection were not level with one another at the end of the test (Fig. 3-16(a)). The shear force produced permanent vertical slip between the two beam flanges, and the angles have an undulating appearance post-test because of this, as shown in Fig. 3-16(b). These permanent deformations indicated that the angles resisted some of the shear force and yielded because of it.

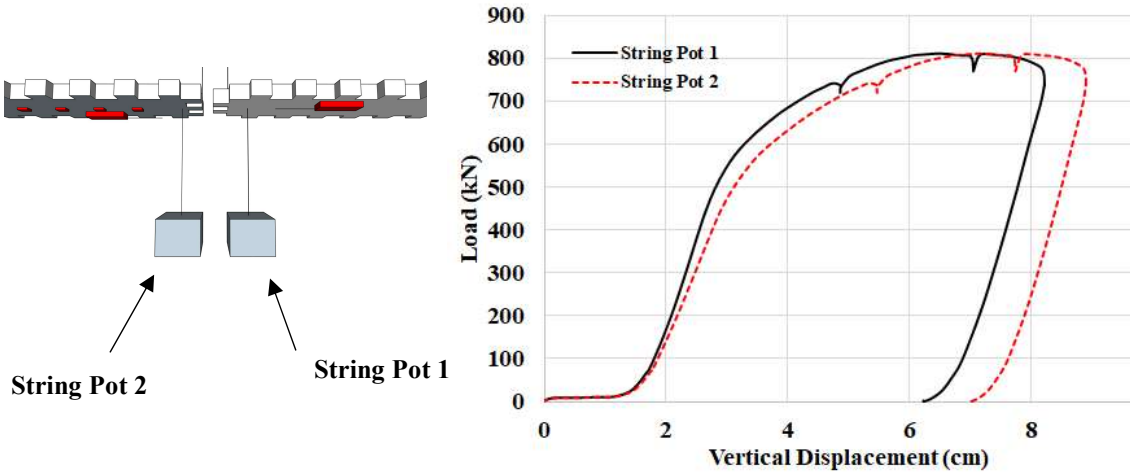

(a) String potentiometers in place of LVDTs 1 and 2

(b) Test 2 load vs. vertical displacement

Fig. 3-15: Test 2 instrumentation and results

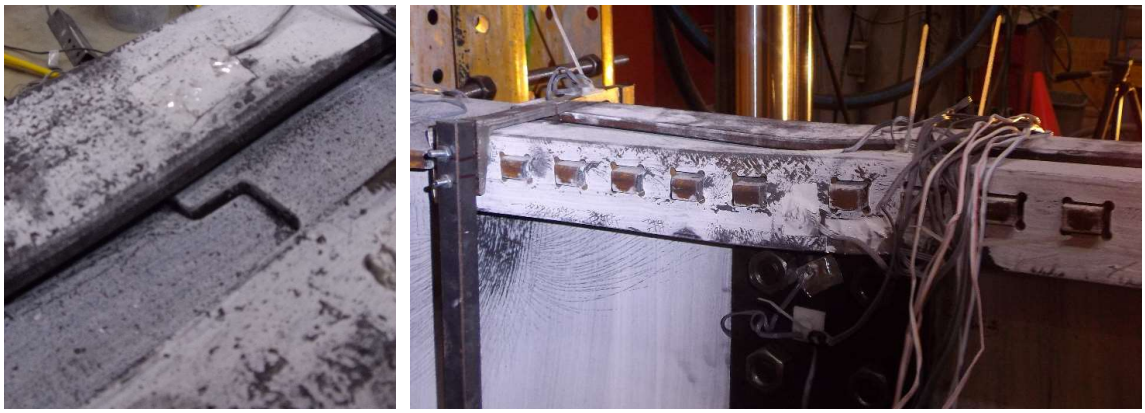

(a) Uneven top flanges

(b) Undulating angles

Fig. 3-16: Shear deformation in the connection region

The third beam, made using a W21×57 section, was tested with one point load and was subjected to a combination of bending moment and shear force (Table 3-1). The lateral bracing was effective in restraining the system until the peak load (1032 kN) was reached. A maximum vertical displacement of nearly 6.3 cm was measured at the connection location in Test 3 (see Fig. 3-17(a)). Similar to Test 2, vertical misalignment of the flanges gradually occurred once load was applied. The beam flanges once again did not record any inelastic behavior, until nearly the peak load.

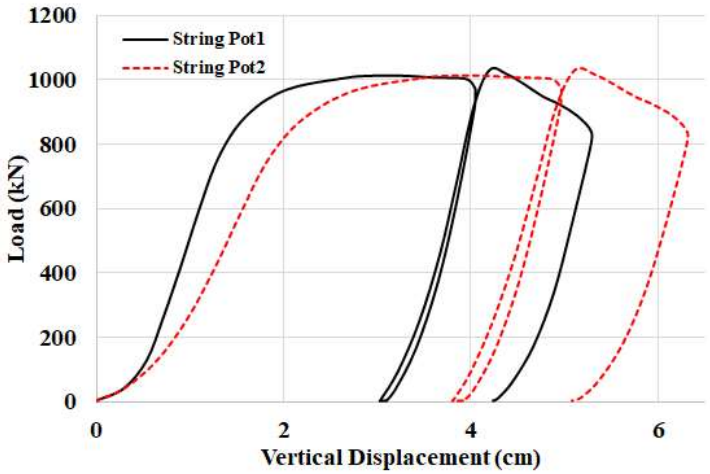

(a) Load vs. vertical displacement

(b) Yielding in the beam web

Fig. 3-17: Test 3 results

In Test 3, yielding of the beam web in shear was visible (Fig. 3-17(b)). This action is assumed to be due to the formation of tension fields in the web aided by the restraint provided by the top and bottom flanges, as well as the stiffeners on either side of the panels. The plastic moment of the beam section developed, due to adequate lateral restraint.

In Fig. 3-18(a), LVDT 6 and LVDT 7 show similar load displacement curves with higher displacements than LVDT 8. LVDTs 6 and 7, located on the left side of the connection, were closer to the point load and therefore experienced higher moments than LVDT 8, as shown in Fig. 3-18(b). Higher moments led to higher resultant axial forces and consequently larger displacements on the left side of the angles.

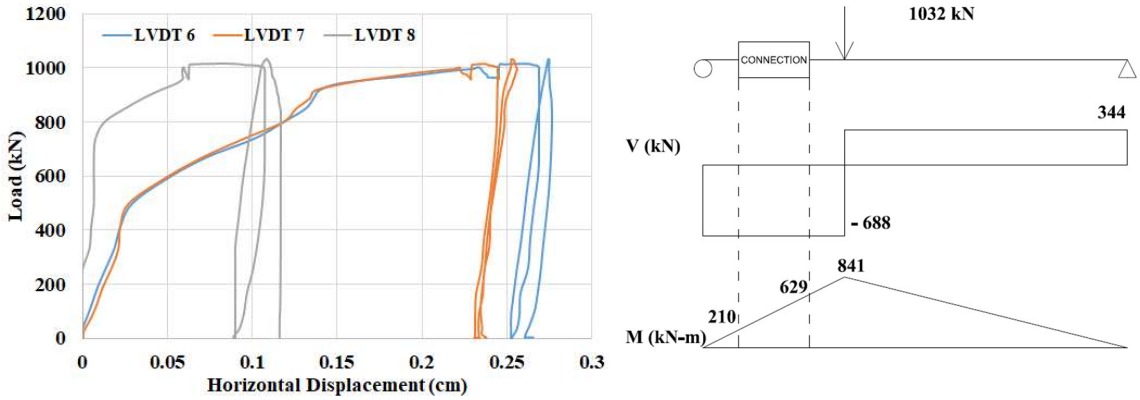

(a) Load vs. angle LVDT displacement (b) Test 3 free diagram

Fig. 3-18: Unequal demand on the tension angles in Test 3

The load versus deflection data of Test 4 is included in Fig. 3-19(a), which indicates unequal vertical displacements, where the String Pot 2 was closer to the point loads than String Pot 1. The unequal displacements were due to the presence of shear, similar to Tests 2 and 3. A peak load of 1277 kN was recorded, and the beam section reached peak load at its plastic moment capacity. The beam data was consistent with the measurements from each of the other tests. The instruments on the bottom of the beam flange within the connection recorded inelastic behavior only in Gage 35 and Gage 36 (Fig. 3-23 (a)).

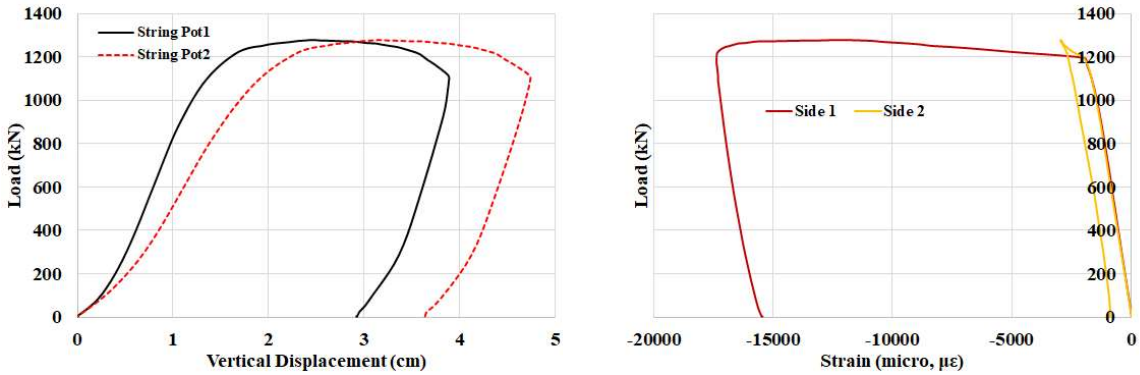

(a) Load vs. vertical displacement (b) Top flange load vs. strain

Fig. 3-19: Test 4 results

The beam flanges, once again, did not record any inelastic behavior until near the peak load (Fig. 3-19(b)). Most of the plasticity in the flanges of the beam sections occurred in the constant moment region of the span, where the bending moment value was the highest. Yield lines due to both moment and shear were visible in several areas along the span of the beam. The center span of the beam was in a constant moment region, and Fig. 3-20(a) shows the yielding of this region after the plastic moment had been reached. After the top flange and the top part of the web buckled, the force (stresses) migrated downward and developed an inclined orientation in order to bypass the "buckle". This compression field was equilibrated by forces generated in the web near the bottom flange. The inclined yield lines observed in Fig. 3-20(a) are a result of this stress state. While plastification occurred at center span, there was no major damage in the connection region. Gaps were closed, and yielding occurred in some parts of angles and beams, but no large deformation or significant yielding was observed, contrary to observations in the previous tests.

(a) Failure of the beam at center span (b) No major damage in connection

Fig. 3-20: Test 4 specimen after unloading

3.6. Data analysis

The experimental program results demonstrated globally and locally how the beam and the connection behaved at various loading stages. All four tests generally showed satisfactory behavior with a load bearing capacity larger than the target design loads. In each beam, linear elastic behavior was observed within the design load level which was in agreement with the assumptions in the design procedure. A ductile behavior with a smooth transition between different phases was recorded, as each beam vertically deflected 6.3 to 9.4 cm over a 3.7-m span (about $L/60$ to $L/40$) when tests were stopped. The summary of the results from Tests 1 to 4 is presented in Table 3-3.

Table 3-3: Summary of the experimental results

Test	F_{max} (kN)	$M_{C,\,max}$ (kN-m)	$V_{C,\,max}$ (kN)	δ_{max} (cm)	$\varepsilon_{A,\,max}$ (%)	$\varepsilon_{F,\,max}$ (%)
Test 1	1001	457	0	8.6	2	1.9
Test 2	810	371	205	8.9	2.8	1.6
Test 3	1032	420	689	6.3	3	1.7
Test 4	1277	390	641	4.7	2.8	1.3

3.6.1. Moment resistance of the specimens

Table 3-4 shows the design moment for each section and the maximum moment observed in each test. Based upon the values in the fifth column of this table, the plastic moment was almost reached in Tests 2, 3, and 4. It was not reached in Test 1, because of the early occurrence of lateral torsional buckling due to inadequate bracing. Notably in Tests 2, 3, and 4, the connections were not subject to the maximum moment in the beams due to their location along the beam.

Table 3-4: Moment capacity of the specimens

Test	$M_{C,\,design}$ (kN-m)	$M_{C,\,max}$ (kN-m)	$M_{B,\,max}$ (kN-m)	$M_{B,\,max}$ / $M_{B,\,plastic}$	$M_{C,\,max}$ / $M_{C,\,design}$
Test 1	171	457	457	0.79	2.67
Test 2	171	372	557	0.96	2.17
Test 3	243	420	841	1.02	1.73
Test 4	243	391	780	0.95	1.61

Only in the first test was the connection located in the region of maximum moment, and this moment was constant over the connection length. This was also the only test where the plastic moment capacity of the beam was not developed at the peak load. In each of the other tests, the maximum moment occurred away from the connection and caused a failure in a portion of the beam section not containing the connection. Thus, in Tests 2, 3, and 4, but the beam section reached its peak load and controlled the failure of the specimen, and the connection was not brought to failure. Similarly, in Test 1 the beam may have been able to resist more load if the bracing system preventing lateral-torsional buckling had been in place.

The peak moment that was reached during the tests indicated that the connection possessed more capacity than initially calculated. In all cases, the connection was designed to develop at least 1/3 of the plastic moment capacity of the section, and a number of generous factors were used to ensure a conservative design. The last column of Table 3-4 compares the maximum moment observed in connection during the experiment to the target moment, for which the connection was designed. In other words, these values represent the moment overstrength in each test. After the test, analysis was performed to decompose the moment overstrength of the connection in Test 1. Test 1 was selected since the angles experienced the highest stresses in this test. The intermeshed connection of this

specimen resisted 2.67 times the moment that it was designed to resist. The following calculations explain why this overstrength was observed.

Although the connection was designed assuming that only the angles would resist bending moment, moment resistance was afforded by the shear plates as well. The strain data recorded in the shear plates was used to estimate how much moment they contributed to the connection. In the shear plate strain gages (see Fig. 3-9(b)), approximately linear elastic behavior was recorded (Fig. 3-21). Because of the linear elastic behavior recorded in the plate, the distribution of strains could be used to estimate curvature, κ, in the shear plate. Curvature can then be used to solve for moment using the moment-curvature relation for slender beams made using a linear, elastic material:

$$M = EIk \qquad \text{Equation 3-1}$$

Moment in the shear plates were calculated using the expected elastic modulus E of steel (2.07×10^5 MPa) and the tabulated values for I the moment of inertia of a vertical section of the shear plates. Applying this procedure and based upon the strain data obtained from the experiments, moments in the shear plates could be as large as 8% of the connection moment [43].

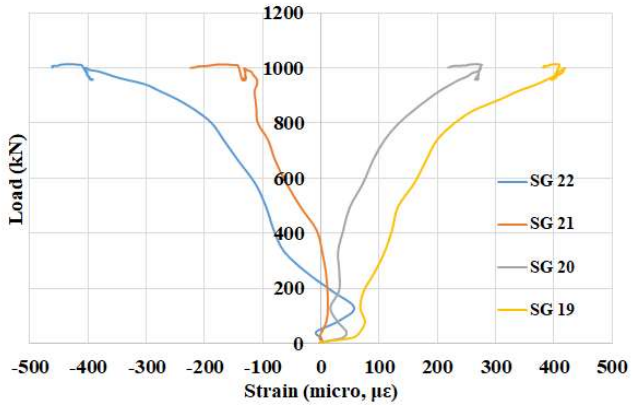

Fig. 3-21: Jack load vs. horizontal strain in shear plates for Test 3

Moment forces at the connection were also resisted by bearing contact between the two beam faces. As load increased, the top flanges of the two beams moved closer together until contact was established. Additional resistance at the top flange would have theoretically elevated the neutral axis of the connection region. The couple comprising the compression from bearing in the top flange and added tension in the shear plates can be calculated using the strain data in the shear plates (see reference [43] for more details). These calculations could be performed using the strain data from the experiments. For Test 1, the moment from the bearing-plate tension mechanism was calculated to be roughly 8% of the total moment at the connection. Additional contribution from post-yield straining of the tension angles could also be about an extra 19% [43].

The yield stress considered in the design process was 248 MPa (nominal yield strength of A36), while the coupon tensile test showed a much higher value of 400 MPa. This adds an overstrength equal to 61% to the connection capacity. Also, in the design procedure and when calculating the failure load of the angles, a safety factor of 1.1 was included which was patterned after the capacity design approach for seismic design [44]. Taking into account all the aforementioned overstrength sources and multiplying their corresponding factors will result in:

$$Overall\ overstrength = 1.1 \times \Omega_{sp}\,\Omega_{bb}\,\Omega_{sh}\,\Omega_{mo} \qquad \text{Equation 3-2}$$

Equation 3-2-2 estimates an overall overstrength factor of 2.5 which is very close to the 2.67 overstrength factor observed in the experimental test of first specimen. Thus, it may be concluded that moment overstrength in Test 1 was likely due to the mechanisms and safety factors outlined in this section.

3.6.2. Demands on angles

The distribution of strains in the tension and compression angles demonstrated that the magnitude of plasticity experienced in the angles varied. Before any yielding occurred, the strain measurements recorded in tension and compression angles were roughly equal. After yielding was initiated, however, variations among strain measurements were recorded. This is demonstrated in strain distribution data from Tests 3 and 4 (Fig. 3-22).

In Test 1, the pure moment test, the angles were loaded symmetrically and recorded similar strains on each side of the angle. In the tests that included shear (Tests 2-4), the angles clearly began yielding on one side of the centerline before the other. Since these tests did not load the specimen with constant moment along the entire length of the connection, the moment at one end of the connection region was higher than it was at the other. For example, in Test 3, the difference was over 300% at peak load (see Fig. 3-18(b)). When the angles were designed, the entire angle was assumed to undergo the moment experienced at the centerline. Since this was not true and the angles loaded asymmetrically, some plasticity was observed in the tension angles of Tests 3 and 4 before the design loads were reached. These were the only observed instances of non-linearity prior to reaching the design load across the four tests.

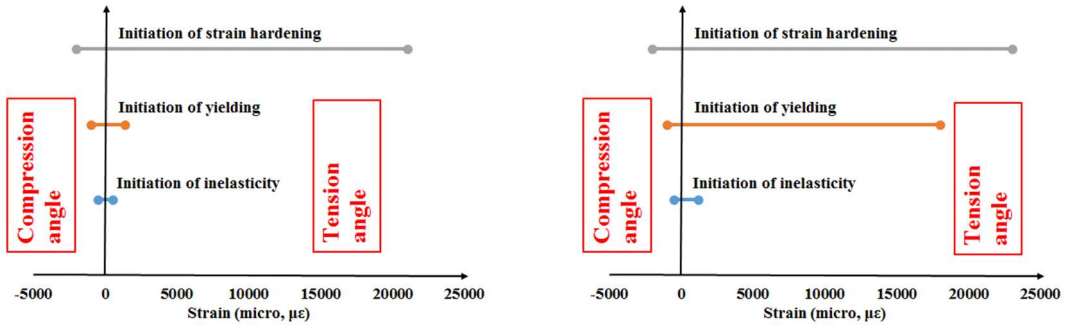

(a) Test 3 (b) Test 4

Fig. 3-22: Distribution of strain measurements in angles

3.6.3. Demands on beam flanges

As intended in the design procedure, the beams remained linear elastic at the onset of the angles yielding. In fact, no significant plasticity was recorded at instrumented locations of any of the beams until the vicinity of the specimen peak load occurrence. In each test, the first instance of nonlinearity in the beam was recorded at the centerline of the bottom flange of the beam. The highest strains on the bottom flange were recorded at the end of the connection region, and the lowest strains were recorded near the centerline of the connection. This feature is demonstrated in Fig. 3-23(b). The left side of the image is at the centerline of the connection (i.e. the end of a beam segment that is joined to another segment by means of the intermeshed connection). In this region, strain accumulation occurs from left to right along the flange. As the strains accumulate from left to right, the axial force on the flange increases from zero to a maximum value after the rightmost tooth. At the right side of the connection region, load transferred to the flange from all teeth was recorded in the strain measurements. The strains measured at 90% of peak load in Test 4 are extracted from Fig. 3-23(a) and included in Fig. 3-23(b) to demonstrate this phenomenon. All plasticity recorded on the beam bottom flanges occurred after the intended design load had been reached.

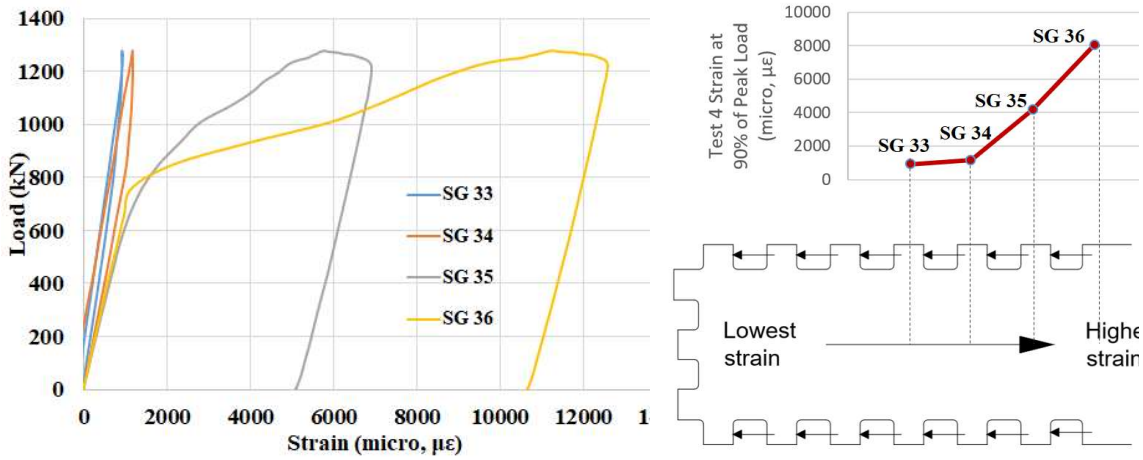

(a) Strain vs load (b) Strain distribution

Fig. 3-23: Test 4 beam bottom flange

The remaining strain gages on the beam recorded flange strain measurements were outside of the connection region. In each test, these instruments recorded only linear elastic behavior until the peak load was reached. This feature indicates that at the peak load, the beam section itself had likely reached its capacity.

3.6.4. Demands on channels

The channels used to restrain the angles proved the importance of a lateral restraint device on the angles. The loads applied on the channels were eccentric and created bending in the web of the channel, as shown in Fig. 3-24. The channels restraining the angles in compression experienced the highest strains. The maximum axial strain that was measured was approximately 0.0004, which corresponds to a stress of 80 MPa and a lateral force of approximately 8 kN. Presence of this axial force in the channel restraints indicated that frictional resistance alone was insufficient to prevent the angles from sliding off the teeth. Thus, a restraining system was essential to prevent the slippage of the compression angles.

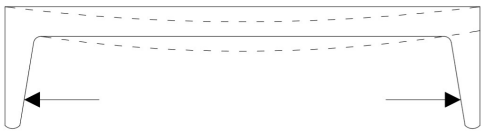

Fig. 3-24: Channel loading

3.6.5. Initial settlement

At the beginning of Test 1, and due to the gaps between different pieces, there existed an initial settlement region before the specimen could resist loads. This region became smaller as shear was applied to the connection region in Test 2, and almost disappeared as shear-to-moment ratio was larger in Tests 3 and 4. So, it seems that the existence of shear load helps with closing up the gaps faster in the specimen, and placement of the connection near the supports appears to have helped alleviate this effect. The connection location is also important since deflection is a function of the beam rotation. A closer connection to the support in Tests 3 and 4, left a shorter end beam in the specimen, which led to a smaller deflection in the connection location.

These observations are important because the intermeshed connection is intended to be used near the ends of the beams in steel frames, similar to what was tested in Tests 2 and 3. Furthermore, when used in a frame, the connection would receive additional restraint offered by the connection to the column. It is likely that such restraint would further reduce the initial settlement of the connection.

3.7. Conclusions

Four simply supported beams featuring the intermeshed connections were fabricated using plasma and waterjet cutting, and tested for different gravity load scenarios.

Forces, strains and displacements were measured in each test, and data analysis was performed to verify the procedure that was developed to design the connection. The intermeshed steel connection was shown to be a robust and ductile component that could transfer bending moment and shear forces. Side angles resisted most, but not all, of the bending moment force, and they are also subject to some shear forces. Shear plates resisted most, but not all, of the shear force in the connection, and they contributed to bending moment resistance, thus increasing the total bending moment capacity of the connection. In conclusion, the angles served to transfer loads across the joint between beam sections, and eventually became the sacrificial component of the connection once the beam capacity was reached. The geometry of the teeth in the beam flanges and the sockets in the angles, supplemented with the stress-reducing radii at the corners, performed as intended and no undesirable local failures occurred.

In all four tests, the intermeshed connection showed higher moment capacity than the design target moment. By virtue of a larger actual yield stress and a conservative design procedure, which is patterned after the capacity design approach for seismic design, the connection developed a large moment capacity. The measured overstrength for Test 1 was 2.67, of which 2.5 was reconciled as contributions from shear plates, beam bearing, strain hardening, material overstrength, and safety factor.

Although the results from this experimental program were largely positive, modifications to the design procedure could lead to more optimal results. During all four tests, the shear plates resisted some of the bending moment forces. Their contribution could be factored into future design procedures to create a less conservative connection.

4

Advanced Manufacturing for the Assembly of Structural Steel[1]

This chapter describes an investigation into the use of advanced manufacturing techniques for the creation of a new class of 'intermeshed steel connections' that rely on neither welding nor bolting. The project herein lays the groundwork to transform the steel building construction industry by advancing the underlying science and engineering precepts for intermeshed connections created from precise, volumetric cutting. The proposed system enhances the integration between design, fabrication, and installation. Fully automated, precise, volumetric cutting of open steel sections poses challenges regarding the load-transfer mechanisms and failure modes for intermeshed connections.

[1] This chapter is adopted from the following manuscript:
M.E. Shemshadian, A.E. Schultz, J.-L. Le, R. Labbane, D.F. Laefer, S. Al-Sabah, L. Truong-Hong, M.P. Huynh, P. McGetrick, T. Martin, P. Matis, AMASS: Advanced Manufacturing for the Assembly of Structural Steel, Pract. Period. Struct. Des. Constr. (in press)

Implementation of the intermeshed connection would cause a discontinuity in the beam, therefore, the effects of such configuration on the behavior of the steel frame were investigated in the current chapter. Load resistance and design of these connections were also explored with physical tests and finite element modeling to investigate the mechanics of intermeshed connections including stress and strain concentrations, fracture potential and failure modes, and connection geometry optimization.

4.1. Introduction

Despite field welding and bolting being time-consuming and/or expensive, the steel building market has not adopted a new, universally applicable, structural steel connection system since before World War II. To improve construction efficiency and heightened material reuse, computer controlled, advanced manufacturing techniques in high-definition plasma, laser and waterjet cutting could be exploited [17]. This chapter envisions the harnessing of those technologies to create an entirely new class of "intermeshed" steel connections.

Precise steel cutting can create notches in beam flanges and webs that can intermesh with other beam parts or external connectors, like puzzle pieces. This type of approach could radically change how structural steel is fabricated, assembled, deconstructed, and reused [8]. Without relying solely on bolting or welding to assemble a connection in the field, the simplicity and efficiency of the construction process may be significantly improved. To date, this class of advanced manufacturing equipment has only been used to accelerate traditional processes for cutting sheet metal or other conventional fabrication

activities (e.g. cutting instead of drilling holes). Such approaches have not capitalized on the equipment's full potential.

Because on-site assembly and inspections costs are high for welded and bolted connections, intermeshed connections offer the potential for lower erection costs, even though manufacturing costs are likely to be higher. There is also the potential for life-cycle savings, as deconstruction costs would be significantly lower, as an intermeshed connection can be designed specifically for disassembly and reuse. However, unlike traditional bolted or welded connections, where the industry has more than 100 years of experience, precise cutting of steel for an intermeshed connection is not yet part of the culture or expectations. While maintaining the same concept, different details can be proposed for the intermeshed connection. In this chapter, two variations of the intermeshed connection are presented and studied.

4.2. Automation in Steel Construction

Construction is one of the largest sectors in the world economy and approximately 7% of the world working population is employed in construction-related services. However, the industry's productivity has been largely stagnant for decades, unlike many other industries. For example, since 1945 America's overall productivity has grown 400%, without any contribution from the construction sector (Fig. 4-1) [45]. Arguably, one reason for underperformance is the extensive regulation of the construction industry. Another reason is that common construction techniques have not been updated in years. The McKinsey Global Institute further states that steel construction as a subcategory of the

construction sector has also suffered from restrictive design specifications, underinvestment in skill development, and insufficient innovation. Consequently, alternatives for steel connections have failed to gain traction in the construction sector during the past 50 years.

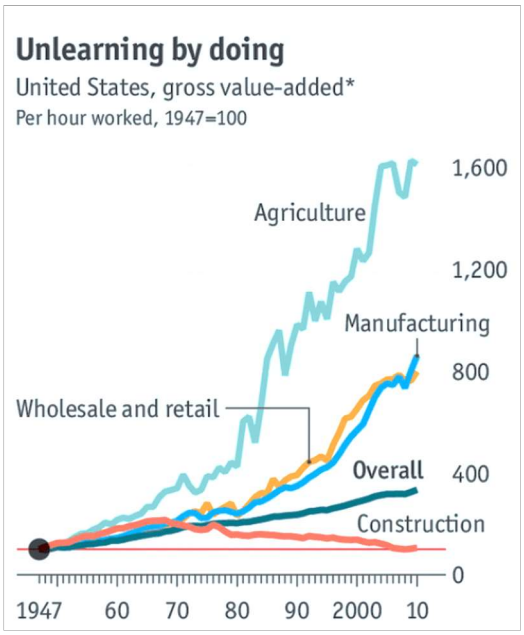

Fig. 4-1: Productivity of different sectors in United States [45]

Developing new construction methodologies such as prefabricated, volumetric construction and digital technologies supported by robotics can further facilitate off-site fabrication [1,2]. Specifically, in the steel construction industry, 'advanced manufacturing techniques' such as plasma cutting and waterjet cutting could be utilized. These fully automated cutting techniques could enhance the fabrication process and consequently increase construction productivity.

Traditionally, steel plates are cut using saws or oxy-fuel for structural purposes. These techniques are mainly applied manually, which results in highly variable speed and accuracy. The new computer-controlled cutting techniques would help improve the

precision of fabrication, and by combining them with robotic arms, faster and more flexible operation would ensue. Although a variety of options are available based on project needs, this research focuses on the implementation of plasma and waterjet cutting in steel fabrication.

High definition plasma cutting is a thermal process achieved through a concentrated high-speed plasma stream [46]. The plasma stream is extremely hot at up to 30,000 K and cuts through material by melting it [47]. The plasma cutter may be attached to a robotic arm with multiple degrees of freedom, thereby giving it unlimited possibilities regarding the position and configuration of the cut surfaces. Waterjet cutting can also be used to precisely cut various materials, including structural steel. High pressure waterjets with abrasive additives are used to cut material by eroding the surface [46]. Waterjet cutting may be a more desirable alternative to plasma cutting due to its lower energy demands and absence of negative thermal effects on the cut material [48]. Moreover, waterjet provides more precise cuts in a wider range of plate thickness. As an emerging technology with certain advantages over other cutting methods, use of waterjet cutting may become more widespread in the future. This technique relies on 'erosion' cutting, which avoids the formation of 'heat affected zone' and keeps the material properties uniformly distributed. Although these advantages make waterjet an attractive cutting technique to use, it is more costly than plasma cutting. Furthermore, it is difficult to integrate waterjet technology into a typical steel fabrication production line [49].

High-definition plasma and waterjet cutting afford the opportunity to create alternative steel connections that rely on intermeshed (i.e. interlocked) components, instead of regular welding or bolting. Intermeshed connections, transfer force through direct

contact bearing of multiple, precisely shaped surfaces of the interlocking elements. However, due to the absence of welds or bolts in the connection detail, intermeshed connections are unlikely to behave as fully rigid connections. Therefore, in the next section, the effects of implementing such connections is evaluated by investigating the response of steel frames equipped with intermeshed connections. Subsequently, two details for the intermeshed connection are suggested and examined in the following sections. Load resistance and design of these connections were also explored with physical tests and finite element modeling.

4.3. Moment Frames with Intermeshed Connection

Structural connections are frequently assumed as being ideally pinned or fixed in numerical modeling. However, neither assumption is likely to represent the behavior of intermeshed connections accurately. In reality, the connection stiffness is expected to be somewhere between the two extremes due to the cuts in section which cause load path discontinuities. Thus, a spring with an assigned stiffness is more representative of this class of connection and helps achieve reasonable accuracy in the frame responses. However, the inclusion of the connection stiffness in analysis may affect the distribution of internal forces and deformations in a frame and, thus, needs further investigation.

Members and connections in gravity framing are typically designed to resist vertical loads. However, most building structures are subjected to lateral loads with wind and seismic forces being the most common. Even though lateral load resisting systems such as structural cores and braced frames are often used to resist these loads, the gravity frames

must undergo the associated lateral displacements with little or no loss in vertical load capacity. This ability can be quantified by determining the changes in internal forces (moment, shear, and axial forces) that occur under the imposed lateral drifts. Large increases in these internal forces would be indicative of a gravity frame at risk.

To determine the influence of connection rigidity on frame response, a series of linear analyses was conducted on variety of frames with different connection properties. The goal herein was to understand the influence of connection rigidity on frame overall stiffness, as well as stress distribution in different frame members. Creation of such information will enable the formulation of practical recommendations for the 'optimal locations' and 'suitable stiffness range' for intermeshed connections. To investigate the impact of lateral displacements on vertical load capacity for an intermeshed connection, a two-dimensional (2D) pushover analysis was conducted with the commercial software SAP2000. In that, the axial (K_1), shear (K_2), and rotational (K_3) stiffnesses of the intermeshed connection were idealized as elastic springs in linear elastic models of prototype steel frames, and the models were analyzed under various load schemes. First, gravity (dead and live) loads were applied. Then the frames were pushed to 2% of their height to simulate the maximum expected drift from lateral loading. A range of 2D frames with different geometries for 3-story and 9-story frames, with span-to-height ratio of two and three, were considered.

Changes in internal forces are affected by the location and stiffness of the spring. Therefore, to find the optimal location of the connection, the position of the connections (a) in the span length (L) was changed from 0.0 to 0.25 of L gradually (i.e., a/L= 0, 0.05, 0.1, 0.15, 0.2, and 0.25). Since the detail of the connection had not been defined at this

stage, the translational and rotational stiffness coefficients of the connection were unknown. Therefore, a wide range of spring stiffnesses were assumed: 20, 10, 5, 1, 0.5, 0.2, and 0.1 times of the beam stiffness, which were defined for axial stiffness (EA/L), shear stiffness (GA/L), and flexural stiffness (EI/L). Each were calculated using geometric properties of the beam section (A and I), beam length (L), and elastic material properties of the structural steel (E and G). In each case, the spring stiffnesses had a constant value, so, more than 300 frames were modeled and analyzed to fully cover the range of selected variables in frames.

Rotational stiffness of the connection, K_3, was found to affect strongly the frame's lateral stiffness (Fig. 4-2) and beam deflection, especially when the connections were located near the beam ends, whereas frame response was found to be relatively insensitive to changes in the axial (K_1) and shear (K_2) stiffness . According to AISC recommendations [33], the minimum value for rotational stiffness of a connection to be categorized as fully rigid is 20 ($K_3 \geq 20EI/L$). Fig. 4-2 also shows that beyond that stiffness limit, increasing rotational stiffness produces no appreciable change in fundamental period, regardless of the connection location. Considering $K_3 \geq 20EI/L$ (i.e. a fully rigid frame) to be the benchmark case, a comparison was performed to capture the reduction effect in the connection's rotational stiffness on the fundamental period of the frame. Fig. 4-2 shows changes in the frame fundamental period based on changes in the ratio of connection rotational stiffness to beam flexural stiffness ($K_3 / (EI/L)$). This demonstrates that while a reduction of this ratio below 20 increases the fundamental period of the frame, the increases are limited to a range of 10% to 20%, even when the ratio drops to 10 and 5 respectively. This is a promising discovery, since connection rotational stiffness values of $5EI/L$ to

10EI/L in the intermeshed connection may be possible without requiring large elements or complicated geometry.

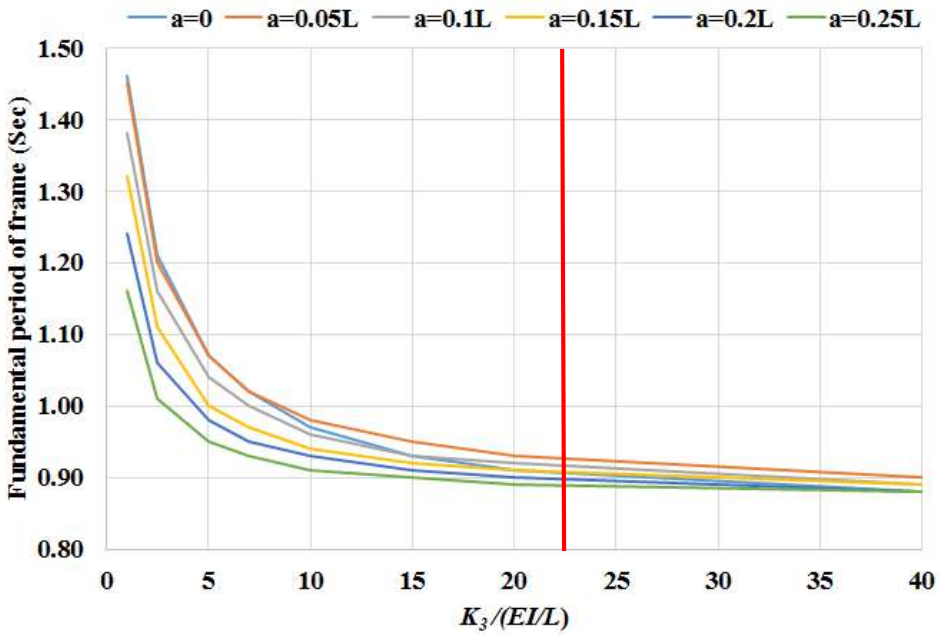

Fig. 4-2: Effects of connection rotational stiffness (K_3) and connection location (a) on fundamental period of the frame

As noted, the benchmark cases are frames in which (1) all the connections are fully rigid and located at the beam ends and (2) all the beams and columns are continuous. Variant frame cases consist of new connection locations and/or new connection rotational stiffness values using the same beams and columns section sizes. In the next stage of frame analysis, the maximum *P-M* (axial load combined with moment) stress ratio in each frame was calculated based on the following equation:

$$\text{Stress ratio} = \frac{P_r}{P_a} + \frac{M_r}{M_a}$$

where P_r and M_r are required axial and flexural strength, and P_a and M_a are the available axial and flexural strength, respectively.

Fig. 4-3 shows that the optimum stress ratio existed at a smaller stiffness ratio, when the connection was located closer to the beam ends. Therefore, it is easier to control the stress ratios of the beam, when the connection is located closer to the beam ends. The optimal location of the connection was defined at *0.1L* from the beam ends. Having the connection at this location led to smaller beam stress ratios for a wider range of stiffness ratio, which is a result of a more uniform moment distribution in the beam length. Another words, in this case, the maximum positive and negative moments were approximately equal in the beam span. Table 4-1 shows the frame responses when the intermeshed connection was placed at *0.1L* from the span ends. Selecting a connection rotational stiffness of *5EI/L* or *10EI/L* (or any value in between), resulted in reduction in the frame *P-M* stress ratios, while the fundamental period underwent a slight increase, which means that the frame's lateral stiffness does not drop significantly.

Table 4-1: Change of the frame responses when *a=0.1L*

K_3	*2EI/L*	*5EI/L*	*10EI/L*
Reduction in *P-M* stress ratios	25%	23%	16%
Increase in fundamental period of frame	35%	16%	7%

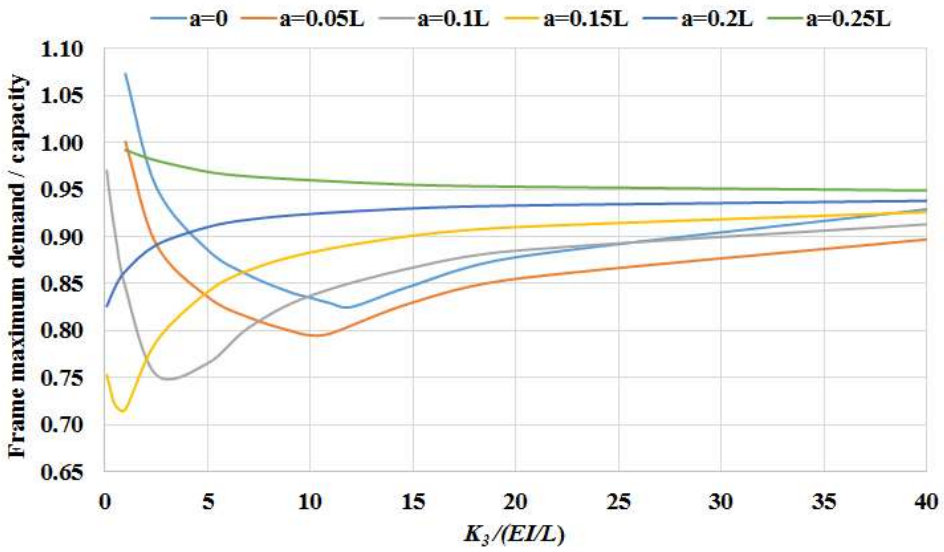

Fig. 4-3: Effects of connection rotational stiffness (K_3) and connection location (a) on beam stress ratio

4.4. Front-Intermeshed Connection

Two possible intermeshed connection designs were investigated. The first was a relatively simple connection named the "Front-Intermeshed Connection" [21]. This connection was composed of a three-dimensional (3D) interlocking through the top and bottom flanges and through the web. The flanges were designed to carry the tension and compression resulting from the bending moment at the connection, while the web was designed to carry the shear force. The connection was intended to transfer shear and compression from one beam section to the next through direct contact bearing of multiple, precisely shaped faces (Fig. 4-4a). The arrangement was envisioned for connecting beams at (or near) ideal inflections points to create gravity load framings. For practical use of this new type of connection, an understanding its mechanical behavior, especially in terms of the load carrying capacity under mixed mode loading scenarios is essential.

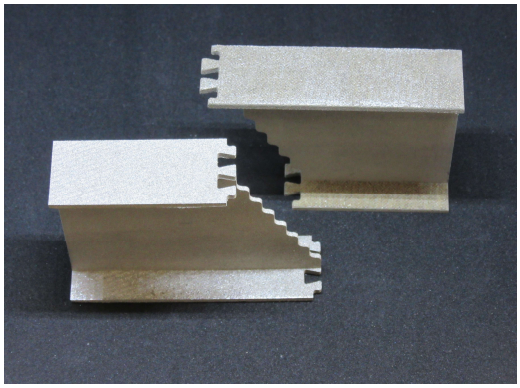

(a) Idealized connection in printed stainless steel

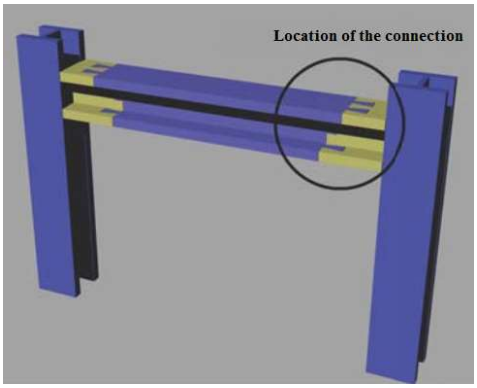

(b) Assembly of the connection in a frame

Fig. 4-4: Front-intermeshed connection

Load is transferred between flanges through bearing and friction via the intermeshed dovetails of the flanges. The connection has the advantage of simplicity and requires no additional parts to create the flange connection, although a locking mechanism can be added to provide resistance against uplift. However, field-assembled locking connections are unlikely to be able to fully transmit the flexural, axial, and shear capacities of the connected steel sections and may reduce the corresponding stiffness components of a continuous steel member, due to interruptions in the load path.

The stepped web connection was designed to promote easy site assembly, as the middle beam part can be dropped from above, similar to current practice for bolted connections. In Fig. 4-4b, the ends (shown in yellow) are shop welded as stubs to the column. No other welding is required, and bolting is fully avoided in this configuration.

To understand better how this type of precise interlocking performs structurally, initial laboratory testing was conducted for the 2D meshed “dovetails” [50]. Based on the success of those initial tests, a 3D numerical model was created in Abaqus [27]. Finite element analyses were performed under different load combinations to investigate the

general behavior, failure modes, and peak capacity of the connection. Under flexure, the connection showed a uniformly monotonic behavior with a relatively low flexural resistance. Failure occurred when the dovetails on one side of the top flange slipped out of the sockets on the other side (Fig. 4-5a), so there was no capacity to carry the tension force, which means that moment capacity cannot be developed. Moreover, in the case of combined tension and shear, the presence of the shear force causes relative vertical movement between the two sides of the connection and, consequently, the flanges may slip out of their intermeshed positions. If this phenomenon happens (Fig. 4-5b), there is no component to resist tension, and the connection will fail.

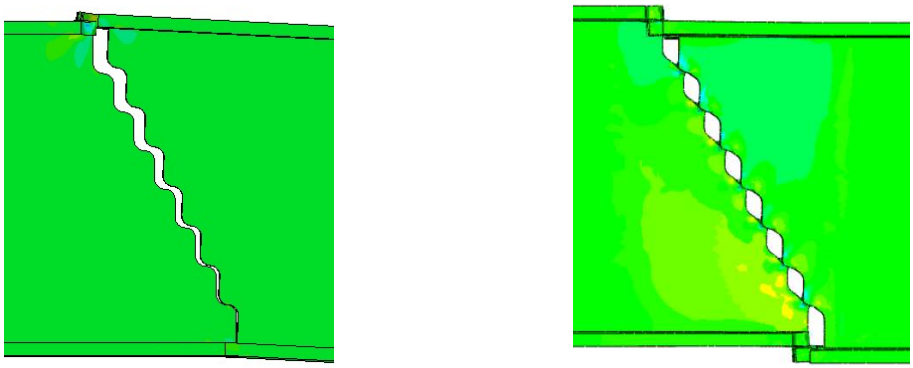

(a) In pure flexure, top flange slips out

(b) In combined tension and shear, top and bottom flanges slip out

Fig. 4-5: Performance of the front-intermeshed connection under different load conditions

The finite element analyses indicate that the front-intermeshed connection would not be able to generate sufficient strength, stiffness and ductility for effective use in practice under many cases. Based on current code standards, the connection is classified as non-ductile and partially restrained [33,35]. This classification is due to the cuts in the flanges, which reduce load carrying capacity in tension and, consequently, significantly limit the moment capacity. Therefore, the front-intermeshed connection is not recommended for use

where demands for 1) large moments, 2) large moments in combination with large shears, or 3) axial tension is possible. A further drawback to this type of connection are the tightness of the tolerances and the lack of adjustability in the erection process.

4.5. Side-Intermeshed Connection

Given the limitations of the front-intermeshed connection in transferring loads, especially when combined loads are present, and the requirement for strict tolerances, another intermeshed connection is proposed in the form of the "Side-Intermeshed Connection" [23], which employs intermeshed external connectors to transfer flanges tension and compression forces.

Two versions of side-intermeshed connection were developed. The 'initial conception' (Fig. 4-6) sought to meet the original goals of requiring no welding nor bolting, while maximizing erection speed and construction tolerance. A modified version (Fig. 4-7) was also developed for greater acceptance in the construction industry. The remainder of the chapter focuses on the modified side-intermeshed connection.

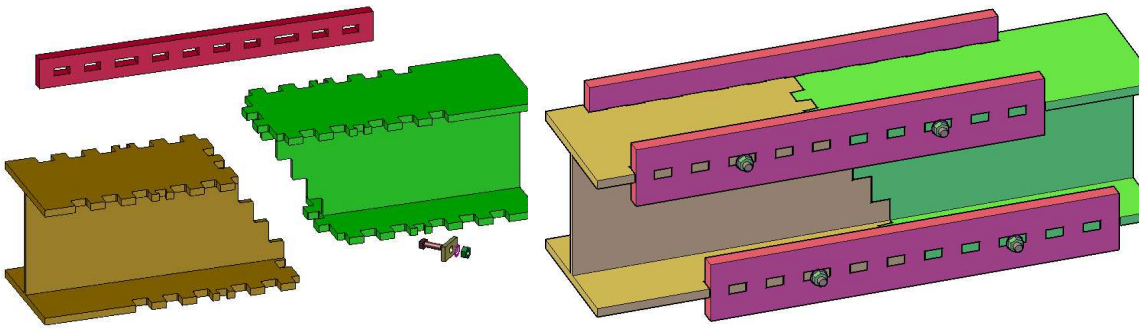

(a) 3D Exploded view (b) 3D View of assembled connection

Fig. 4-6: Side-intermeshed connection (initial conception)

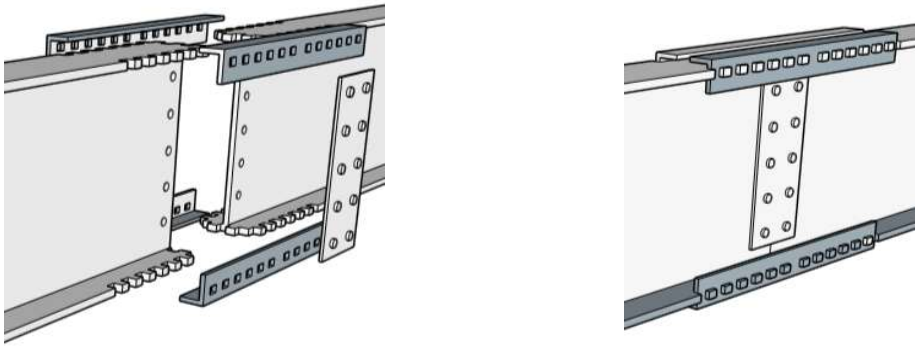

(a) 3D Exploded view (b) 3D View of assembled connection

Fig. 4-7: Side-intermeshed connection (modified version)

In this connection, flange edges are cut to create a set of tooth-shape notches (i.e. 'teeth'). To connect different sides of the beam, an angle is used on each edge with rectangular holes (sockets), which match the teeth (see Fig. 4-7). Having the beam flanges connected, the section was designed to transfer moments via connector angles. However, for shear transfer, a pair of shear plates were bolted to the beam webs.

The side-intermeshed connection was devised to allow larger fabrication tolerances and easier erection, for a better potential for wider acceptance in practice. An early concern was addressed related to possible stress concentrations at the sharp corners of the angle sockets. Depending on the length-to-width ratio of the angle sockets, previous studies have shown that the stress concentration factor can be up to five [40], which can result in a premature rupture. To avoid any undesirable failure modes, circular holes were added to the sharp corners in the angle sockets. A finite element model proved the effectiveness of such a change by reducing the stress concentration factor to 1.7. Fig. 4-8 shows the configuration of the socket and the resulting stresses.

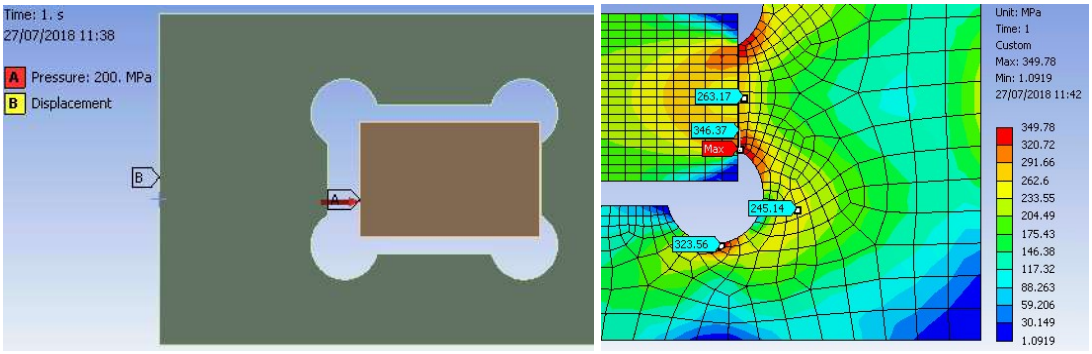

(a) Load and boundary conditions (b) Equivalent stress around the corner

Fig. 4-8: Finite element analysis on the effect of the shape on the stress concentration around the socket

4.5.1. Design procedure and analysis method

A procedure was developed for analyzing and designing the modified side-intermeshed connection (Fig. 4-7) using fundamentals of structural mechanics. The design procedure was based upon the requirements of the current American steel design standards [33,41,44] to ensure the practicality and sufficiency of the connection.

In traditional structural design, the connection would be proportioned after the appropriate beam sections had been selected to resist a given combination of loads. Thus, some properties such as the beam section size and beam material properties were assumed here, prior to the connection design. This means that the thickness of the teeth was equal to the beam flange thickness and would not be adjusted when the connection was being designed. Other geometric parameters, such as the length of a single tooth, the number of teeth, and the size of the angles were dependent upon one another and had to be chosen iteratively during moment design of the connection.

Another basic assumption in this design procedure was that the connection would transfer the moment and shear loads separately; meaning the angles would take all the load

due to moment, and the plates would take all the load due to shear. Therefore, the design procedure of the side-intermeshed connection combines two different procedures: 'shear design' and 'moment design'. The shear design follows a conventional shear tab design according to the AISC recommendations [33] which results in the selection of suitable shear plates and bolts. The moment design, however, requires several steps, and multiple iterations are likely to be required due to the more complex load transfer mechanism of the intermeshed segments. The moment design process will be discussed in detail in the following paragraphs.

As mentioned previously, these connections are not recommended for placement near the location where maximum moment will be experienced. Therefore, the full plastic capacity of the beam section is not required to be developed by the connection, and a fraction of this capacity becomes a design choice. In this research, one-third the plastic moment capacity of the beam was selected as the design moment (M_d). As previously stated, a basic assumption is that the angles take all the moment without any contribution from other connection elements. This means that the design moment, M_d, transfers through the angles in form of a force couple, i.e. compression in the top angles, P_d, and tension in the bottom angles, T_d (assuming positive bending moment). Assuming that all four angles are identical, each top angle takes an axial force of $P_d/2$, and each bottom angle takes $T_d/2$. Then, the angles are proportioned at these demand levels for 'yielding at the gross section' as well as 'rupture at the net area' based upon the AISC recommendations [33].

The radius for the circular cuts (R) at the socket corners were chosen so that an adequate amount of stress could be relieved, without significantly reducing the angle's cross section. Socket dimensions in the angles are a function of the teeth size, plus the

considered tolerances, g_1 and g_2, on top/bottom and left/right side of the teeth, respectively, as shown in Fig. 4-9a. Importantly, the horizontal dimension of the teeth was considered as an unknown quantity as opposed to the vertical dimension which equaled the beam flange. Consequently, an initial value had to be assumed. This value was later adjusted during the tooth strength design (as described subsequently). The adjusted value would change the socket size and, consequently, affect the angle design. Thus, this design procedure needed several iterations until the sizes converged.

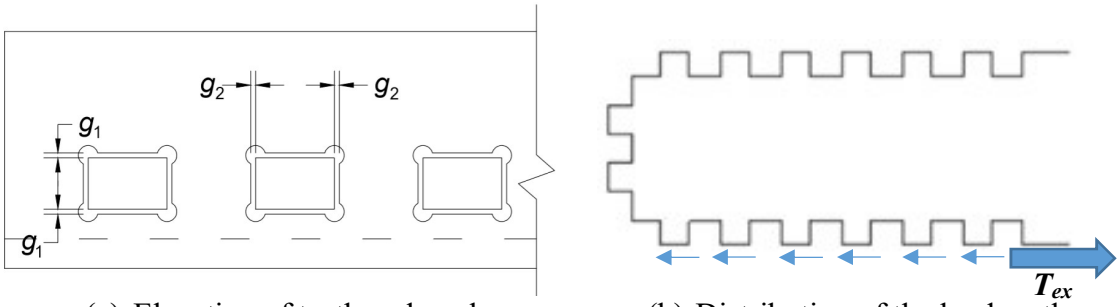

(a) Elevation of teeth and angle (b) Distribution of the load on the tension angle

Fig. 4-9: Detail of geometry and load path in the connection

In this design step, the teeth were sized for the maximum expected forces based on the connector angle capacity, which is symbolized as T_{ex} for the tension angle and P_{ex} for the compression angle. This concept, known as 'Capacity Design', assures that the failure in the angles occurs before the teeth failure. Such a mechanism is desirable, since the replacement of the angles is easier and faster following any case of damage-inducing overloading. Assuming all the teeth had an equal contribution in transferring the angle load, each tooth had to bear T_{ex}/n (or P_{ex}/n), where n was the number of the teeth on one side of the connection (see Fig. 4-9b). Therefore, each tooth needed to resist the combined shear and moment stresses caused by the external load.

Once all geometries and material properties were established, the capacity of the connection could be checked against the demand. The size of the connection components could then be increased or decreased to produce an adequate and optimally efficient configuration. Several iterations may be necessary to develop an arrangement that is appropriate for a given moment. The flowchart shown in Fig. 4-10 helps understand the step-by-step process of the moment design for the side-intermeshed connection.

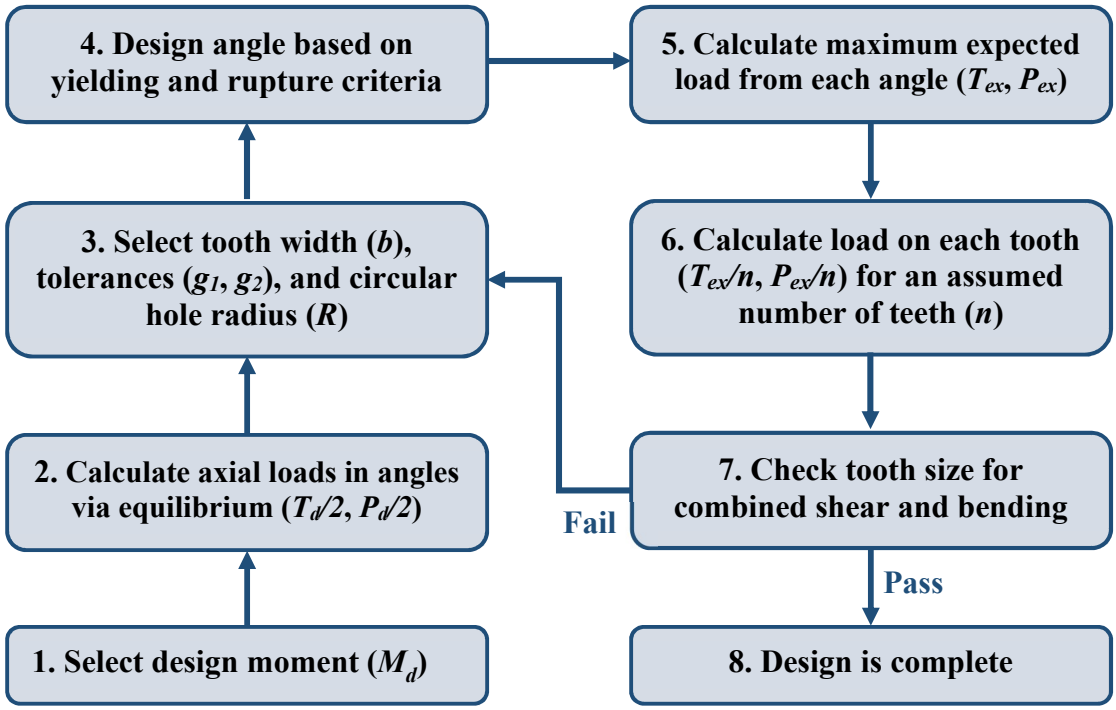

Fig. 4-10: Moment design of side-intermeshed connection

4.5.2. Fabrication process and challenges

An experimental program at the University of Minnesota was aimed at investigating the performance of the side intermeshed connection under different load conditions. For this purpose, two beam sizes, W18x46 and W21x57, were selected from commonly used members based upon engineering judgment. Side intermeshed connections were designed

for these beams according to the procedure described in the previous section, which resulted in angle sizes L2½×2×3/8 and L3×2×3/8 respectively.

A tolerance of 1.6 mm was specified for all the connection components, except for the circular holes in the angle sockets, which needed a more precise tolerance of 0.8 mm. Additionally, the cutting equipment had to be able to penetrate the thickest steel element (16.5 mm for the beams and 9.5 mm for the angles), while maintaining the required precision level.

High-definition plasma and waterjet cutting were selected for manufacturing different parts of the connection, since both techniques are capable of cutting structural steel with high precision. Plasma cutting, which works based on a 'melt and blow' mechanism, can be used to cut metal plates to a maximum thickness of 60 mm with a 0.25-0.4 mm precision. However, the process is relatively slow. Waterjet cutting, on the other hand, is a very fast technique that provides an smooth cut finish with high precision (0.05-0.2 mm) for pieces of up 75 mm in thickness [39,51].

Local and regional fabricators were contacted to investigate the feasibility of fabricating the beams, angles, and shear plates for the side-intermeshed connection. Plasma cutting was selected for the fabrication of the beams and shear plates. The manufacturer used a Python X Robotic CNC (Computer Numerical Control) Plasma Cutting System for their fabrication. The plasma cutting of one of the beam specimens is shown in Fig. 4-11a. Although plasma cutting could achieve the precision of 1.6 mm required for the beams, it could not guarantee the 0.8-mm precision in the angles sockets. Therefore, waterjet cutting was selected to fabricate the angles. The manufacturer used an OMAX A-Jet waterjet cutting machine to cut the angles and successfully achieved the specified precision. The

waterjet cutting had the added advantage of preventing heat affected zones to build around the sockets, which was a concern due to the large plasticity expected to occur in the angles. Fig. 4-11b shows waterjet cutting of one of the angles.

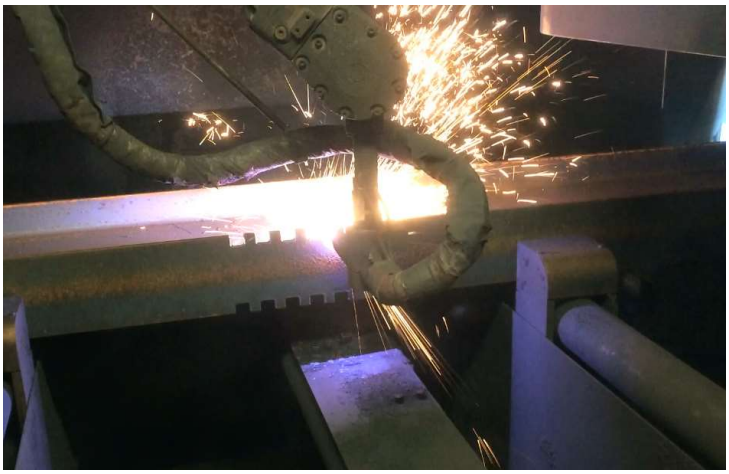

(a) Plasma cutting performed by an industrial robot

(b) Waterjet CNC cutting machine

Fig. 4-11: Connection fabrication through advanced cutting techniques

The required capability to manufacture the specimens was found at steel fabrication shops near the University of Minnesota and was achievable without significant changes to existing fabrication procedures. The specimens were measured with calipers at the University of Minnesota to check fabrication accuracy. On the beams, every single tooth was measured, and the maximum deviation was found to be 1.4 mm, which was within the specified tolerance value of 1.6 mm. Every socket on every angle was also measured. The maximum deviation in both the width and the height of each socket was found to be 0.4 mm, which was well within the allowable tolerance value of 0.8 mm. The measurements verified that both plasma cutting and waterjet cutting were acceptable for the precision required for the side-intermeshed connection.

4.5.3. Structural performance - experimental study

Four full-scale beam specimens with the side intermeshed connection were designed using the procedure in Section 4.5.1, and fabricated as described above. An experimental testing program was conducted with these specimens to study the behavior of intermeshed connections under gravity loads. The validity of the proposed design procedure also needed to be verified with experimental testing in order to gain acceptance for adoption by design and construction codes.

Four major-axis beam tests were tested. Two different locations for the intermeshed connection were investigated to study the positional effect on the specimen's global behavior. In Tests 1 and 2, the connection was in the middle of the beam, while in Tests 3 and 4, the connection was located at the beam end (Fig. 4-12). In Test 1, the connection was placed in the pure moment region, whereas in the other three tests, the connection was subjected to a combination of bending moment and shear forces with different ratios (see Table 4-2). Structural steel used for the beam and angles were Grade 50 and Grade 36, respectively, as specified by the American Society for Testing and Materials (ASTM) [30,52]. The specimens were quickly and easily assembled for each test and required no special skills.

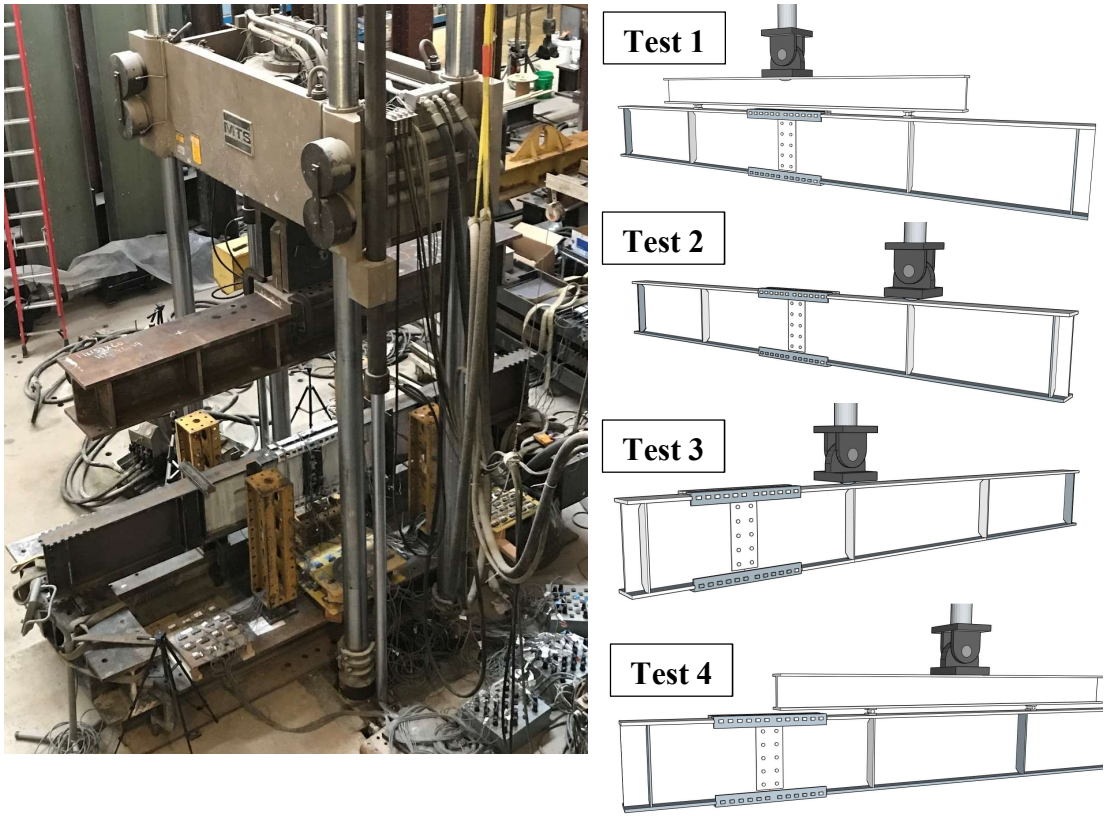

(a) Loading jack and specimen in the laboratory

(b) Loading conditions of Test 1 to Test 4

Fig. 4-12: Test setup

Table 4-2: Description of test specimens

Test #	Loading condition			Specimen sizes*	
	Loads at connection	Point Loads	Moment to shear ratio (m)	Beams	Angles
1	Pure bending	2	N.A.	W18×46	L2½×2×3/8
2	Bending plus shear	1	1.84	W18×46	L2½×2×3/8
3	Bending plus shear	1	0.61	W21×57	L3×2×3/8
4	Bending plus shear	2	0.61	W21×57	L3×2×3/8

* US designations for hot rolled steel shapes

Fig. 4-13 shows the results of all four tests in terms of load-displacement curves, where load was recorded in the loading jack and the vertical displacement was recorded at the connection location. In all cases, the specimens exhibited ample load carrying capacity and ductility. Table 4-3 summarizes some of the experimental results in terms of

performance criteria such as deformability, capacity, and stiffness. In this table, the deformability is defined as the ratio of the displacement at the peak load (Δ_P) over the displacement at which the specimen starts yielding (Δ_y). Results show a displacement ratio range of 2.7 to 3.9, which shows the ability of the specimens to undergo significant plastic deformation before reducing peak load. While demonstrating excellent deformability, the specimens exhibited ample load resistance, as the generated loads in the specimens were as high as 0.79 to 1.02 of M_p, the plastic moment capacity of the beam sections. This confirms that load could be transferred in the intermeshed steel connection via direct contact of different parts and without using welding or major bolting. Thus, beams with intermeshed steel connections were shown to be able to resist the gravity loads expected in typical moment frames.

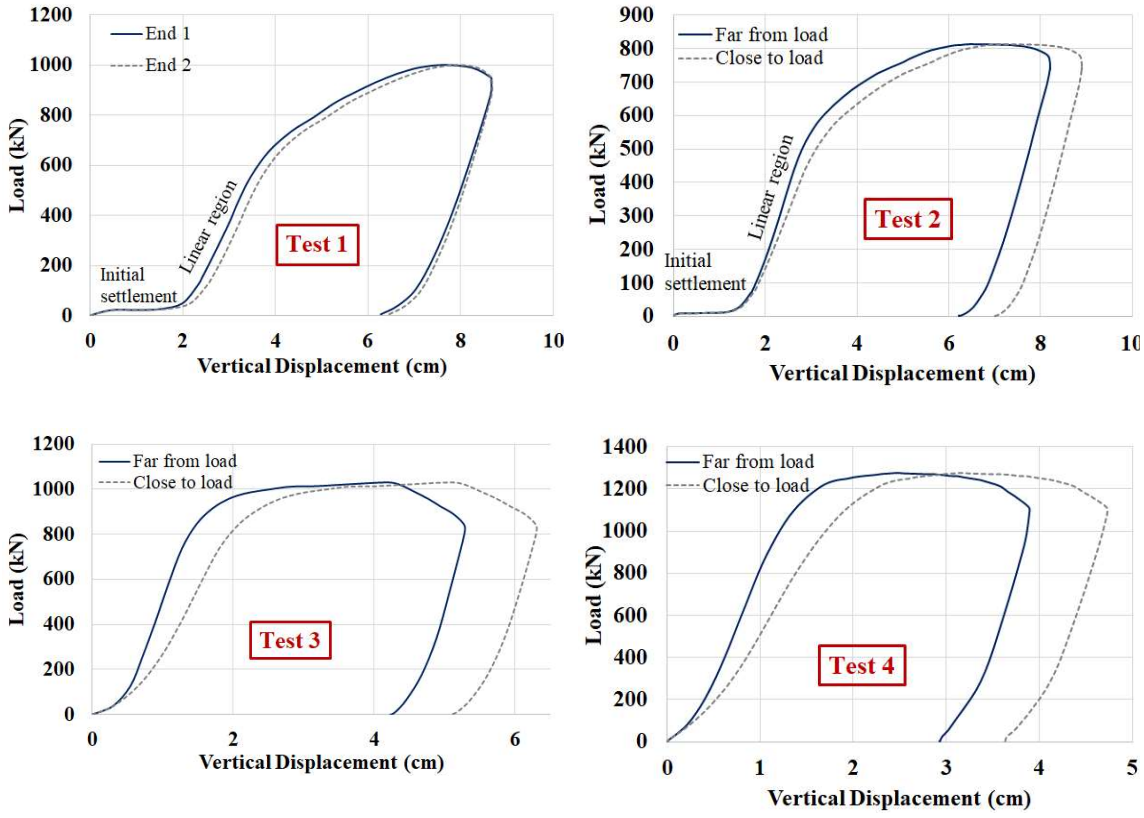

Fig. 4-13: Load at jack versus vertical displacement at connection ends for Test 1 to Test 4

Table 4-3 indicates that the vertical stiffness of the specimens (K_s) was only a fraction of the values calculated for the corresponding beam without the connection (K_b). In other words, installation of the intermeshed connection in a continuous steel beam causes a reduction in the elastic stiffness of the beam, which could be as large as 47% to 55%. This is due to the discontinuity at the connection region. Although closing the specimen gaps in the loading process helps with stiffness formation, not all gaps will close completely and some contacts are likely not to be fully established because of manufacturing tolerances. As a result, the intermeshed connection can only attain a fraction of the ultimate beam stiffness of a continuous member. This stiffness loss might raise some concerns for the application of the intermeshed system in steel moment frames. However, results shown in Section 4.3 demonstrate that when the intermeshed connection is located away from the beam ends, the reduction in connection stiffness has no major effect on the stress or deflection responses of the frame.

Table 4-3: Summary of the test results

Test #	Deformability* (Δ_P / Δ_y)	Load Capacity (M_{max} / M_p)	Initial Stiffness* (K_s / K_b)
1	3.8	0.79	0.50
2	3.9	0.96	0.53
3	3.3	1.02	0.45
4	2.7	0.95	0.48

* Not including the 'initial settlement' region of Tests 1 and 2

In all four tests, the specimen started to exhibit out-of-plane movement after reaching peak load, and eventually failed due to lateral-torsional buckling. This occurred in later stages of loading, when the specimens experienced high plasticity, which caused a significant reduction in material stiffness and subsequently in sectional and member stiffness. Fig. 4-14 shows the specimens after the test was completed. As illustrated, the

out-of-plane failure mode was a product of pure lateral buckling in Test 2 and Test 4 and a combination of lateral and torsional buckling in Test 1 and Test 3. In all cases, the out-of-plane deflection occurred somewhere between the lateral braces and caused the specimen to lose some of its load bearing ability. Thus, the bracing design was modified as the program progressed from one test to the next due to the need for additional lateral restraint. Table 4-3 shows the effectiveness of such modification, as the 'Load Capacity', as evidenced by M_{max}/M_n, of the specimens improved from Test 1 to Tests 2-4.

(a) Test 1

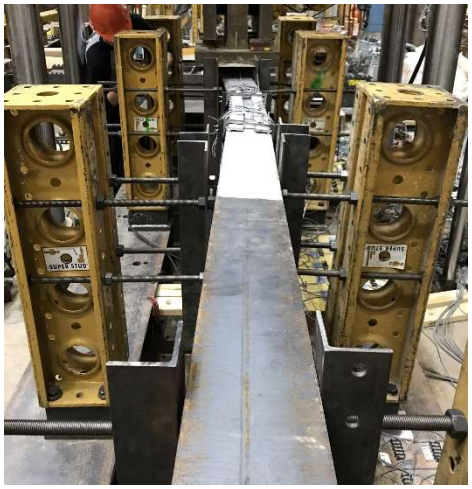

(b) Test 2

(c) Test 3

(d) Test 4

Fig. 4-14: Failure of the specimens due to lateral-torsional buckling

Fig. 4-13 shows an almost flat initial branch in the load-deflection curves of Tests 1 and 2 (labeled as 'initial settlement'). During this phase, Test 1 and 2 specimens deflected 2 cm and 1.3 cm, respectively, under small loads. Visual observations during the tests showed that in this stage of loading, the 'teeth and sockets' were moving towards each other and the 'bolts and shear plates' were slipping towards one another. In fact, the connection did not develop full stiffness the connection elements came into contact and, subsequently, engaged in the load resistance.

While the initial settlement was relatively large in first two tests, this phenomenon was minimal in Tests 3 and 4, and those specimens began gaining load almost immediately (see Fig. 4-13). A major reason for the difference was the location of the connection. In Test 3 and 4, the intermeshed connection was placed near the end of the specimen resulting in the formation of a shorter lever arm. In these specimens, gaps closed faster since the horizontal movement is a function of the lever arm length.

As illustrated in Fig. 4-4b, the intermeshed connection was designed with the intention of it being placed at the ends of a steel beam in a moment frame. Therefore, the initial settlement is not much of a practical concern, as it would be small in that configuration. Additionally, there are practical ways to control the deflections, if needed, including the introduction of some camber to eliminate deflections from floor deck weight. Tighter tolerances could also be used in the connection region, as the assembly process definitely showed some leeway in fitting all the connection parts together.

4.6. Conclusions

This study analyzed a radically new connection for structural steel members, which uses multi-degree of freedom, volumetric cutting to reduce fabrication labor and vastly simplify and speed erection. These fully automated cutting techniques could enhance the fabrication process and, consequently, increase the productivity of construction. Based on this concept, two different intermeshed connections were investigated via finite element modeling in Abaqus and large-scale, physical testing.

Results showed that the front-intermeshed connection exhibited excellent shear resistance but axial and flexural behavior were affected by the alignment of the intermeshed flanges. Based on the flexural characteristics of the connection, the front-intermeshed connection showed low stiffness and resistance rendering it a simple connection. For these reasons, this version of the intermeshed connection was not pursued further in this study.

In keeping with the intermeshed connection concept, another alternative was proposed that offered larger load capacity potential and larger erection tolerances. The resulting side-intermeshed connection was designed, fabricated, and tested in the laboratory. Python X Robotic CNC plasma and OMAX A-Jet waterjet cutting machines successfully met the designed precision of the connection. These techniques, which were easily accessible in local fabrication firms, made the manufacturing process fast and easy. The experimental results on four large-scale samples demonstrated high load carrying capacity, as well as ample ductility and stiffness. This showed the effectiveness of the adopted ‘design procedure’ in proportioning the connection elements, which led to some desired failure modes in the specimens. All four specimens failed due to lateral-torsional

buckling, even though the lateral restraining system was improved progressively from Test 1 to Test 4. However, in practice, the lateral-torsional buckling of this system would be of much less concern, since the top flanges are usually restrained by the floor deck.

5

Structural Mechanics Characterization of Steel Intermeshed Connection Using Nonlinear Finite Element Analysis

The aim of the present study is to develop insight on structural performance of a recently developed 'intermeshed' steel connection which transfers mainly loads through direct contact rather than by welds or bolts. This investigation was conducted through a step-by-step state assessment of the intermeshed connection subjected to multiple scenarios of gravity loading and by use of a nonlinear finite element platform. Implementation of the intermeshed connection would cause a discontinuity in the beam, so this chapter addresses concerns regarding the load-transfer mechanisms and failure modes for these connections. The finite element simulations were performed in Abaqus, which is capable of handling material and geometrical nonlinearity, as well as contact between individual surfaces. In order to verify the accuracy of these simulations, the numerical results were compared with

experimental data from four physical tests. Finally, some important factors of influence such as connection segments sizes, lateral constraint, support conditions, and failure modes were also explored using finite element modeling. The results of finite element analysis on different prototypes of steel intermeshed connection showed that the specimens equipped with this connection could provide sufficient ductility and resistance to meet external demands.

5.1. Introduction

In recent decades, alternatives to traditional steel connections have been proposed and investigated. Some of these innovative connections focused on ease of fabrication and erection [6,8], some prioritized sustainability and reducing construction waste through enabling the disassembly [9,10], and others had an emphasis on seismic applications [11,12]. Many of these studies remained in the research phase and could not find commercial application, while a limited number resulted in proprietary connection solutions [15]. Therefore, there is still a need for a universally applicable steel connection mechanism that could offer solutions to current shortcomings such as high waste demand of steel material and excessive labor cost.

In the recent years, and in response to the aforementioned needs in the steel industry, a new class of steel connections has been developed by the AMASS research group, referred to as the 'Intermeshed Connection' [22,53]. The intermeshed connection is essentially a gravity connection which focuses on offering easier assembly/disassembly options over existing approaches, through eliminating/minimizing the use of the traditional

connecting techniques of welding and bolting. Instead, this connection relies on precisely-cut connecting parts which 'intermesh' into each other to form a connection and operate through direct contact to transfer loads (Fig. 5-1(a)). With this configuration, the intermeshed connection could be easily assembled on site (Fig. 5-1(b)) and could be disassembled without cutting.

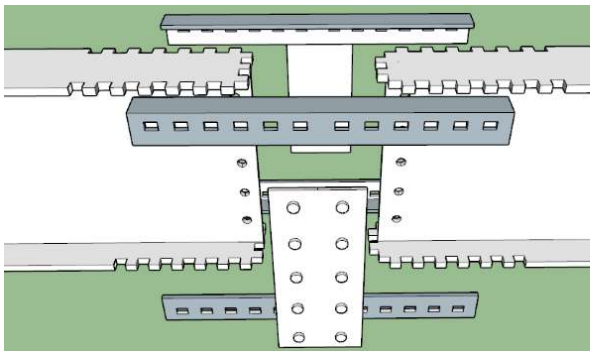

(a) Multiple pieces 'intermesh' into each other to form the connection

(b) Assembly of the connections in the laboratory

Fig. 5-1: The intermeshed connection

The main idea behind the intermeshed connection is to exploit the potential in the recent advances of the cutting techniques and harness them to create a platform for speedy production of steel connections. To date, plasma, laser, and waterjet cutting have only been used to accelerate traditional processes by cutting sheet metal, but the proposal here is that they be used to cut parts of a steel section such as I-shape or angles [17,18]. Consequently, the connection would be able to transfer forces and moments through bearing at multiple contact points on these precisely-cut surfaces in the section.

In 2019, an experimental testing program was conducted at the University of Minnesota that focused on the behavior of intermeshed connections under various vertical

load scenarios. Four full-scale specimens with an intermeshed connection were designed to resist gravity loading in steel frame members, and then manufactured by using plasma and waterjet cutting machines. The results from this study showed that the intermeshed connection is capable of providing sufficient amounts of bending moment and shear force, through the direct bearing between individual components. However, in many cases, the load carrying capacity of the tested samples was significantly larger (up to 167%) than the target load during the design process [43].

The present chapter further investigates different observations from the physical test specimens and provides engineering explanations of the phenomena that resulted in such observations. To obtain such insight, extensive knowledge is generated on the stress and stain states state of the beams, angles, shear plates, and bolts, using nonlinear finite element (FE) analysis of the intermeshed specimens. The first numerical phase is devoted to developing a platform in Abaqus that can accurately simulate the behavior of the intermeshed connection, by choosing the suitable analysis methods and adjusting the parameters to meet the conditions of the experimental setup. The second phase, however, implements the assumptions from the first phase and further expands the numerical investigation by modifying the specimen designs to optimize connection geometry. Results of the FE analyses on the 'modified connections' show that, when smartly designed, the intermeshed connection can still provide enough resistance and ductility using smaller sizes for the connecting parts.

5.2. Finite Element Model Description

Due to the limitations that come with using measuring instruments and sensors in a physical experiment, as well as constraints in budget and schedule, there is much information that is often not recorded or measured in the laboratory. In the case of the experimental study of the intermeshed connection, it was not possible to install strain gages in the teeth and bolts, since they were encased by the angles and shear plates respectively. Therefore, there is no test data to indicate whether bolts experienced plasticity or to determine the load share for each tooth. To answer these and other questions, a finite element model was developed for each test specimen and nonlinear analyses were conducted for both verification and investigation. Such model would help to better understand the behavior of the intermeshed connection by learning in detail the underlying mechanics behind the phenomena observed during the tests. The FE simulations were performed in Abaqus, which is capable of handling material and geometrical nonlinearity, as well as contact between individual surfaces [27].

Fig. 5-2 shows the connection region of the specimen assembled in the laboratory, and the equivalent simulated connetion in Abaqus. In order to maintain the authenticity of the specimen and increase the accuracy of the model, the small geometric details were also incorporated in the Abaqus model including tolerances and special socket shapes. Therefore, the numerical model also included an extra 1.5 mm of space that was provided in the experiments between the teeth and sockets, as well as between bolts and their holes. Furthermore, a 6-millimeter gap was left where the beam faces meet each other at the center of the connection, as per the nominal design values (Fig. 5-2(c) and (d)). The special socket

cuts that can be seen in Fig. 5-2(e) were a result of adding circular holes (with a 3 mm radius) to the rectangular sockets, in order to reduce stress concentration in the corners.

(a) Assembled connection in the laboratory

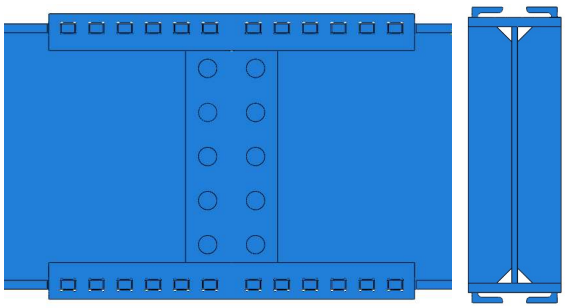

(b) Side/front elevation of the connection in Abaqus

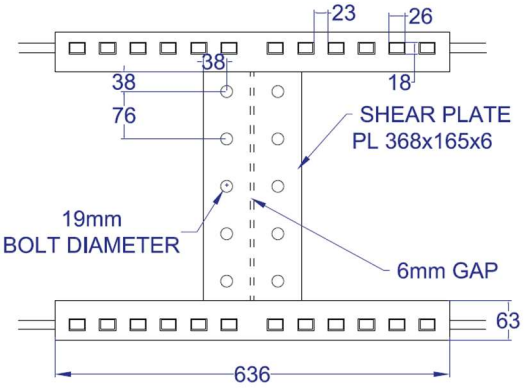

(c) Connection in W18×46 specimen

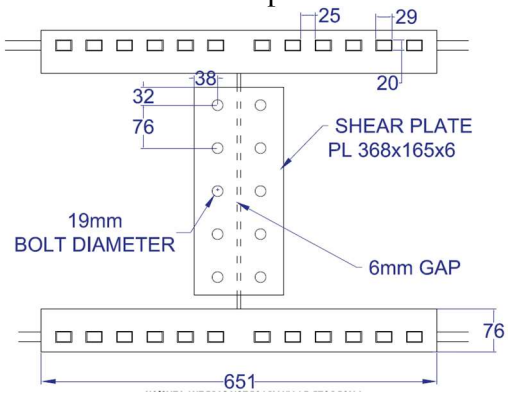

(d) Connection in W21×57 specimen

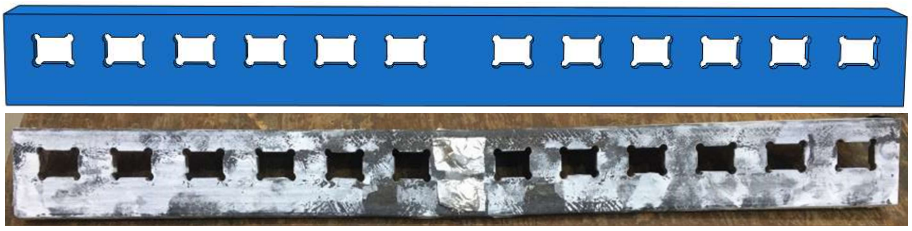

(e) Typical angle with special socket cuts in it

Fig. 5-2: Intermeshed connection; reality vs simulation vs schematics (unit is millimeter)

The material behavior was characterized with uniaxial tensile tests in accordance with ASTM E8/E8M [42]. This behavior was then introduced to Abaqus using stress-strain curve. Fig. 3-5 shows an example of such constitutive behavior for a tensile sample cut from the flange of a W21×57 section. Isotropic hardening was considered to describe the

deformation hardening behavior for a material under monotonic loading. Isotropic hardening assumes that the initial yield surface expands uniformly without distortion or translation as plasticity develops.

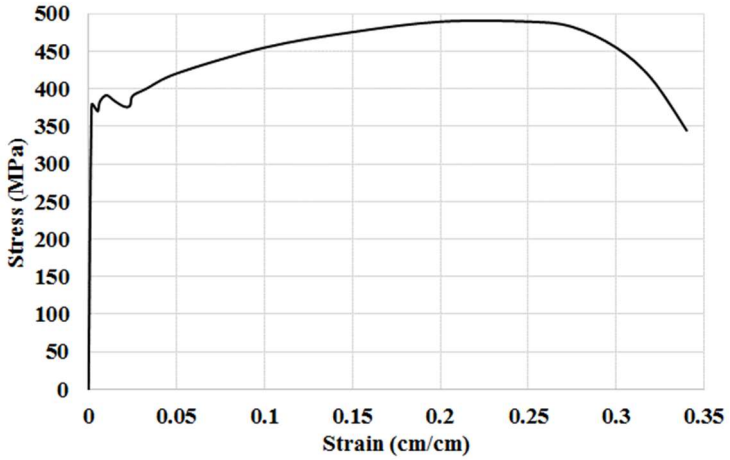

Fig. 5-3: Material behavior introduced to Abaqus for W21×57 flange

5.2.1. Model Assumptions

The intermeshed connection consists of multiple elements that work together through bearing and/or friction, or their combination, to transfer force and moment in the splice region. A key factor in modeling the connection properly is to understand the interaction between different components of the connection. To do so, the potential contact area of each element and its counterpart should be determined and the suitable contact properties should be assigned. Based on this approach, six different contact areas were defined between different segments of the intermehsed connection as shown in Fig. 5-4. Surface-to-surface contact with small sliding was used, which assumes that although two bodies may undergo large motions, there will be relatively little sliding of one surface relative to the other [31]. In the contact model, tangential behavior was introduced with a

friction coefficient of 0.3. This value was suggested as a result of an experimental study on the components of the intermeshed connection [50].

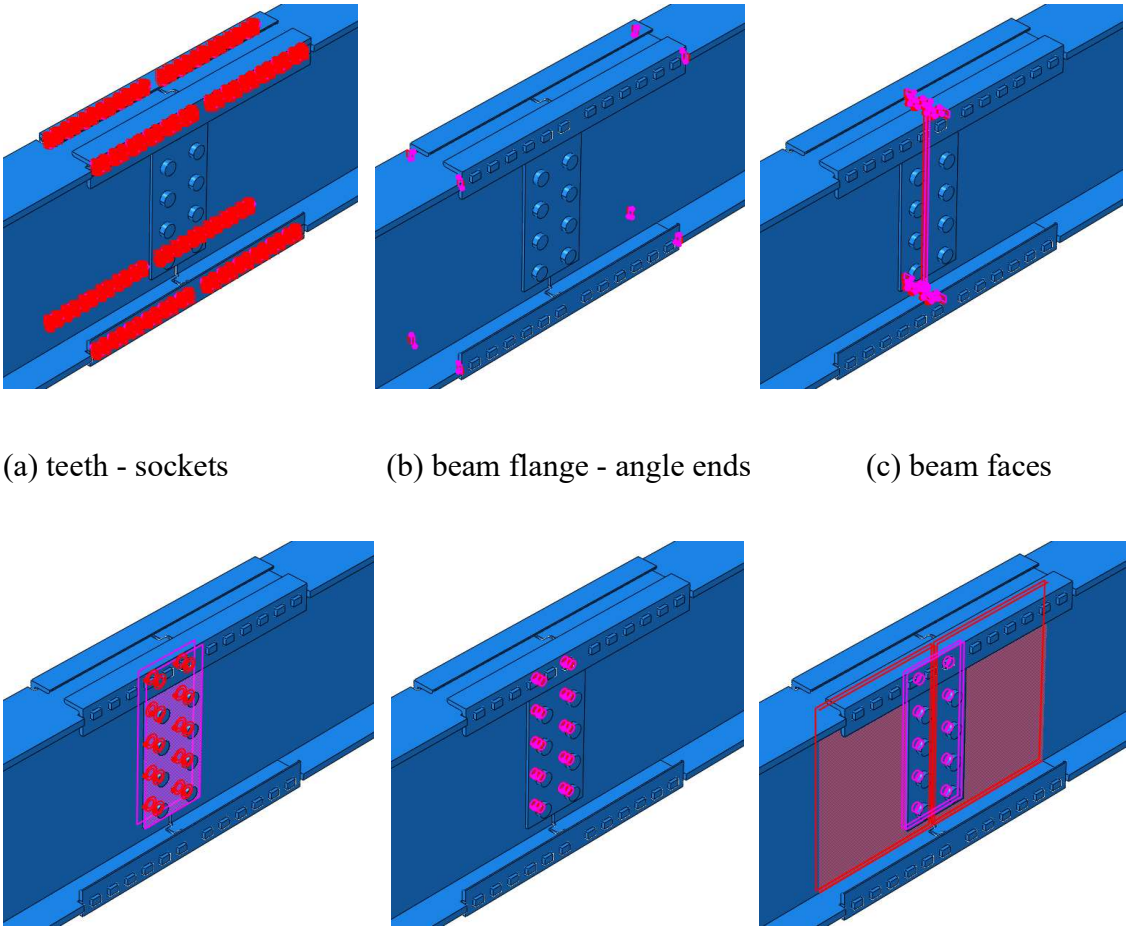

(a) teeth - sockets (b) beam flange - angle ends (c) beam faces

(d) bolt nuts - shear plates (e) bolt shank - plate thicknesses (f) beam web - shear plates

Fig. 5-4: Different contact areas in the connection region

To account for erection tolerances in systems with intermeshed connections, some gaps were used when designing and manufacturing the specimens. Because of these gaps, there was a lag at the start of load bearing during the experimental studies which was reported as “initial settlement” [54]. In the numerical models, on the other hand, the gaps hold the described contact areas (see Fig. 5-4) from developing any interaction in the very

early steps of the analysis. This results in an unstable system as there is no stiffness formed in the system due to the voids. To solve this problem, some contact areas, such as 'bolt nuts-to-shear plates' and 'beam web-to-shear plates' (areas (d) and (f) in Fig. 5-4), were forced to be in touch at the initiation of the analysis. Also, some of the teeth on both top and bottom flanges were assumed to be in touch with the corresponding socket on the top and bottom angles. This selection was made based on observations in the laboratory related to the settlement of the specimens due to self-weight during the assembling stage, and in the initial loading stage.

The structure was discretized by eight-node 3-dimensional solid brick elements (C3D8R) with linear displacement interpolation, which is suitable for complex nonlinear analyses involving contact, plasticity, and large deformations. [28]. The mesh size was limited to a maximum of 6 mm in angles, bolts, shear plates, and other components in the connection region, as higher accuracy was needed in that region due to the likelihood of complex phenomena. Everywhere else in the model, a coarser mesh was used which had a maximum mesh size of 25 mm. It is worth mentioning that other mesh sizes and patterns were also tested at this stage, but the mesh sizes above were found to be the optimum case, as using a finer mesh did not increase the accuracy of the results. Using this pattern, a total of 58,000 elements were defined in the models of Specimens 1 and 2, and 74,000 elements in the models of Specimens 3 and 4. The final mesh pattern can be seen in Fig. 5-5

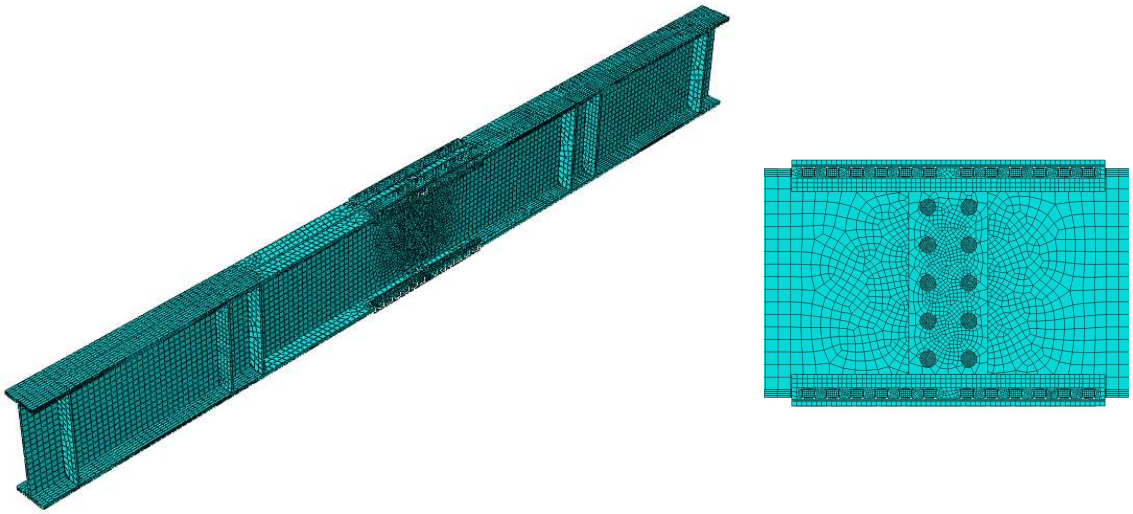

(a) The entire beam model (b) Connection region

Fig. 5-5: Mesh pattern in the W18×35 beam

5.2.2. Loading and Boundary Conditions

Two specimens featuring W18×46 sections with intermeshed connection in the middle, and two specimens with W21×57 sections and intermeshed connection in one end, were tested in the structures laboratory of the University of Minnesota. What separated the identical specimens was the loading scenario, as each section was tested under single or double point loads. A full description of the specimens, instrumentation, and failure modes could be found in reference [54].

The experiments were conducted using a displacement-controlled protocol at small increments. As a result, the testing process could be considered quasistatic since the inertial effects were negligible. Based on this description, a 'Static General' FE analysis was used, in which the jack displacement was applied to the loading point(s) of the specimen, as shown in Fig. 5-6. However, before vertical load could be applied, another step was used to include the effects of preloading in the bolts used to connect the shear plates. During this step, the bolts develop a pretension load which helps engage the friction between the shear

plates and beam web at the initiation of vertical load loading. However, this pretension load was relatively small, since all the bolts were hand tightened using a wrench in the laboratory. Bolt preload is represented in yellow on each bolt in Fig. 5-6(c).

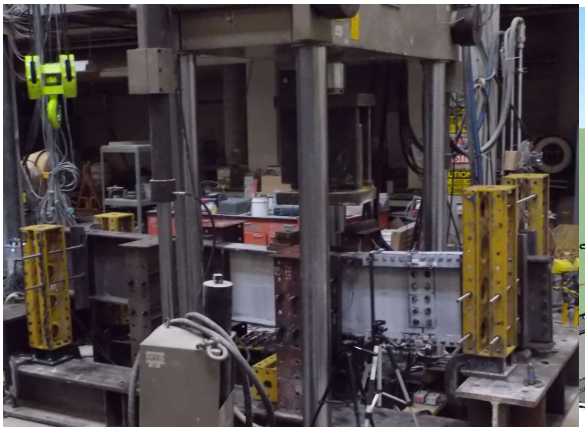

(a) Laboratory

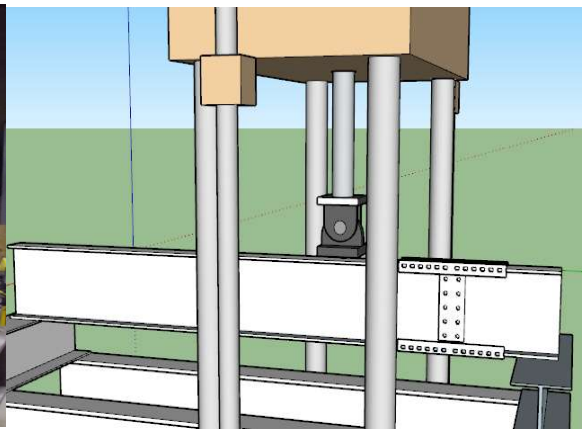

(b) Schematic

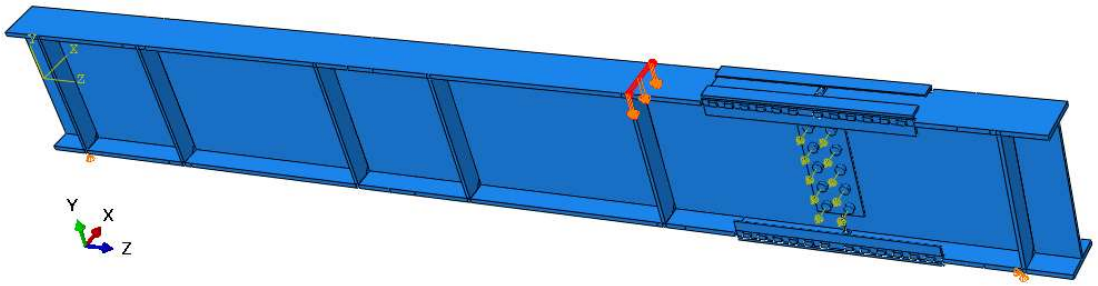

(c) Abaqus

Fig. 5-6: Loading and support condition of Specimen 3

Roller supports had been utilized underneath the first and last stiffeners during the tests. Similarly, in the FE models, the movement of the beam was restrained in Y direction in the same locations (see Fig. 5-6(c)). To avoid a lateral-torsional buckling failure and permanent twisting deformation in the tests, bracing restraints were added to the test setup at multiple locations. This bracing system differed from a test to another, since an augmentation was crucial in the braces due to an undesirable failure mode in Test 1, and excessive lateral motion in Test 2. Although these braces helped significantly to restrain undesirable out-of-plane movement, they deformed themselves at high-level loads during

the tests. To take into account the effects of this flexibility in the FE model, springs were added to the FE model at the locations of the brace points in the test specimens as can be seen in Fig. 5-7. These springs with constant stiffness and a degree of freedom in the X direction (see Fig. 5-6(c) for the general coordinate system), connect points on the beam flange to the fixed reference (i.e. the ground). Estimating the stiffness of the bracing system was complicated given the variety and complexity of the brace connections. Therefore, to provide a realistic estimation of the possible range of spring a simple but rational model was developed based on first principles. A summary of such calculation is provided in Appendix C.

(a) Using EFCO members for lateral bracing in Specimen 1 (left) and Specimen 2 (right)

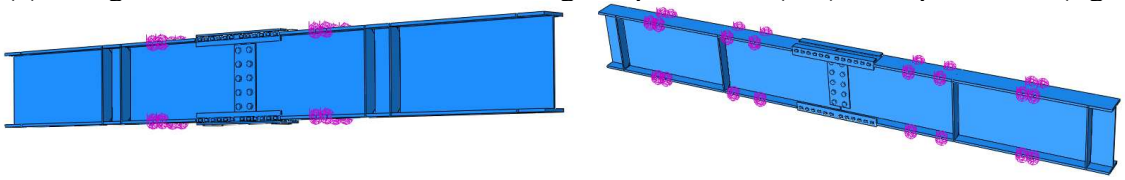

(b) Using springs with axial stiffness in Model 1 (left) and Model 2 (right)

Fig. 5-7: Restraining out-of-plane movement in the laboratory versus FE model

5.3. Verification Against Experiment

To ensure the validity of the assumptions implemented in the FE models, results of the simulated specimen tests needed verification with the experimental data and visual observations. But before the complete specimens were modeled, some primary FE models

of the connection components were prepared to investigate the behavior of the intermeshed parts.

5.3.1. Structural performance of the intermeshed components

To ensure that the angles and shear plates can facilitate the load transfer in the flanges and web, respectively, a set of numerical studies was performed with the focus on the individual flange and web. The main assumption in designing the intermeshed connection was the separation of moment and shear in the connection [53]. Based on this assumption, shear forces would transfer only through the shear plates in the beam web; while the bending moment would transfer entirely through its corresponding axial force resultants in the beam flanges. The intermeshed connection was imagined to provide such performance through angle-tooth interaction in the flanges as well as shear plates-bolt interaction in the web.

To test the ability of the intermeshing mechanism to provide enough capacity, three Abaqus models of the connection region were created and analyzed under several loading scenarios. In the first two models, the four angles in the connection are the only connectors between different beams parts, while the third FE model relies only on the shear plates for connecting the beam segments (see Fig. 5-8). The connection was assumed to be cut from W18×46 sections and L2½ × 2 × 3/8 angles, as in Specimens 1 and 2 in the laboratory tests. Grade 50 structural steel was considered for the beam section, Grade 36 for the angles and shear plates, and A325 for bolts, according to the corresponding ASTM standards [30,52,55].

In the models, the left side of the connection was connected rigidly to its support, while the right side was subjected to different pure load cases. In the first two models, pure tension and compression along the beam axis were applied respectively, while the third FE model was subjected to pure shear force in the transverse direction. In each case, the analysis was continued until loss of load capacity and the corresponding force-deformation curves are shown in Fig. 5-8 along with the failure modes. The results showed that the performance of the samples was satisfactory, and that the mechanisms of tensile load transfer in the flange and shear load transfer in the web occurred as assumed in the connection concept as long as the tension, compression and shear mechanisms are separable.

Fig. 5-8(a) presents the measured load-displacement response under tension, which displayed a softening behavior in the post-peak regime. The failure mode indicates that this behavior is a result of necking around the middle sockets in the angles. In fact, earlier in the analysis it was observed that only the first sockets from the connection centerline on either side tolerate large elongations, while the other sockets deform slightly. Eventually, the majority of the applied displacement was concentrated in the first sockets which led into necking and consequently fracture. In Fig. 5-8(b), the same sample was subjected to pure compression and buckled after showing significant load bearing capacity. The buckling, expectedly, happened in the middle of the angles, where the longest unbraced length existed. Finally, Fig. 5-8(c) shows the behavior of the shear plates under pure shear load applied to the right side of the sample. The connection fails after showing ample capacity and ductility is the shear behavior.

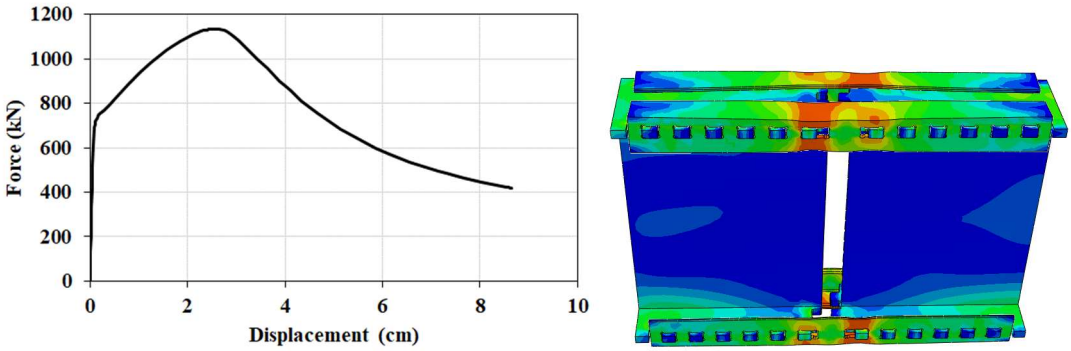

(a) Pure tension on the angles

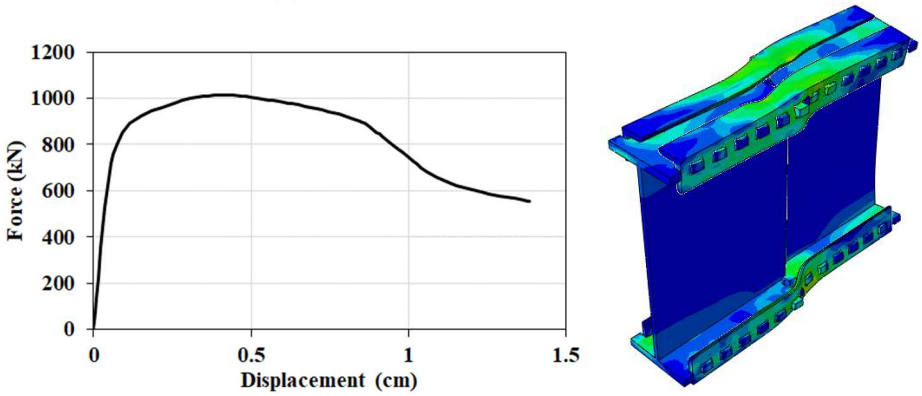

(b) Pure compression on the angles

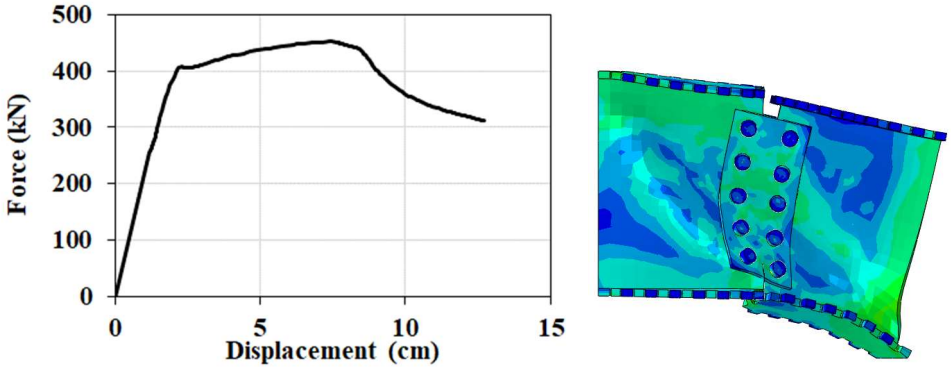

(c) Pure shear on the shear plates

Fig. 5-8: Behavior of the connection component under pure loading

All three samples showed desirable performance as they could successfully transfer large forces and failed only after showing a satisfactory ductility. Based on the force-displacement curves in Fig. 5-8, the peak loads resisted by each sample are 1134 kN under pure tension, 1014 kN under pure compression, and 452 kN under pure shear. If the peak

loads of the first two samples are compared with the plastic capacity of the beam flanges under axial load, it turns out that the connection could develop 76% of the flange capacity under tension and 68% under compression. The third sample was also able to generate a large shear capacity equal to 61% of the plastic capacity of the beam web under shear load. Therefore, the configuration considered for the intermeshed connection is able to provide large amount of load capacity and ductility. At the same time, the capacity of the connector components is well below the ultimate capacity of the beams section, which ensure failure in these elements before significant damage in the main beam section. This is in line with the design philosophy if the intermeshed connection.

5.3.2. Simulation of the experimental studies

Four numerical models were developed in Abaqus (Models 1-4) to replicate the response of the four specimens (Specimens 1-4) which were tested in the laboratory. Geometry, material properties, and boundary conditions were assigned to the FE model in a way that describes the experiments conditions best as possible, as discussed in detail in the previous section. Four different load scenarios, including a pure moment and three combined moment-shear loads, were considered for Models 1 to 4, respectively. Nonlinear finite element analysis was then conducted in Abaqus so that the models could be validated by comparing numerical results with the experimental data observations from the intermeshed beam test program. Both global observations, such as failure modes and force-displacement relations, and local observations, such as strain distributions and regional deformations, are presented. Investigating and comparing these results with the data from

the experiments indicates good agreement at both global and local levels, which is reported in detail in the following section.

Model 1, a W18×46 steel beam, was analyzed under two vertical point loads, which resulted in constant moment in the intermeshed connection region. The analysis was displacement controlled and it stopped at the same displacement level as the Test 1. At this step of the FE analysis, the beam had gone through large out-of-plane displacement and the peak load capacity had dropped 7%. This was similar to the failure mode in Test 1, as the tested beam buckled out of plane due to inadequate lateral bracing. Comparison of the global behavior through force-displacement curves, further proves that the FE model was able to simulate Test 1 accurately. Fig. 5-9 summarizes the comparison between the global numerical and experimental results for the first test.

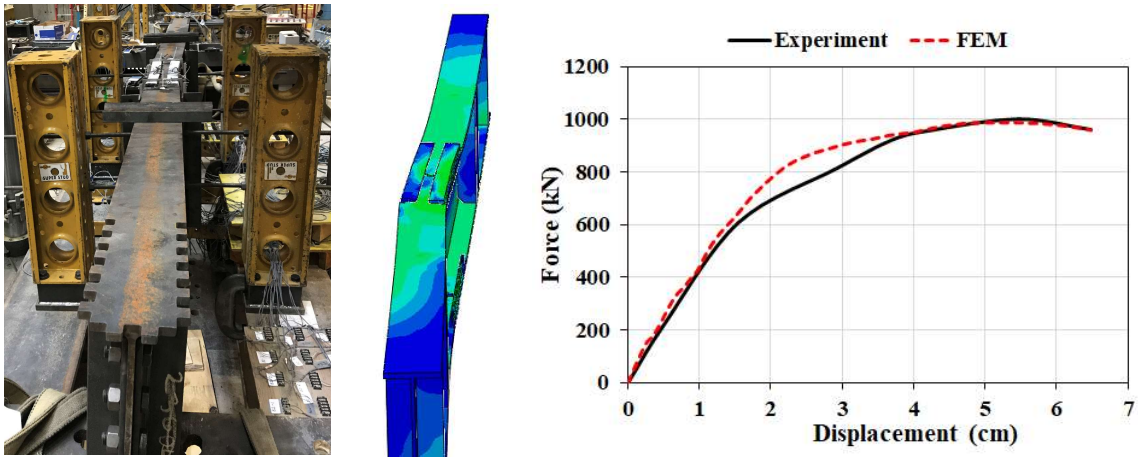

(a) & (b) Failure mode (c) Force-Displacement behavior

Fig. 5-9: Experimental versus numerical results of Test 1

Fig. 5-10 shows the deformed shape of each connection component at the failure stage for both Specimen 1 and Model 1. In the tension region (bottom flange and angles), the beam segments started separating and the initial gap was enlarged about three times its

initial dimension. The gap in the flange hole became wider as a result of plastic deformation in the tension angle. The width was larger for the holes located closer to the beam centerline as can be seen in the figure.

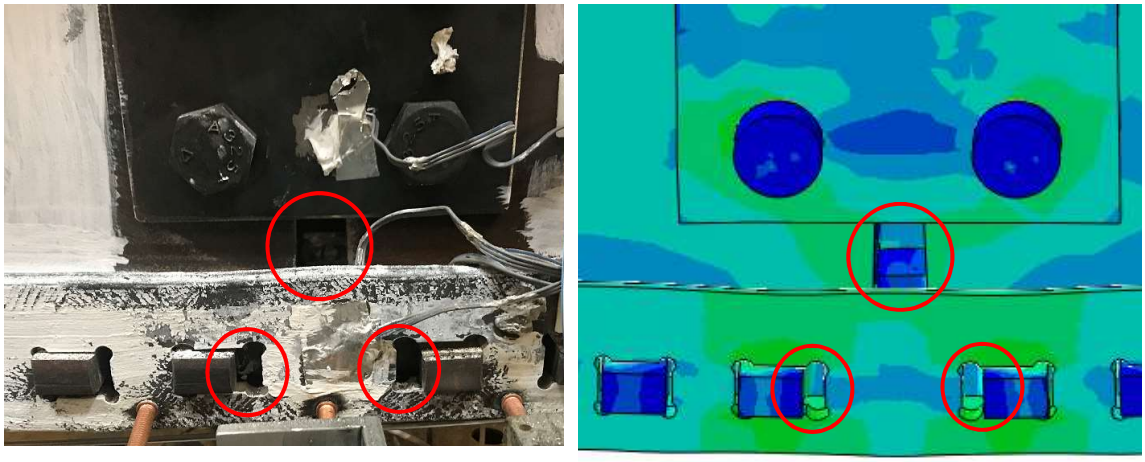

Fig. 5-10 Imposed gaps of the tensile area from the side view (Specimen 1 vs Model 1)

On the other hand, in the compression region (top flange and angles), the initial gap between the beam segments was closed entirely by the end of the test. This imposed a large axial deformation to the middle part of the length of the angles which resulted in plastic deformation and local kinking as shown in Fig. 5-11. Given the asymmetric cross section of the angles, the central portion of the compression angles rotated towards the beam flanges and webs. Consequently, the ends of the angles were required to separate from the beams, and the locks limited that movement. The locking mechanism, which consisted of channel sections, had been placed around the angles to keep them from a potential outward slippage. The analytical model successfully simulated this phenomenon as can be seen in Fig. 5-11.

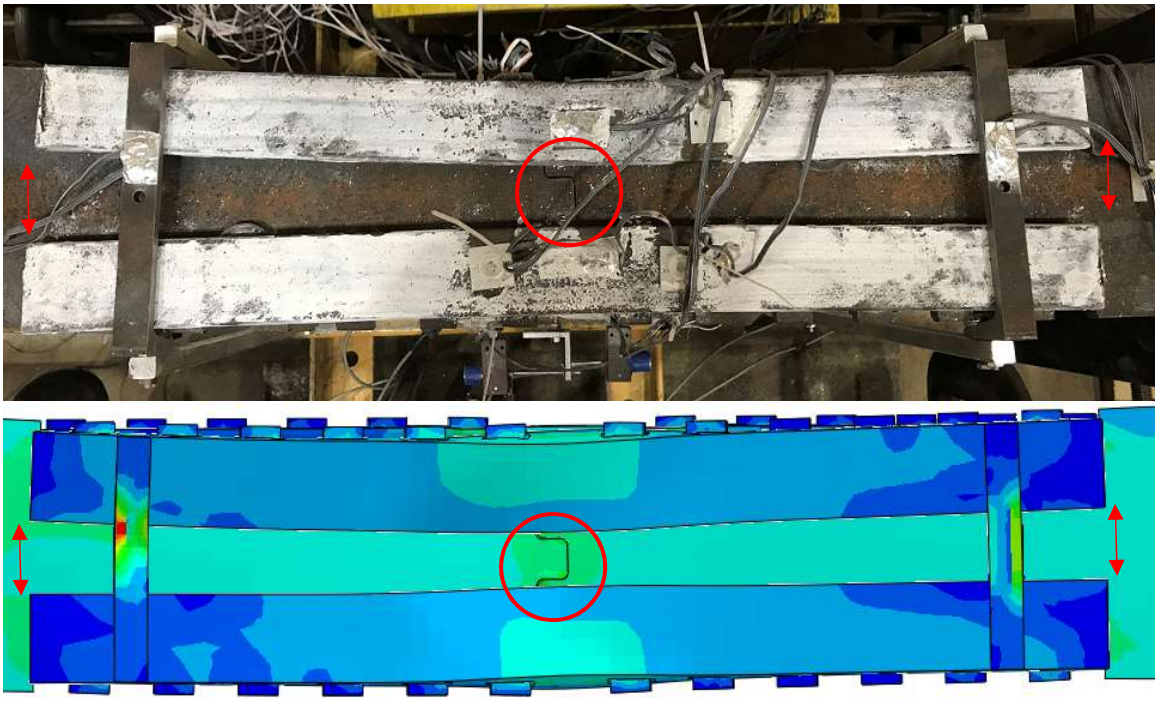

Fig. 5-11 Deformations of the compressive area from the top view (Specimen 1 vs Model 1)

In the second test, same beam section (W18×46) with same connection detail and location, was tested with a single point load over a stiffener, and with the connection under both shear force and bending moment. Fig. 5-12 shows a comparison of the force-displacement behavior of the second specimen in the laboratory and the Abaqus model which were in a good agreement. In both cases of the experimental test and numerical simulation, lateral-torsional buckling was the cause that resulted in the failure of the beam. In fact, during the analysis, small lateral displacements were observed which indicated that the beam was experiencing the initiation of lateral buckling (Fig. 5-12). During the analysis, these out-of-plane movements were increasing to a point that caused out-of-plane instability in the FE model and consequently stopped the analysis.

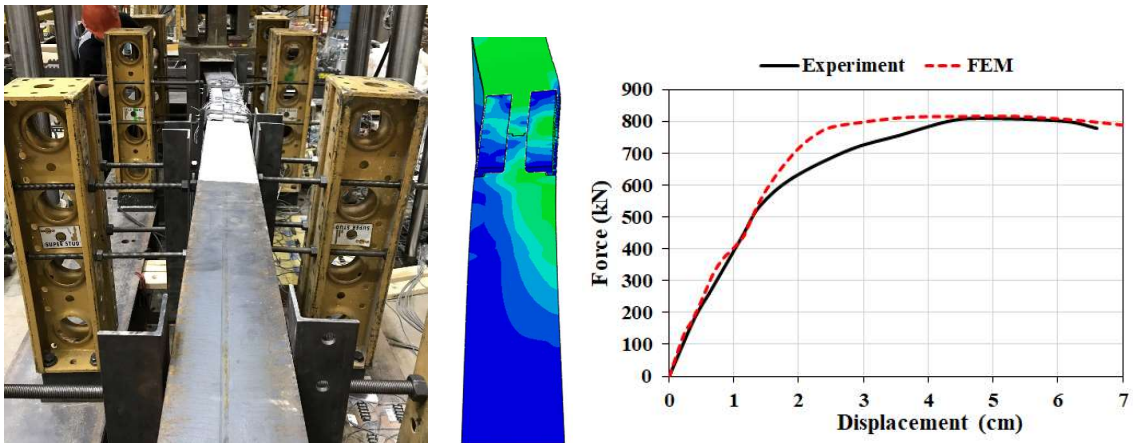

(a) & (b) Failure mode (c) Force-Displacement behavior

Fig. 5-12: Experimental versus numerical results of Test 2

Concentrating the jack load in one spot, also resulted in buckling in the stiffener as well as deforming the flange underneath the load. A closer look at the Model 2, showed the similar phenomenon at the failure stage which is shown in Fig. 5-13. At this step of the analysis, the beam web adjacent to the loading area demonstrated yielding which contributed to the stiffness drop in that area and consequently buckling of the stiffener. This was also reported from the experimental studies of Test 2 [43].

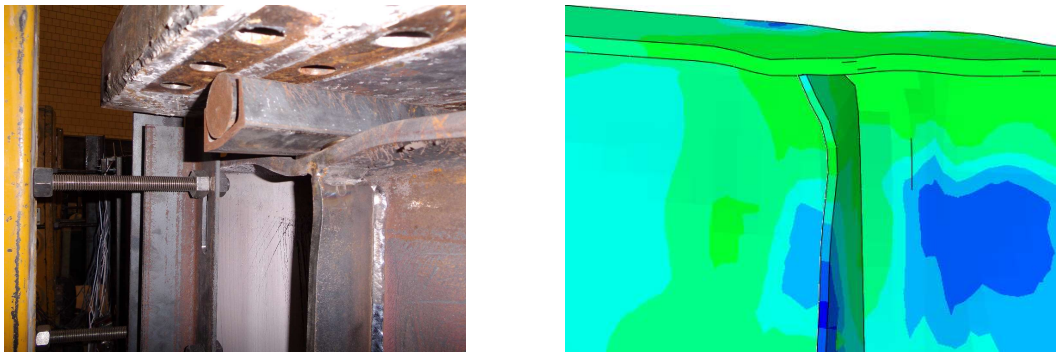

Fig. 5-13: Buckling of the stiffener and deforming the top flange under the point load (Specimen 2 vs Model 2)

Tests 3 and 4 were conducted on a W21×57 beam section with an intermeshed connection located at one end of the specimen. Different load scenarios were considered for the two specimens, as Specimen 3 was tested with one point load and Specimen 4 was

tested with two point loads. However, both load scenarios subjected the connection zone to a combination of bending moment and shear force with a moment-to-shear ratio (*M/V*) of 0.61 m. Therefore, Specimens 3 and 4 were more susceptible to shear than Specimen 2 with moment-to-shear ratio of 1.84 m.

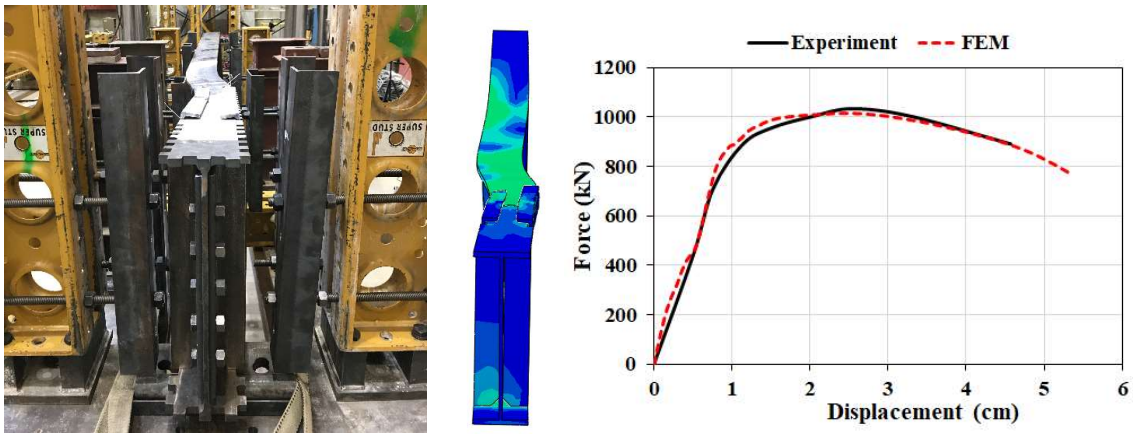

(a) & (b) Failure mode (c) Force-Displacement behavior

Fig. 5-14: Experimental versus numerical results of Test 3

Numerical studies of Models 3 and 4 in Abaqus showed that both models stopped running due to lateral instability of the FE model caused by lateral buckling of the beam. This out-of-plane movement took place under the point load in Model 3 (Fig. 5-14), whereas in Model 4 it occurred between the loads and in the beam centerline (Fig. 5-15). These were the same locations in the specimens during Tests 3 and 4 that did not have enough lateral braces attached to the beam and eventually experienced lateral buckling. Comparing the experimental and numerical Force-Displacement curves of both tests in Fig. 5-14 and Fig. 5-15, further confirms the ability of the FE models to predict the behavior of specimens with the intermeshed connection.

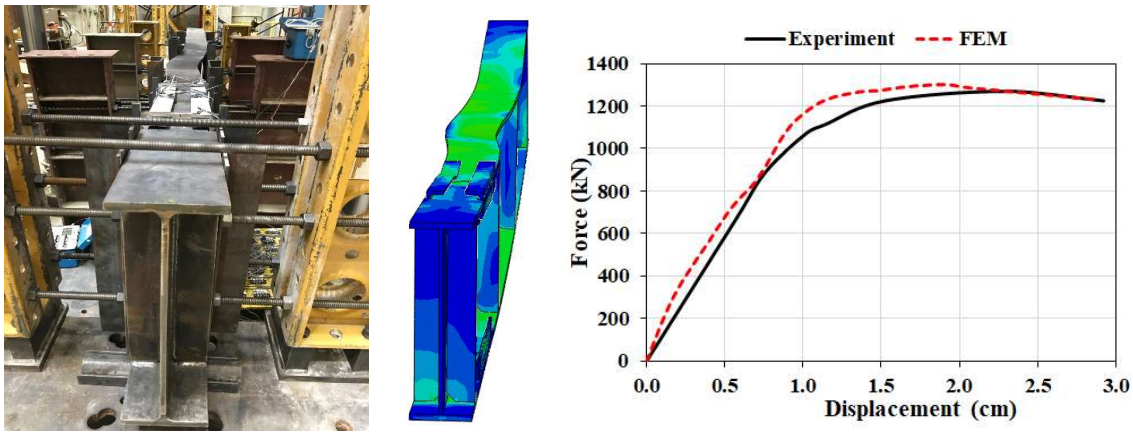

(a) & (b) Failure mode (c) Force-Displacement behavior

Fig. 5-15: Experimental versus numerical results of Test 4

As mentioned earlier, in the Test 3 and Test 4, the connection region was subject to large shear demand. Therefore, the effects of this demand on the connection behavior during the analysis was essential. Models showed that as a result of the shear deformation in the connection region, the beam faces started slipping against each other and consequently formed a step between different sides of the flange in the connection. At the same time, the angles deformed in an undulating manner, because they unexpectedly contributed in resisting shear. Fig. 5-16(a) and Fig. 5-16(b) show the described deformations for the third beam as an example, but it is worth mentioning that similar phenomena were observed in the fourth beam.

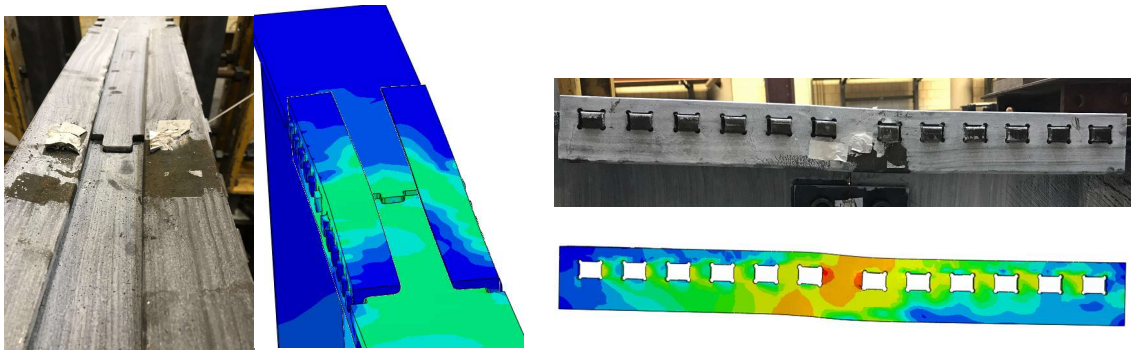

(a) Misalignment of the top flanges (b) Undulating of the angles

Fig. 5-16: Effects of shear presence in the connection region (Specimen 3 vs Model 3)

As can be seen in Fig. 5-15, the fourth beam failed because the beam buckled between the braces at the center span. This region happened to be the constant moment region of the beam as well, in which the moment demand was maximum. Fig. 5-17 shows the yielding of this region after the plastic moment had been reached, caused the top flange and the top part of the web to buckle in both Specimen 4 and Model 4.

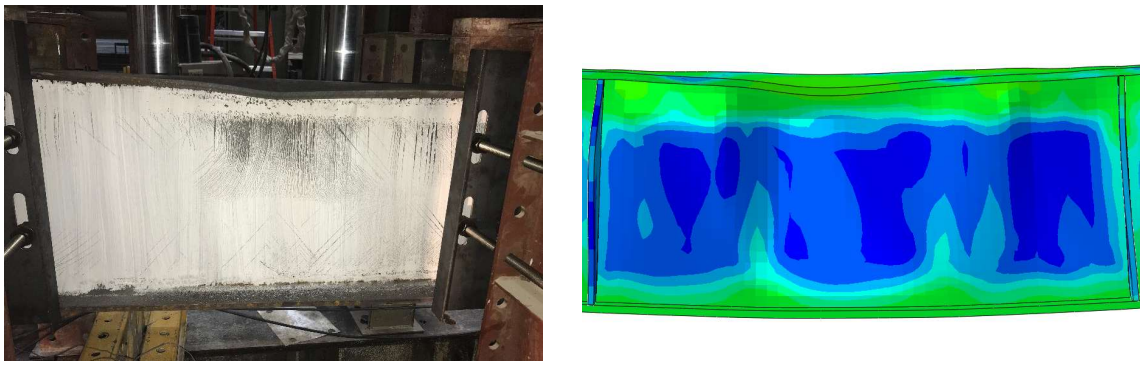

Fig. 5-17:Yielding of the web and kinking of the top flange in the center span (Specimen 4 vs Model 4)

5.4. Investigating Structural Mechanics of Intermeshed Connection

After verifying the accuracy of the finite element model by comparing the results with the experiment, some case studies were conducted in Abaqus to investigate the effects of changes in the initial assumptions in the FE models. These studies provide further insight on how the beam with intermeshed connection would behave in a structural condition, different from the condition in the laboratory experiments.

5.4.1. Sensitivity of the behavior to initial touch in the angles

As mentioned in Section 2, in order to avoid zero stiffness in the numerical models, some of the flange teeth were assumed to be initially in contact with their correspondig

sockets in the angles. Selecting the right combination of teeth for this so-called 'initial touch' was decided with consideration of the data from the experiments. In all specimens, during the test, the majority of the load was taken by the first tooth on either side of the centerline, both on the compression and tension angles. In the copression angle, however, the gap between the beam faces closed and beam faces came into contact in early stages of the test. Thereafter, beam segments contributed in load resistance in the compression region through direct contact, which prevented the teeth 2 through 6 on each side from receiving major loads. Based on this rationale, only the first tooth on each side of the splice was selected to be in contact initially for the compression angles. In the tension flange, beside the first tooth, three more teeth were selected on either side of the connection to counteract the forces generated by direct contact of the beam faces. This pattern of initial touch was then introduced in Abaqus as can be seen in Fig. 5-18(b). It needs to be mentioned that although only the selected teeth were in contact initially, the other teeth could still come into contact with their corresponding socket later in the analysis.

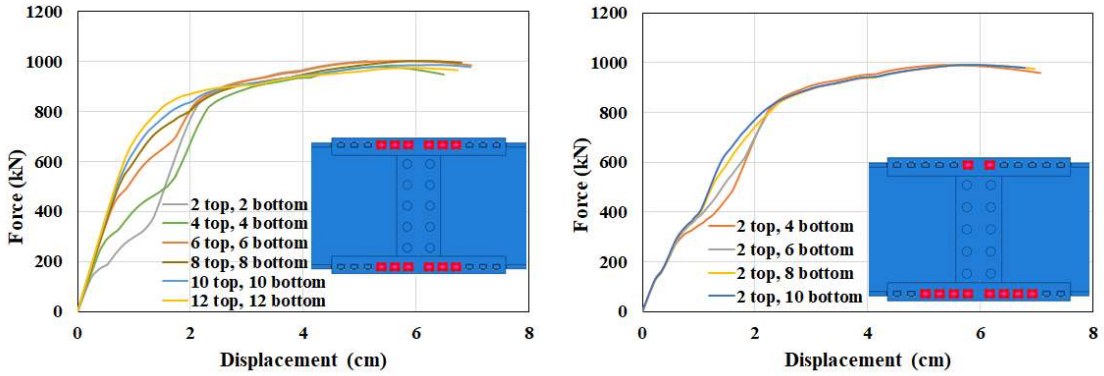

(a) Using the similar initial touch in tension and compression flanges

(b) Using unbalanced initial touch in tension and compression flanges

Fig. 5-18: Effects of different initial touch patterns on the behavior of Model 1

A case study on the initial touch was conducted to show the sensitivity of the numerical model to the selection of teeth initially in contact. In the first part of this study, similar initial touches were assumed in tension and compression flanges. Six different cases were considered, starting with only two teeth in contact to the ultimate case of all 12 teeth in contact in top and bottom flanges (the third case with six teeth is shown in Fig. 5-18(a)). Comparing the results of these cases showed that only the region between the displacement of 0.25 cm and 2.75 cm in the force-displacement curve is affected, while the rest of the behavior remains almost unchanged. This range of displacements represents about 35% of the full range in the tests, and it occurs prior to the initiation of global yielding of the connection. Exhibiting the same peak load and ductility in different cases indicates that all the models ended up with the same stress and strain state at the end of the analysis. This means that all the teeth eventually generated contact with the corresponding angle, independent from the assumed initial touch. However, choosing different initial touch determines what teeth take major loads at the beginning, which causes different plasticity pattern in the corresponding angle. This causes changes in the force-displacement paths between 0.25 cm and 2.75 cm, and differences in the pre-yield stiffness.

In the second part of this case study, the initial touch in the top flange (compression flange) was kept constant at two teeth, based on the rationale explained earlier in this section. Then, the number of in-touch teeth were altered from four to 10 in the bottom flange (tension flange). Similar to the other case study, results of all cases are identical except for a limited region, which was from 0.75 cm to 2.25 cm. Fig. 5-18(b) shows that even within this range, the difference are very short lived, and the behavior of the specimen is not highly dependent on the selected initial touch.

5.4.2. Effects of boundary condition

In the laboratory, all the specimens were tested in a simply supported condition, as both ends of the beams were placed on rollers. But the intermeshed connection is conceptualized for use in moment frames, in which the beam ends are clamped to the column to form a fixed connection. In other words, the main body of the beam is attached to the beam stubs via the intermeshed connection, while the stubs are connected to the columns using welds or bolts. Fig. 5-19 shows this concept in a prototype mockup frame in Dublin, Ireland.

Fig. 5-19: Moment frame with the intermeshed connection

To take into account the realistic support conditions in the W18×46 specimens, Models 1 and 2 were modified with clamped supports in lieu of the original simple supports. Aside from the support conditions, the remainder of these Abaqus models remained unchanged. Fig. 5-20 shows the force-displacement behavior of these FE models under the load scenarios used in the laboratory for Tests 1 and 2.

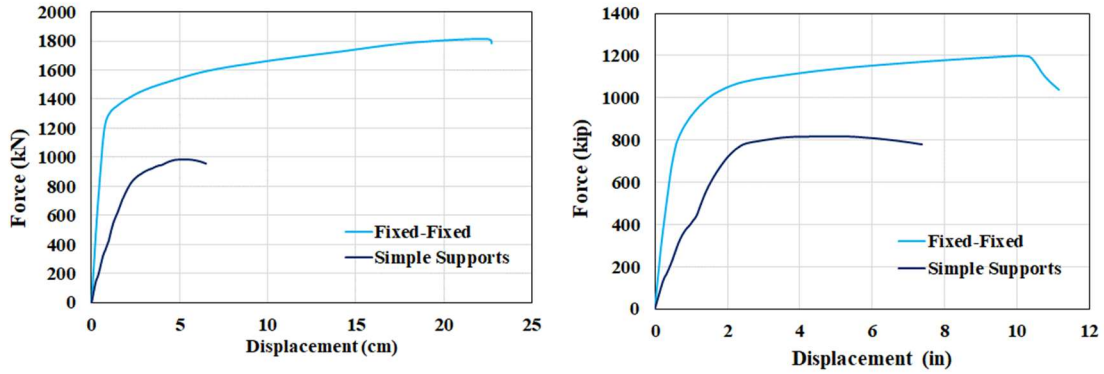

(a) Model 1 (b) Model 2

Fig. 5-20: Comparing the W18×46 model numerical results after updating the boundary condition

The FE results reveal that changing the support conditions from simple to clamped, increases the stiffness, load capacity, and ductility of the specimens as expected. Both models with new boundary condition, showed initial stiffness of approximately four times bigger than that of their original models. Also, Model 1 experienced an increase of 84% and 250% in the load capacity and maximum displacement respectively, while those values are 67% and 47% for Model 2. This shows that if utilized in a moment frame with fixed beam ends, the intermeshed connection is capable of offering an even larger resistance and stiffness range than the conducted experimental studies. The fixed-end boundary conditions enable the beams to develop plastic mechanisms that allow moment redistribution, with the net effect of increasing force and deformation capacities. In a frame, the boundary conditions for a beam will depend on the relative stiffness of the beams and columns. Nonetheless, an increase in moment and deformation capacities can be expected.

Investigating the ultimate state of these models revealed that no major out-of-plane movement was visible. In fact, the fixed end conditions helped the beam maintain the original web plane until the end of analysis, and therefore, produce larger load capacity.

Both models finally lost their ability to carry load as a result of buckling in the beam web due to large shear forces near the supports (Fig. 5-21).

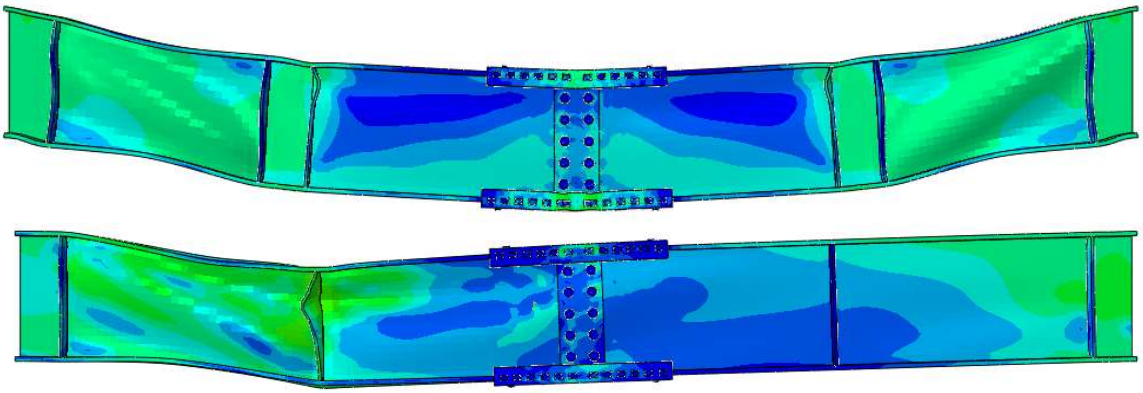

Fig. 5-21: Failure modes of Model 1 (top) and Model 2 (bottom) with fixed boundary conditions

5.4.3. Moment overstrength

The intermeshed connection showed good moment resisting capacities in the experiments. However, the peak moment that was reached in the connection during Test 1 was larger than initially targeted. The intermeshed connection of this specimen resisted 2.67 times the moment that it was designed to resist [54].

The design procedure for the intermeshed connection intended for the angles to be the only component of the specimens that would resist bending moment. Although the shear plates were originally placed in the connection to transfer the shear load, their contribution in providing extra moment capacity is not negligible. To determine the magnitude of the shear plate contribution, two extra Abaqus models of Specimen 1 (pure bending moment case) were developed. In the first model, only angles were used in the intermeshed connection, so that the effect of shear plate elimination could be investigated.

The second model, on the other hand, only contained the shear plates (i.e. the side angles were eliminated) to study their behavior under bending moment.

Fig. 5-22(a) compares the results of these two models with the original Model 1. Comparison of the 'Angles Only' case with the original connection shows that the behavior of these two cases are very similar up to the displacement of 1.5 cm. Beyond this point, the case with angles only loses its stiffness significantly due to yielding in the angles. In contrast, the presence of the shear plates the original connection (Model 1) helps with a desirable and gradual transition of stiffness beyond the yielding point of the angles, by providing extra help with moment resistance. The additional load path for flexure offered by the shear plates makes the intermeshed connection robust. Furthermore, the shear plates provide extra moment capacity for the connection, as elimination of the shear plates from the original connection caused a drop of 36% in the peak load (Fig. 5-22(a)). When beam faces start developing contact at the top flanges, a compression force will form which moves the neutral axis upward. Consequently, a tension force will develop in the shear plates that counteracts the compression force in the top flange. This is a coupled force mechanism that provides extra moment capacity for the connection, as demonstrated in Fig. 5-22(b). Another phenomenon that contributes to generating this extra moment resistance in the bending of the shear plates. In fact, the shear plates bend and develop a nearly linear distribution of axial stresses which results in the formation of an internal moment [43,54].

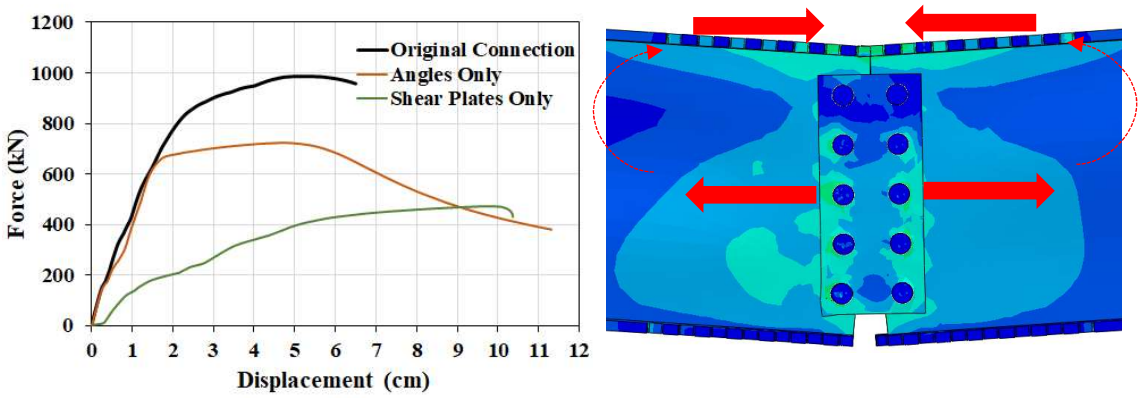

(a) General behavior of the connection (b) Extra moment capacity

Fig. 5-22 Effects of using shear plates on the moment capacity of Model 1

5.5. Modified Intermeshed Connection

There is a need for modification of the intermeshed connection design procedure that was used to design the Specimens 1 to 4 [53], so that the connections can meet the design goals with less excess conservatism. The moment overstrength that was observed in Test 1 which was 2.67 times the design moment, should be reduced to a value that is closer in line with structural steel flexural design. Whatever value of overstrength is targeted for a simply supported beam will be larger if the beam has fixed end conditions or is part of a moment frame.

5.5.1. Updating the design procedure

A detailed procedure had been developed which was inspired by the AISC recommendations For analyzing and designing the intermeshed connection [33,41,53]. A basic assumption in this design procedure is that the connection would transfer the moment and shear loads separately; meaning the angles would take all the load due to moment, and

the plates would take all the load due to shear. But Section 5.4.3 of the present chapter showed that this assumption is not necessarily accurate and that shear plates can contribute to the moment resistance of the connection as much as 36% of the total capacity. Therefore, a modification was made in the design procedure to take into account the contribution of shear plates in moment.

In the first step of the modified design procedure, shear plates and bolts are sized based on a conventional shear tab design according to the current code recommendations. The considered shear demand (V_d) in this step is obtained from the linear elastic analysis of the beam, assuming a target design moment (M_d) in the connection location. In this research, one-third the plastic moment capacity of the beam was selected as the design moment (M_d). A detailed sample calculation of the shear plate design is presented in the Appendix B.

After the shear design is finalized and shear plates sizes are determined, the bending moment that could be resisted by these plates would be calculated (M_{plates}). The second step of the design, the moment design of the connection, is devoted to sizing the angles and teeth. While in the original design approach, the angles and teeth were sized for the total target design moment (M_d), the modified approach considers only a share of M_d to be taken by these elements. In fact, the angles moment (M_{angles}) is assumed to be the remainder of the total design moment, after deducing the shear plates share ($M_{angles} = M_d - M_{plates}$).

Including this modified step in the design procedure, a new design was undertaken for the connection in Specimens 1 to 4. New sizes for the angles and shear plates as well as new numbers of teeth and bolts were determined and are summarized in Table 5-1. Results indicate that, using this modified approach, smaller sizes for the angles and shear

plates, as well as fewer numbers of teeth and bolts are acceptable for the same design objectives.

Table 5-1: Size comparison of the original and new specimens

Specimen	Beam*	Angle*	Number of teeth	Shear Plate (mm)	Number of bolts
1 & 2 Original	W18×46	L2½×2×3/8	48	PL368×152×6	10
1 & 2 New	W18×46	L2×2×1/4	40	PL229×152×3	6
3 & 4 Original	W21×57	L3×2×3/8	48	PL368×152×6	10
3 & 4 New	W21×57	L2.5×2×5/16	48	PL305×152×3	8

* US designations for hot rolled steel shapes

5.5.2. Behavior of the redesigned specimens

In order to make sure that the new specimens will meet the selected design objectives, numerical models for all four new specimens were developed in Abaqus. Similar load scenarios as the original FE studies were considered for these new analyses, so that the results could be compared. Fig. 5-23 to Fig. 5-27 present the numerical results of the newly designed Specimens 1 to 4 respectively, and compare them with the force-displacement curves and failure modes of the original FE models.

Numerical investigation of the new Specimen 1 results showed that this specimen could meet the design strength, and the peak load is above the target design load[1] by an acceptable margin (Fig. 5-23(a)). Large displacements were exhibited by the specimen, while the majority of the deformation was concentrated in the connectors such as the angles and shear plates (Fig. 5-23(b)). Such a mechanism is desirable, since the replacement of

[1] For all specimens, the target design load is the load that generates a design moment equal to one-third the plastic moment capacity of the beam in the connection location.

the angles is easier and faster following any case of damage-inducing overloading. In fact, it is a design objective to assure that the failure in the angles occurs before the teeth failure.

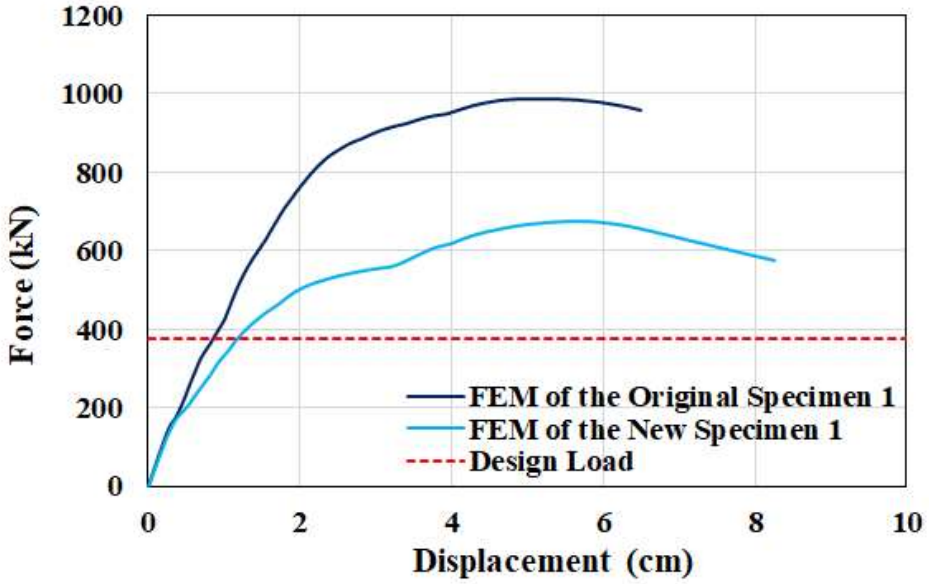

(a) Force-displacement comparison of the original and new Specimen 1

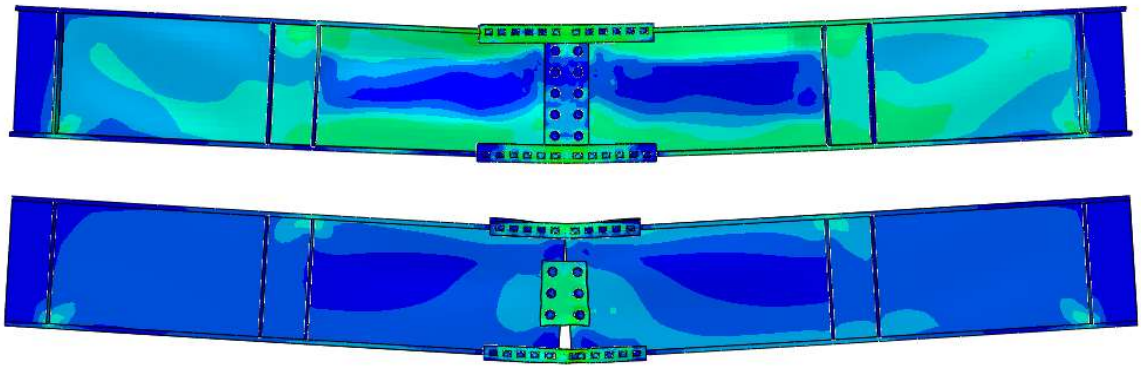

(b) Failure modes of the original (top) and new (bottom) Specimen 1

Fig. 5-23: Numerical results of the new Specimen 1

Fig. 5-24 shows the area of plastic deformation in different components of the connection region for both original and new Specimen 1. The grey area indicates stress level is in the elastic range, and the colored area demonstrates the region that has deformed into the plastic range.

In the case of the original Specimen 1 (Fig. 5-24(a)), only the top flange and top angle are shown, since all other components remained elastic. In fact, even in the angles, which are meant to yield as sacrificial elements, no major yielding happened up to the design load level. This was possible due to the help from the shear plates which kept the angles from taking enough load to yield. This issue was mentioned earlier as the 'overstrength' phenomenon in the intermeshed connection.

On the other hand, in the new Specimen 1, the angles showed major plasticity at the design load while other components either showed no plasticity (e.g. bolts) or minor plasticity (e.g. beams and shear plates). The yielded area in the angles is concentrated around the first tooth of the angles on either side of the connection splice. In the case of the top angle, direct bearing from the compressive flange caused plasticity between the middle sockets; while in the case of the bottom flange, necking caused plasticity above and below the first socket on either side of the splice. Comparing these results with the plasticity patterns in the original connection, proves the effectiveness of the modification in the design procedure. This modification helped to force the angles to their capacity, which in turn protected the beams from major damage form inelastic deformation.

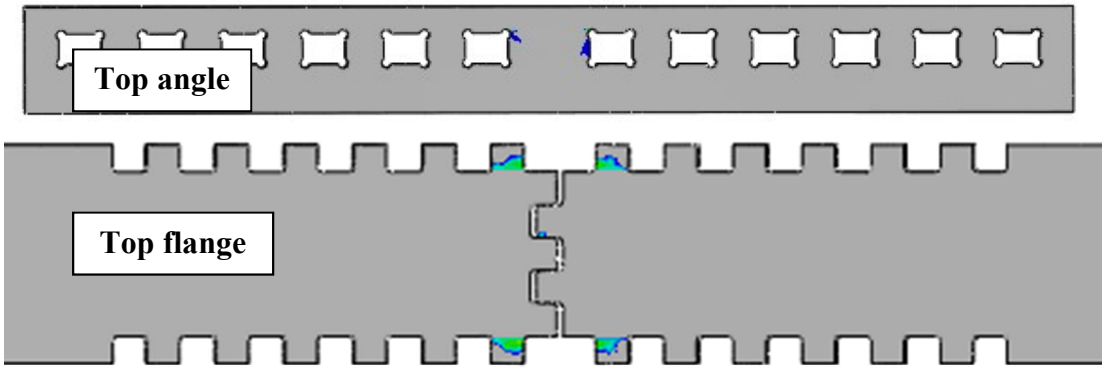

(a) Original Specimen 1

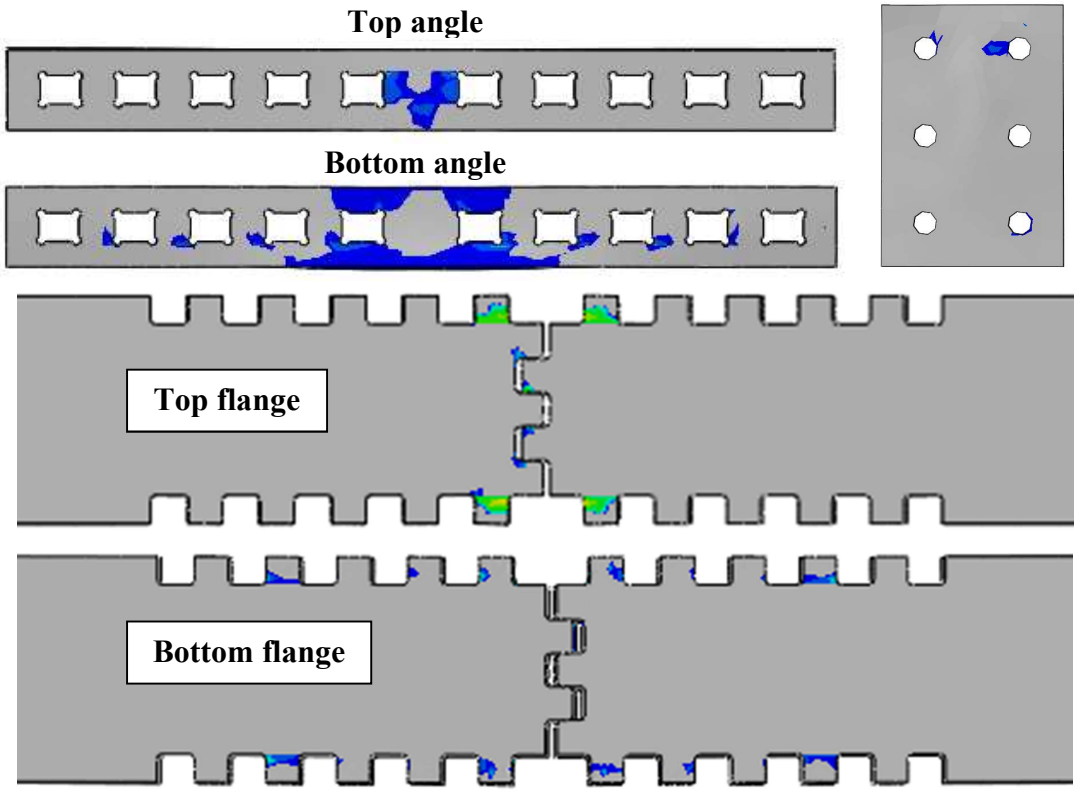

(b) New Specimen 1

Fig. 5-24: Plasticity of different components of the connection at design load level

Similarly, the FE analyses of the newly designed Specimens 2 to 4 showed satisfactory results as they provided ample strength above the design load over large deformations (Fig. 5-25 to Fig. 5-27). All the original specimens failed due to lateral backling which caused major damage in the beam sections. These phenomena were not observed in the redesigned specimens and they remained in plane even after large deformations. Contrary to the original specimens in which the major damage was observed in the beam sections, the angles and shear plates underwent major failure in the FE analysis of the redesigned specimens. For instance, in the original Specimen 2, the beam section underneath the load deforemed significantly, the top flange kinked due to buckling, and the adjacent stiffener buckled (see Fig. 5-13). Fig. 5-25 shows that none of these happened in

the new Specimen 2 and the significant plasticity and kinking in the angles and shear plates were the failure mechanisms.

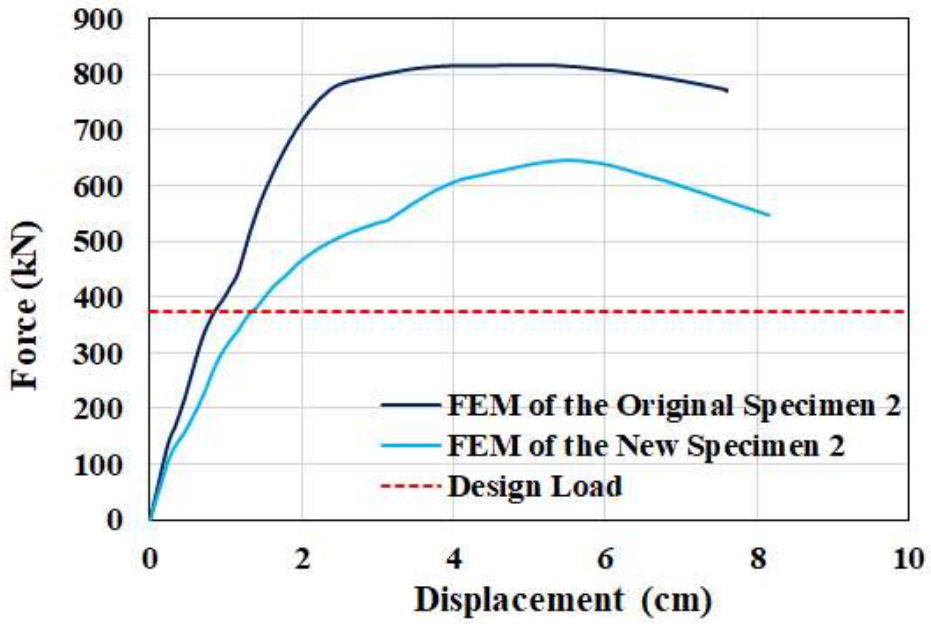

(a) Force-displacement comparison of the original and new Specimen 2

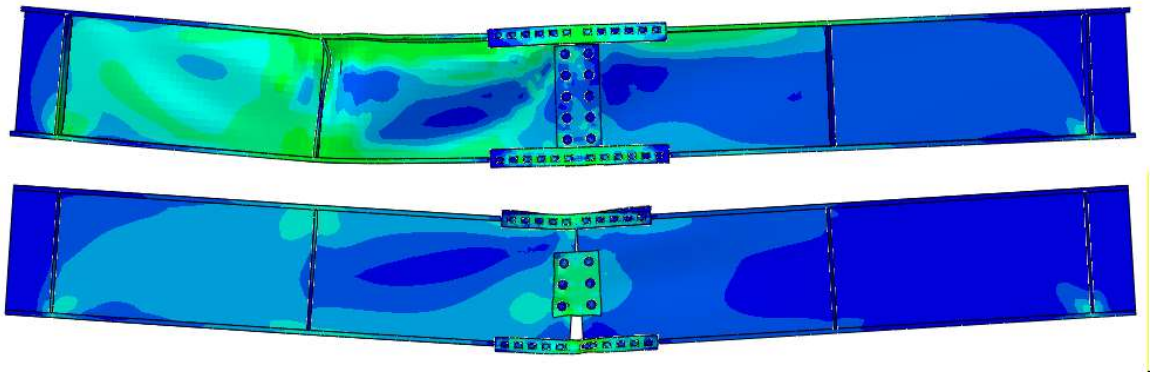

(b) Failure modes of the original (top) and new (bottom) Specimen 2

Fig. 5-25: Numerical results of the new Specimen 2

This was also the case for Specimens 3 and 4 (Fig. 5-26 and Fig. 5-27) and failure in the load points was replaced by damage in the connection zone. It is worth remembering that the intermeshed connection is meant to be the fuse in the specimen that protects the

beam from bearing large deformations. Therefore, the modified design approach enabled the selection of connection details which meet this design objective in all cases.

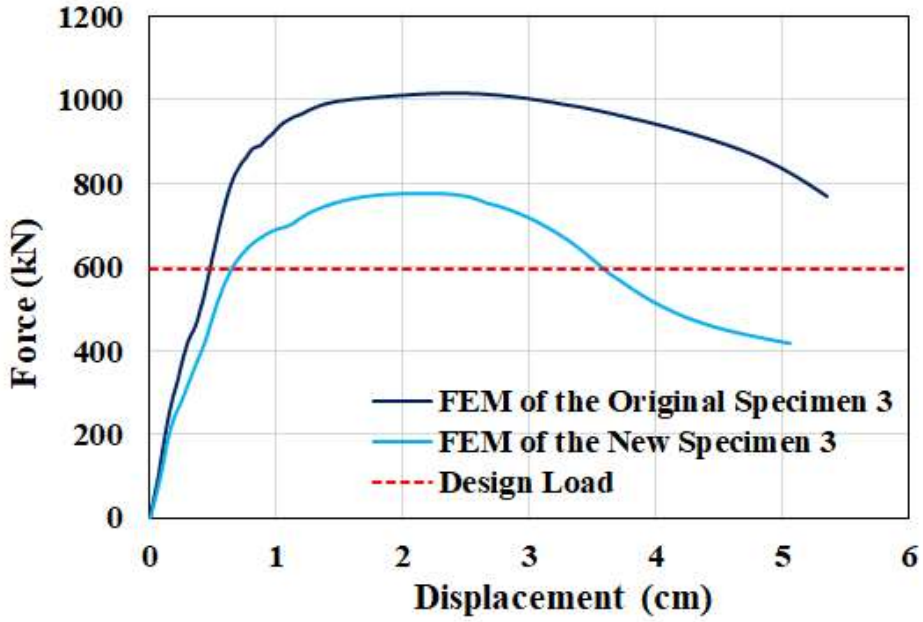

(a) Force-displacement comparison of the original and new Specimen 3

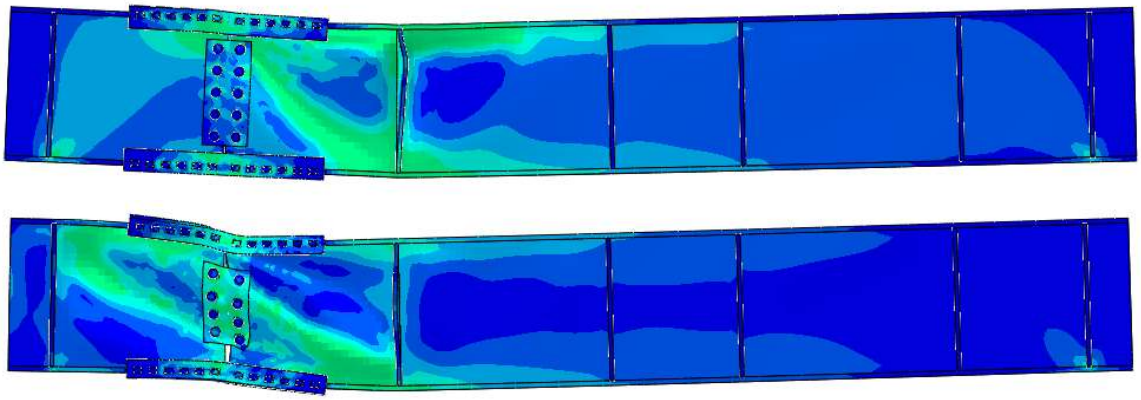

(b) Failure modes of the original (top) and new (bottom) Specimen 3

Fig. 5-26: Numerical results of the new Specimen 3

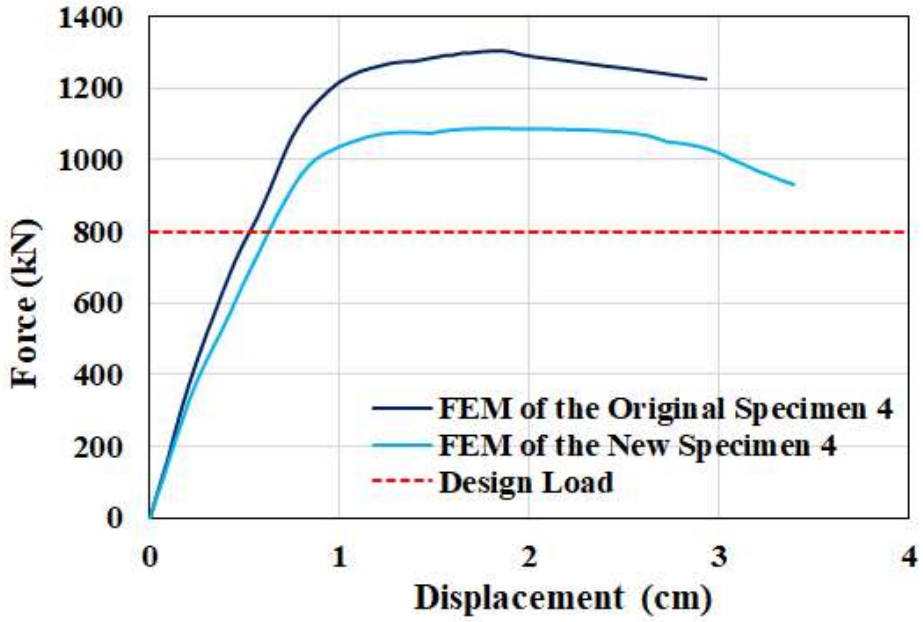

(a) Force-displacement comparison of the original and new Specimen 4

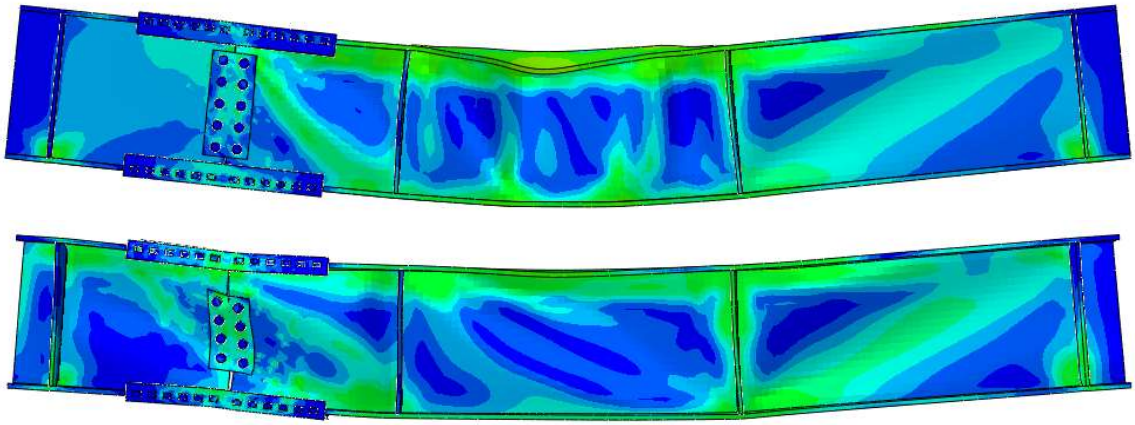

(b) Failure modes of the original (top) and new (bottom) Specimen 4

Fig. 5-27: Numerical results of the new Specimen 4

As mentioned previously, all four redesigned specimens provided ample load and deformation capacity, and therefore met the strength criteria by a reasonable margin. Table 5-2 shows this margin for different cases in the 'Overstrength' column. Based on the results, the maximum overstrength value is 1.80 in the first specimen which is noticeably smaller than 2.67 in the original Specimen 1. Therefore, the modified design procedure

was effective in maintaining overstrength to acceptable levels. Besides the strength limit, the specimen also needs to meet deflection serviceability requirements (i.e. allowable deflection limits) in current codes.

The first column of Table 5-2 provides the ratio of maximum deflection of the redesigned specimen at the design load level (Δ_{max}) to the allowable deflection (Δ_{all}). As per AISC Specification, the appropriate limiting value of deformations is $L/240$, where L is the span length of the beam [33,41]. Knowing that the span length for all the specimens is 3.7 m, the allowable deflection could be calculated. Comparison of the maximum deflection values with this limit shows that all redesigned specimens could meet the deflection limitation except for the new Specimen 2. This specimen shows 8% more deflection than the allowable deflection and barely fails this check.

The second block of Table 5-2 is devoted to the comparison of the basic parameters of the force-displacement behavior in the redesigned specimens to the original specimens. In this part of the table, 'Initial Stiffness' refers to the elastic portion of the curve, while 'Load Capacity' is the peak tolerated load. Also, the 'Deformation Capacity' is defined as the ratio of the displacement at the peak load (Δ_P) over the displacement at which the specimen starts yielding (Δ_y). Results show that, despite using smaller connectors in the connection zone, the new specimens could develop a large portion (at least 60%) of the original initial stiffness, deformation capacity, and load capacity. Therefore, if smartly designed, the intermeshed connection could provide enough strength and stiffness to meet current code recommendations, even while using smaller connector elements.

Table 5-2: Summary of the numerical results of the redesigned specimens

	New Specimen Results		*Compared to Original Specimens*		
Specimen No.	$\Delta_{max} / \Delta_{all}$	**Overstrength**	**Initial Stiffness**	**Deformation Capacity**	**Load Capacity**
1	0.90	1.80	73%	82%	68%
2	1.08	1.73	62%	67%	79%
3	0.98	1.30	72%	64%	76%
4	0.82	1.37	84%	82%	84%

5.6. Conclusions

This study focused on the performance of intermeshed connections as well as improved design methodology by performing nonlinear finite element analyses in Abaqus. The main goals were to generate further insight on the previously tested intermeshed specimens, and to improve the structural behavior of the connection via modifications in the design procedure with a view to more efficient connections.

Four detailed models including six contact zones were developed to simulate the response of the four beam specimens, with intermeshed connection and two different beam sizes of W18×46 and W21×57, that were tested in the laboratory. Results of these models were presented at global and local level scales to provide a platform with which to evaluate the validity of the FE models to simulate the experimental response data. Comparison of the numerical and experimental results confirmed that by choosing suitable analysis methods and model parameters Abaqus can accurately simulate the behavior of intermeshed connection.

Investigating the structural mechanics of the connection was performed through a number of case studies that focused on the “initial touch” concept, support conditions, and

overstrength decomposition. Based on the lessons learned from this step, the design methodology for the connections was updated and the connections geometry was optimized. The modified design procedure includes explicit consideration of the interaction between moment and shear in the connection, and therefore provides a more realistic estimate of connection strength. The connections for the four beam specimens were designed and investigated numerically in Abaqus. No out-of-plane movement was observed in any of the redesigned specimens and the specimens failed due to damage associated with yielding in the connection zone as planned. This desirable failure mechanism provides the opportunity for the disassembly of the specimen after severe damage and replacement of the angles and the shear plates. All of the redesigned specimens could meet the strength requirement without developing uneconomical margins of overstrength. The maximum deflection at the design level was also within the allowable range, except for the new Specimen 2 in which this value was slightly higher. However, this observation is not concerning because in reality these beams would not be simply supported, thus, the actual deflection would be smaller.

6

Conclusions and Future Perspectives

The objective of the research documented in this thesis was to develop an intermeshed connection for steel frame structures that improves the efficiency of construction and reuse of material using advanced manufacturing techniques. The intermeshed connection consists of interlocking pieces that act together without relying entirely on bolts or welds to transfer forces. Based on this concept, two different alternatives of the intermeshed connection were envisioned, designed, and evaluated. The primary duty of the intermeshed connection is to resist gravity loads; therefore, the loads considered for designing and analyzing the intermeshed system come from gravity (i.e. dead and live) loads. Physical tests and finite element simulations were used to investigate the mechanics of intermeshed connections including stress-strain states, component interaction, and failure modes. The main results of this work are summarized as follows.

6.1. Conclusions

Implementation of the intermeshed connection would cause a discontinuity in the frame, therefore, the effects of such configuration on the behavior of the steel frame were investigated. From analysis of frame structures, the optimal location of the connection was found to be located at *0.1L* from the beam ends. Having the connection at this location led to smaller beam stresses, which is a result of a more uniform moment distribution in the beam length. Results also proved that a connection rotational stiffness anywhere from *5EI/L* to *10EI/L* suffices the stiffness requirements of the intermeshed systems. This observation is important since both alternatives of the intermeshed connection have shown the ability to offer this level of rotational stiffness.

The first alternative of the intermeshed connection is a dovetail joint with no external connectors, called the 'front-intermeshed' connection. Over 200 nonlinear finite element analyses were performed to investigate the complex behavior and failure modes of this connection under various mixed-mode loading scenarios. Results showed that the connection exhibited excellent shear resistance, and the connection was able to develop about 90% the full plastic shear capacity of the beam. However, the axial and flexural behavior were greatly affected by the alignment of the intermeshed flange connection. The *P-M-V* interaction diagram of the connection, simulated by nonlinear FEA simulations, showed that existing code recommendations of *P-M-V* interaction are not applicable to the front-intermeshed connection. Therefore, detailed numerical analysis plays an essential role in determining the load capacity of the intermeshed connection under general mixed-mode loading. Based on the classification requirement by both the AISC specification and the Eurocode, the front-intermeshed connection should be considered a simple connection

with limited ductility. Therefore, this connection is not recommended for cases in which large plastic deformations are required.

The second alternative of the intermeshed connection, the 'side-intermeshed' connection, was proposed in response to the shortcomings of the front-intermeshed connection in transferring mixed loads. This new connection was designed with external connectors such as angles for transferring axial forces in the beam flanges, and plates for transferring shear forces in the beam web. Finite element analysis of the connection components proved that angles can successfully transfer up to 76% of the beam flanges plastic capacity under tension and 68% under compression, while the shear plates offer up to 61% of the beam web plastic capacity. These values ensure failure in the connector elements before significant damages in the main beam section, which is in line with the design philosophy if the intermeshed connection.

In the design process of the intermeshed connection, the tolerances were specified to be as small as 1.6 mm and 0.8 mm in different connection components. Therefore, in order to fabricate the connection, cutting equipment had to be able to meet high precision levels. Python X Robotic CNC plasma and OMAX A-Jet waterjet cutting machines successfully provided such ability with no major changes in their manufacturing routines. These techniques, which were easily accessible in local fabrication firms, made the manufacturing process convenient. The fabricated segments were easily and quickly put together in the lab and the specimens were assembled without the need for special skills.

Finite element models in Abaqus could accurately simulate both the global and local behavior of the intermeshed connection specimens. Results of four specimens demonstrated high load carrying capacity, approaching the beam plastic moment, and with

ratios of deflection to span length of 1/60 to 1/40. These observations demonstrated the effectiveness of the adopted 'design procedure' in proportioning the connection elements, which led to desired failure modes in the specimens. Contact between the connection components at six different locations was sufficient for the numerical model to provide a good representative of the interactions between the beam, angles, shear plates, and bolts. One-dimensional springs with constant stiffness were used to connect the points on the beam flange to the ground (i.e. a fixed reference) to simulate the restraining effect of the lateral bracing system.

All four specimens failed due to lateral or lateral-torsional buckling, even though the lateral restraining system was improved progressively from Specimen 1 to Specimen 4. However, in practice, the lateral-torsional buckling of this system would be of much less concern, since the top flanges would be restrained by the floor deck and the beam ends would be fixed against torsional rotation. The intermeshed steel connection was shown to be a robust connection that could transfer bending moment and shear forces through multiple paths. Side angles resisted most, but not all, of the bending moment force, and they were also subject to some shear forces. Shear plates resisted most, but not all, of the shear force in the connection, and they contributed to bending moment resistance, thus increasing the total bending moment capacity of the connection. In conclusion, the angles served to transfer loads across the joint between beam sections, and eventually became the sacrificial component of the connection once the beam capacity was reached. The geometry of the teeth in the beam flanges and the sockets in the angles, supplemented with the stress-reducing radii at the corners, performed as intended and no fracture was observed at locations of potentially higher stress intensities. In all four tests, the intermeshed

connection showed higher moment capacity than the design target moment. By virtue of a larger actual yield stress and a conservative design procedure, which is patterned after the capacity design approach for seismic design, the connection developed a large moment capacity. The measured overstrength for Specimen 1 was 2.67, of which 2.5 was reconciled as contributions from shear plates, beam bearing, strain hardening, material overstrength, and safety factor.

Although the results of the side-intermeshed connection were largely positive, modifications to the design procedure could lead to more optimal results. In all four specimens, the shear plates resisted some of the bending moment forces. Therefore, a less conservative design approach was developed which included a step that considered the interaction between moment and shear in the connection region. As a result, a more realistic estimation of the connection strength was provided and the connection geometry was optimized. Using this modified approach, four new specimens were designed with smaller angles and shear plates and fewer teeth and bolts, compared to the original specimens. Nonlinear finite element simulations of these new specimens were conducted in Abaqus to compare their performance with the original specimens and the target performance in the design. No out-of-plane movement was observed in the simulated response of any of the redesigned specimens and the specimens failed due to significant damage in the connection zone as planned. This desirable failure mechanism provides the opportunity for the disassembly of the specimen after severe damage. Despite using smaller connection components, the new specimens showed satisfactory performance and on average provided 73% of the stiffness, 74% of the deformability, and 77% of the load capacity of the original specimens. At the same time, all new specimens could meet the design strength level while

not overtly exceeding it. In fact, the maximum calculated overstrength value was 1.80 in the first specimen which is noticeably smaller than 2.67 in the original Specimen 1. Therefore, the modified design procedure was effective in controlling the overstrength issue.

6.2 Recommendations for Future Research

The front-intermeshed connection can be used in gravity bearing structural systems. However, the connection performance could be unsatisfactory if flange alignment is not maintained. Further research is needed to determine strategies to minimize such outcomes.

The side-intermeshed connection is inherently a beam splice, in which the angles and shear plates have essentially the same function as the connectors in a traditional splice connection. In the present research, the side-intermeshed connection served as a beam splice, but with modifications, it has the potential to be used as a column splice too. Angles were proven to be able to tolerate major axial loads, so there is potential for the side-intermeshed connection to transfer high axial loads in column flanges. On the other hand, the shear plates would need further research that investigates the influence of axial compression on the shear strength of the plates.

Large deflections caused by the initial settlement of the beam similar to what observed during the experiments, would be impractical in a building. Using tighter tolerances in the connection pieces and a smaller gap between the beam parts, would likely reduce the settlement deflection. High precision capacity of the advanced cutting techniques would allow for such modification, but in order to prevent a considerable

financial loss, primary numerical models could investigate this idea first. There are also other ways such as cambering to counteract the effects of the initial settlement in the beams with intermeshed connection. Introducing some camber could help to make the floors flat with the self-weight of the floor decks and the intermeshed beams. The results of the present study showed that the initial settlement is a function of the intermeshed connection location, so, the relationship between connection location and the initial settlement could be of interest.

Earlier in this chapter, it was mentioned that having a floor deck on top of the intermeshed beams would prevent the undesirable lateral-torsional buckling of the beams. However, this is not the only influence of floor decks on the performance of the connection system. The presence of the deck that works in compression would likely move the neutral axis upward, which changes the flexural strain distribution over the beam cross section. The effects of such phenomenon need investigation by using the numerical tools, before the intermeshed system is introduced to the practice.

Another step before the intermeshed connection is ready to be adopted to practice, is to develop an accessible and fast analysis tool that can simulate the behavior of the connection properly. Although accurate, the 3-dimensional nonlinear FE modeling is cumbersome and cannot be an every-day tool for structural engineers. So, a future research line could be idealization of the intermeshed connection to develop a practical approach for modeling the connection behavior.

Ultimately, full-scale 2-dimensional frames equipped with the intermeshed connection need to be tested in the lab, where the connections are located at $0.1L$ from the beam ends. Such study could help provide insights on the overall frame responses as well

as any interactions between the connections and the other frame components. However, it could be a challenge to provide enough lateral bracing support for such test setup, so that the out-of-plane failure mode does not occur early in the experiment.

References

[1] J.M. Davila Delgado, L. Oyedele, A. Ajayi, L. Akanbi, O. Akinade, M. Bilal, H. Owolabi, Robotics and automated systems in construction: Understanding industry-specific challenges for adoption, J. Build. Eng. 26 (2019). doi:10.1016/j.jobe.2019.100868.

[2] B.G. Hwang, M. Shan, K.Y. Looi, Key constraints and mitigation strategies for prefabricated prefinished volumetric construction, J. Clean. Prod. 183 (2018) 183–193. doi:10.1016/j.jclepro.2018.02.136.

[3] Wikipedia, Plasma Cutting, (2018).

[4] Wikipedia, Waterjet Cutter, (2018).

[5] C. Castiglioni, A. Kanyilmaz, W. Salvatore, F. Morelli, A. Piscini, M. Hjiaj, et al., EURFCS Project LASTEICON, (2016). www.lasteicon.eu.

[6] A. Kanyilmaz, C.A. Castiglioni, Fabrication of laser cut I-beam-to-CHS-column steel joints with minimized welding, J. Constr. Steel Res. 146 (2018) 16–32. doi:10.1016/j.jcsr.2018.02.039.

[7] A. Kanyilmaz, The problematic nature of steel hollow section joint fabrication, and a remedy using laser cutting technology: A review of research, applications, opportunities, Eng. Struct. 183 (2019) 1027–1048. doi:10.1016/j.engstruct.2018.12.080.

[8] N.D. Perreira, R.B. Fleischman, B. V Viscomi, L.-W. Lu, Automated Construction and ATLSS Connections; Development, Analysis, Experimentation, and

Implementation of ATLSS Connections for Automated Construction, 1993.

[9] S.A. Silverstein, Applying “Design for Disassembly” to connection design in steel structures, Doctoral dissertation at the Massachusetts Institute of Technology, 2008.

[10] J.M. Ricles, R. Sause, M. Wolski, C.-Y. Seo, J. Iyama, POST-TENSIONED MOMENT CONNECTIONS WITH A BOTTOM FLANGE FRICTION DEVICE FOR SEISMIC RESISTANT SELF-CENTERING STEEL MRFS, in: 4th Int. Conf. Earthq. Eng., 4th International Conference on Earthquake Engineering, Taipei, Taiwan, 2006.

[11] B. Rafezy, Q. Huynh, H. Gallart, M. Kheirollahi, An Innovative Method for the Seismic Retrofitting of Existing Steel Moment Frame Structures Using Side Plate Technology, in: Second ATC SEI Conf. Improv. Seism. Perform. Exist. Build. Other Struct., San Francisco, CA, 2015: pp. 144–158.

[12] B. Rafezy, Q. Huynh, A. Jared, Numerical and Experimental Analysis of an Innovative Steel Special Moment Frame Connection, in: 11th United States Natl. Conf. Earthq. Eng., Los Angeles, CA, 2018.

[13] R.B. Fleischman, B.V. Viscomi, L. Lu, ATLSS Connections - Concept, Development and Experimental Investigation, 1991.

[14] K. Gerfen, Pin-Fuse Joint, (2009). retrieved from www.architectmagazine.com.

[15] P.P. Cordova, R.O. Hamburger, Steel Connections: Proprietary or Public Domain?, 2011.

[16] SidePlate Connections: Structural Design Optimization, 2017. www.sideplate.com

(accessed September 30, 2017).

[17] S. Ramakrishnan, M. Gershenzon, F. Polivka, T.N. Kearney, M.W. Rogozinski, Plasma generation for the plasma cutting process, IEEE Trans. PLASMA Sci. 25 (1997) 937–947.

[18] S. Ramakrishnan, M.W. Rogozinski, Properties of electric arc plasma for metal cutting, J. Phys. D. Appl. Phys. 30 (1997) 636–644.

[19] R.O. Hamburger, Prequalified Connections for Special and Intermediate Steel Moment Frames for Seismic Applications, ANSI/AISC 358-05, in: Struct. Congr. 2006, American Society of Civil Engineers, Reston, VA, 2006: pp. 1–8. doi:10.1061/40889(201)5.

[20] D.D. Viana, I.D. Tommelein, C.T. Formoso, Using Modularity to Reduce Complexity of Industrialized Building Systems for Mass Customization, Energies. 10 (2017) 1622. doi:10.3390/en10101622.

[21] S.A. Al Sabah, D.F. Laefer, GB Patent Application No 1718744.4, 2017.

[22] A. Schultz, J.-L. Le, M.E. Shemshadian, R. Labbane, D. Laefer, S. Al-Sabah, L. Truong-Hong, M.P. Huynh, P. McGetrick, T. Martin, P. Matis, AMASS: Advanced Manufacturing for the Assembly of Structural Steel, in: Tenth Int. Struct. Eng. Constr. Conf., Chicago, 2019.

[23] S.A. Al Sabah, D.F. Laefer, GB Patent Application No 1718746.9, 2017.

[24] R. Mahnken, Theoretical, numerical and identification aspects of a new model class for ductile damage, Int. J. Plast. 18 (2002) 801–831.

[25] P. Matis, T. Martin, P. McGetrick, D. Robinson, Modelling and experimental testing of interlocking steel connection behaviour, in: Sixth Int. Symp. Life-Cycle Civ. Eng., Ghent, 2018.

[26] J. Bathe, Finite Element Procedures Second Edition, (2006).

[27] Abaqus 6.13, (2013).

[28] S. Lin, Z. Huang, M. Fan, Modelling partial end-plate connections under fire conditions, J. Constr. Steel Res. 99 (2014) 18–34.

[29] X. Yun, L. Gardner, Stress-strain curves for hot-rolled steels, J. Constr. Steel Res. 133 (2017) 36–46. doi:10.1016/J.JCSR.2017.01.024.

[30] ASTM, ASTM A992 / A992M: Standard Specification for Structural Steel Shapes, 11 (2014) 11–14.

[31] DNV-RP-C208, Determination of Structural Capacity by Non-linear FE analysis Methods, 2013.

[32] S.-W. Han, K.-H. Moon, B. Stojadinovic, Design equations for moment strength of RBS-B connections, J. Constr. Steel Res. 65 (2009) 1087–1095.

[33] AISC, Specification for Structural Steel Buildings (ANSI/AISC 360), American Institute of Steel Construction, 2016.

[34] C. Vogel, C. Rivard, V. Wilken, A. Muskolus, C. Adam, Performance of secondary P-fertilizers in pot experiments analyzed by phosphorus X-ray absorption near-edge structure (XANES) spectroscopy, Ambio. 47 (2018) 62–72.

[35] Eurocode, Eurocode 3: Design of steel structures - Part 1-8: Design of joints, 2005.

[36] H.P. Broom, Construction costs, Chem. Eng. News. 28 (1950) 1109–1111. doi:10.1021/cen-v028n014.p1109.

[37] Y. Shan, J.Y. Kim, P.M. Goodrum, C.H. Caldas, C. Haas, Impact of steel quick connection system on steel erection labor productivity: case studies and simulation based analyses, Can. J. Civ. Eng. 41 (2014) 1036–1045. doi:10.1139/cjce-2014-0079.

[38] M.E. Shemshadian, J.-L. Le, A.E. Schultz, P. McGetrick, S. Al-Sabah, D.F. Laefer, A. Martin, L.T. Hong, M.P. Huynh, Numerical study of the behavior of intermeshed steel connections under mixed-mode loading, J. Constr. Steel Res. 160 (2019) 89–100. doi:10.1016/J.JCSR.2019.04.024.

[39] P. McGetrick, T. Martin, P. Matis, D.F. Laefer, S. Al-Sabah, L. Truong-Hong, M.P. Huynh, A.E. Schultz, J.-L. Le, M.E. Shemshadian, R. Labbane, The AMASS Project: Advanced Manufacturing and Assembly of Steel Structures (under review), Struct. Build. J. (2019).

[40] J. Sikora, A Summary of Stress Concentrations in the Vicinity of Openings in Ship Structures, DAVID W TAYLOR Nav. Sh. Res. Dev. Cent. BETHESDA MD Struct. DEPT. (1973).

[41] AISC, Steel Construction Manual, 15th Ed., American Institute of Steel Construction, 2017.

[42] ASTM, ASTM E8/E8M - Standard Test Methods for Tension Testing of Metallic Materials, Astm. 02 (2013) 1–27. doi:10.1520/E0008.

[43] R. Labbane, Experimental Investigation of the Performance of Intermeshed Steel Beam Connections, Masters thesis at the University of Minnesota, 2019.

[44] AISC, Seismic Provisions for Structural Steel Buildings (ANSI/AISC 341-16), American Institute of Steel Construction, 2016.

[45] McKinsey Global Institute, Reinventing Construction: A Route to Higher Productivity, 2017.

[46] D. Krajcarz, Comparison Metal Water Jet Cutting with Laser and Plasma Cutting, Procedia Eng. 69 (2013) 838–843. doi:10.1016/j.proeng.2014.03.061.

[47] BOC Linde group, Facts about plasma technology and plasma cutting, 2011.

[48] L. Dahil, I. Dahil, A. Karabulut, Comparison of Advanced Cutting Techniques on Hardox 500 Steel Material and the Effect of Structural Properties of the Material, Metalurgua. 53 (2014) 291–294.

[49] S. Al-Sabah, D.F. Laefer, L. Truong Hong, M. Phuoc Huynh, J.-L. Le, T. Martin, P. Matis, P. McGetrick, A. Schultz, M.E. Shemshadian, R. Dizon, Introduction of the Intermeshed Steel Connection - A New Universal Steel Connection, Build. J. 10 (2019) 37. doi:10.3390/buildings10030037.

[50] P. Matis, T. Martin, P. McGetrick, D. Robinson, The effect of frictional contact properties on intermeshed steel connections, in: Civ. Eng. Res. Irel., Civil Engineering Research in Ireland, Dublin, 2018: pp. 547–553.

[51] www.omax.com, Cutting Material with an Abrasive Waterjet, (2019). https://www.omax.com/frequently-asked-questions.

[52] ASTM, ASTM A36/A36M - Standard Specification for Carbon Structural Steel, (2018).

[53] M.E. Shemshadian, A.E. Schultz, J.-L. Le, R. Labbane, D.F. Laefer, S. Al-Sabah, L. Truong-Hong, M.P. Huynh, P. McGetrick, T. Martin, P. Matis, AMASS: Advanced Manufacturing for the Assembly of Structural Steel (under review), Pract. Period. Struct. Des. Constr. (2020).

[54] M.E. Shemshadian, R. Labbane, A.E. Schultz, J.-L. Le, D.F. Laefer, S. Al-Sabah, P. McGetrick, Experimental study of intermeshed steel connections manufactured using advanced cutting techniques, J. Constr. Steel Res. 172 (2020) 106169. doi:10.1016/j.jcsr.2020.106169.

[55] ASTM, ASTM A325−14 Standard Specification for Structural Bolts, Steel, Heat Treated, 120/105 ksi Minimum Tensile Strength, (2014). doi:10.1520/B0221-14.

Appendix

Appendix A: Moment Frames with Intermeshed Connection

The overall goal of the analysis described here is to determine frame behavior under vertical loads and lateral drift, and to determine optimal locations of the intermeshed connections depending on frame geometry and load combination. This aspect of the research utilizes linear elastic analysis of frames equipped with springs that idealize the intermeshed connections as elastic restraints. Independent springs with constant stiffness represent the axial, shear and flexural stiffness of the connection. Objectives for this part of research are to:

- Prepare a tool for analysis of the intermeshed system without the need to run nonlinear analysis.
- Determine the potential locations for the intermeshed connections that optimize the design of the frame.
- Find the effects of different combinations of stiffness for the axial, shear and flexural springs.
- Investigate the behavior of this system with various frame geometries.

Assumptions

To fulfill the abovementioned objectives, a parametric study was conducted using the computer program SAP2000. While the main function of intermeshed systems is to carry gravity loads while they are part of global structural system, the system may be subjected to lateral loads (e.g. wind or earthquake). The system will include other elements to resist the lateral loading, but the frame with intermeshed connections must be able to accommodate the associated lateral drifts while supporting the gravity loads. Consequently, more than 300 pushover analyses were performed in which geometric nonlinearities (P-Delta and large displacement effects) were defined. Both 3-story and 9-story planar frames representing portions of an office building were designed for gravity loads, and these frames were pushed to drifts equal to 2% of their total height.

To idealize the linear behavior of intermeshed connections, frame partial fixity springs were utilized which includes axial, shear, and flexural stiffness. Each of these stiffness values were defined as a ratio of corresponding beam stiffness. For a beam these amounts can be expressed by the following formulas:

$$K_{Axial} = \frac{EA}{L}$$

$$K_{Shear} = \frac{GA}{L}$$

$$K_{Flexural} = \frac{EI}{L}$$

Where A and I are the area and moment of inertia of the beam section, L is beam length, and E and G are modulus of elasticity and the shear modulus, respectively, of the structural steel. In European standards [35] there is a classification for joints based on their flexural stiffness as per the following equation:

Zone 1 (rigid connection)

$K_{connection} > 25(EI/L)_{beam}$

Zone 2 (semi-rigid connection)

$0.5(EI/L)_{beam} < K_{connection} < 25(EI/L)_{beam}$

Zone 3 (simple connection)

$K_{connection} < 0.5(EI/L)_{beam}$

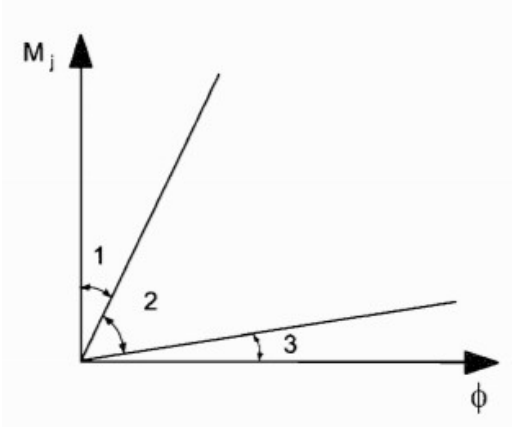

Fig. A 1: Classification of joints by stiffness according to Eurocode 3 [35]

In AISC 2016, the recommended range for semi-rigid connections is from 2 to 20 times beam stiffness [33]. Since the intermeshed connection is considered as a semi-rigid connection, a similar range of stiffness was chosen which also satisfies the Eurocode 3 limits. So, each spring stiffness assumed to be 20, 10, 5, 1, 0.5, 0.2, and 0.1 times of the beam stiffness (seven different cases). The position of the intermeshed connections was changed to find the best possible option. In the first attempt, the connection was located at the end of the beams (0 & *L*). Then it was moved away from the ends to 10% and 20% of the beam length (*0.1L* & 0.9L and 0.2L & 0.8L accordingly). To account for the effects of

geometry, the ratio of each bay to story height was changed from 2 to 3. Also, the total height of the frames was changed from 11 m (3 story) to 33 m (9 story).

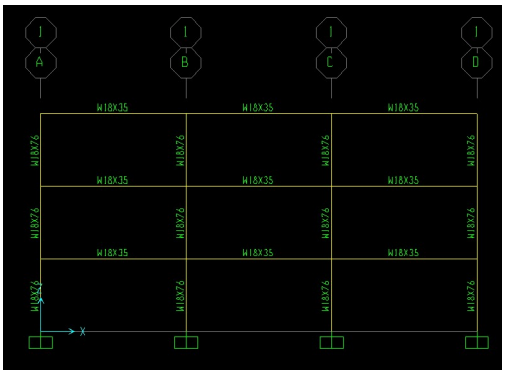

(a) 3-story with span to height ratio 2:1

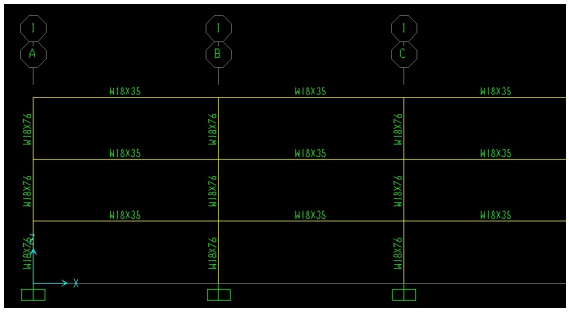

(b) 3-story with span to height ratio 3:1

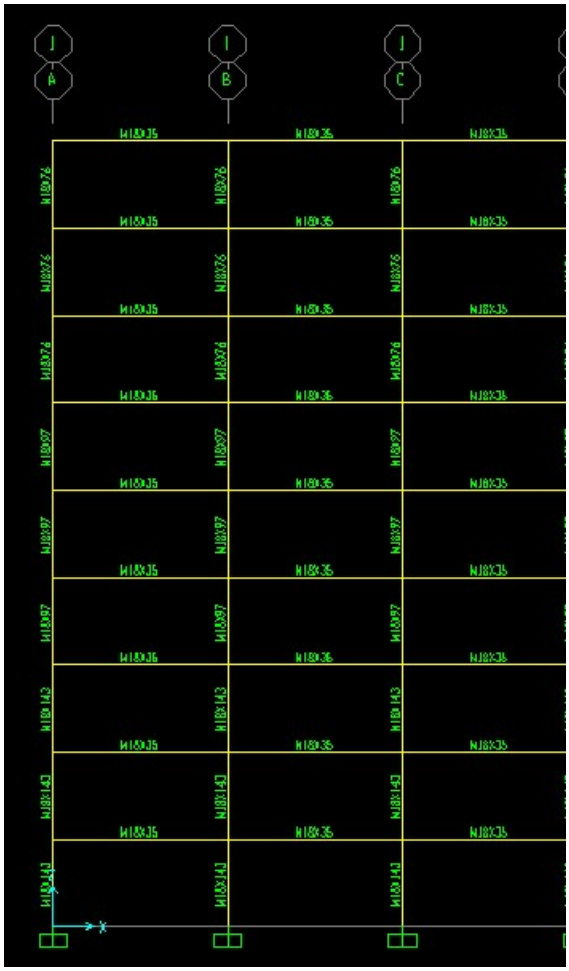

(c) 9-story with span to height ratio 2:1

Fig. A 2: Different frames studied in SAP2000

Summary of the Results

To have a better insight of intermeshed system behavior from both strength and stiffness points of view, results were evaluated in terms of *P-M* interaction ratios, deflection of the beams, patterns of internal forces, and mode shapes and periods. For a comparative understanding of the effects of changing parameters, results are presented in comparison with corresponding benchmark models. In each case of Frame (a), Frame (b), or Frame (c),

the benchmark is the frame before implementation of the intermeshed connection. In such frame, there is no partial connectivity and therefore all the joints are rigid. In comparison with the benchmark frames the following observations were made:

1. For a wide range of stiffness values, there is not much undesirable change in the frame responses such as mode shapes, internal forces, etc.
    - Changing the connection axial stiffness from 20 to 1, changes the results less than 1%.
    - Changing the connection shear stiffness from 20 to 1, changes the results less than 3%.
    - Changing the connection flexural stiffness from 20 to 5, increases the beam deflections by 20% at most while a maximum drop of 35% happens in beam *P-M* ratio.
    - Beam and column forces and the frame stiffness are highly dependent on flexural stiffness, rather than axial or shear stiffness. So, the main concern will be to provide enough flexural stiffness at intermeshed connections.
2. Changing the position of intermeshed connections, may cause a change in results especially in terms of beam *P-M* ratio and mode shapes.
    - When the connection is placed at 20% from both ends, there is an increase up to 30% in beam *P-M* ratio and some undesirable mode shapes happen.
    - Placing intermeshed connection at 10% of beam length, does not change the frame mode shapes and does not cause any major changes in beam *P-M* ratio (up to 10%).
3. The effects of rigid diaphragms resulting from composite action do not affect the results, but they eliminate of higher mode effects caused by partially fixity.

4. Increasing the ratio of span length to story height from 2 to 3, has a significant effect on the beam deflections (up to four times of original deflections) while beam *P-M* ratio increases up to 20% and column *P-M* ratio remains almost the same.

5. Comparing the results of 9-story to 3-story frame shows a significant drop in the maximum *P-M* ratio for the columns. In fact, in most cases the columns will experience one-half of what they had experienced in the 3-story frame. However, beam *P-M* ratios will increase by about 20% of the original value.

Fig. A 3 to Fig. A 11 present the results of the Frames (a), (b), and (c) (see Fig. A 2) in the form of response curves. Each figure shows the frame response (deflection or stress) as a function of the intermeshed connection stiffness and location. In each curve, the vertical axis shows the ratio of the response in the investigated frame to the response in the corresponding benchmark frame.

Results of Frame (a)

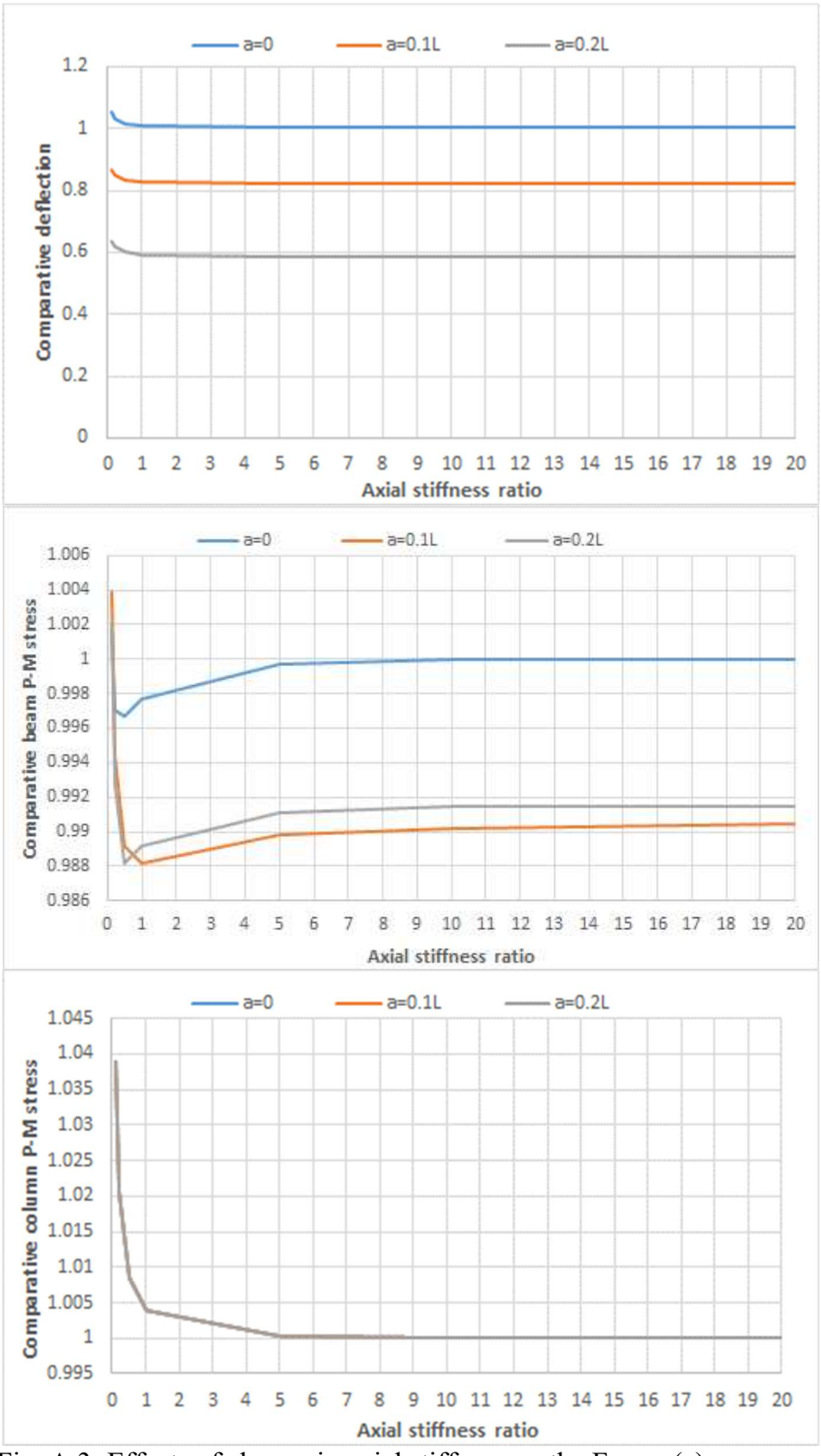

Fig. A 3: Effects of change in axial stiffness on the Frame (a) responses

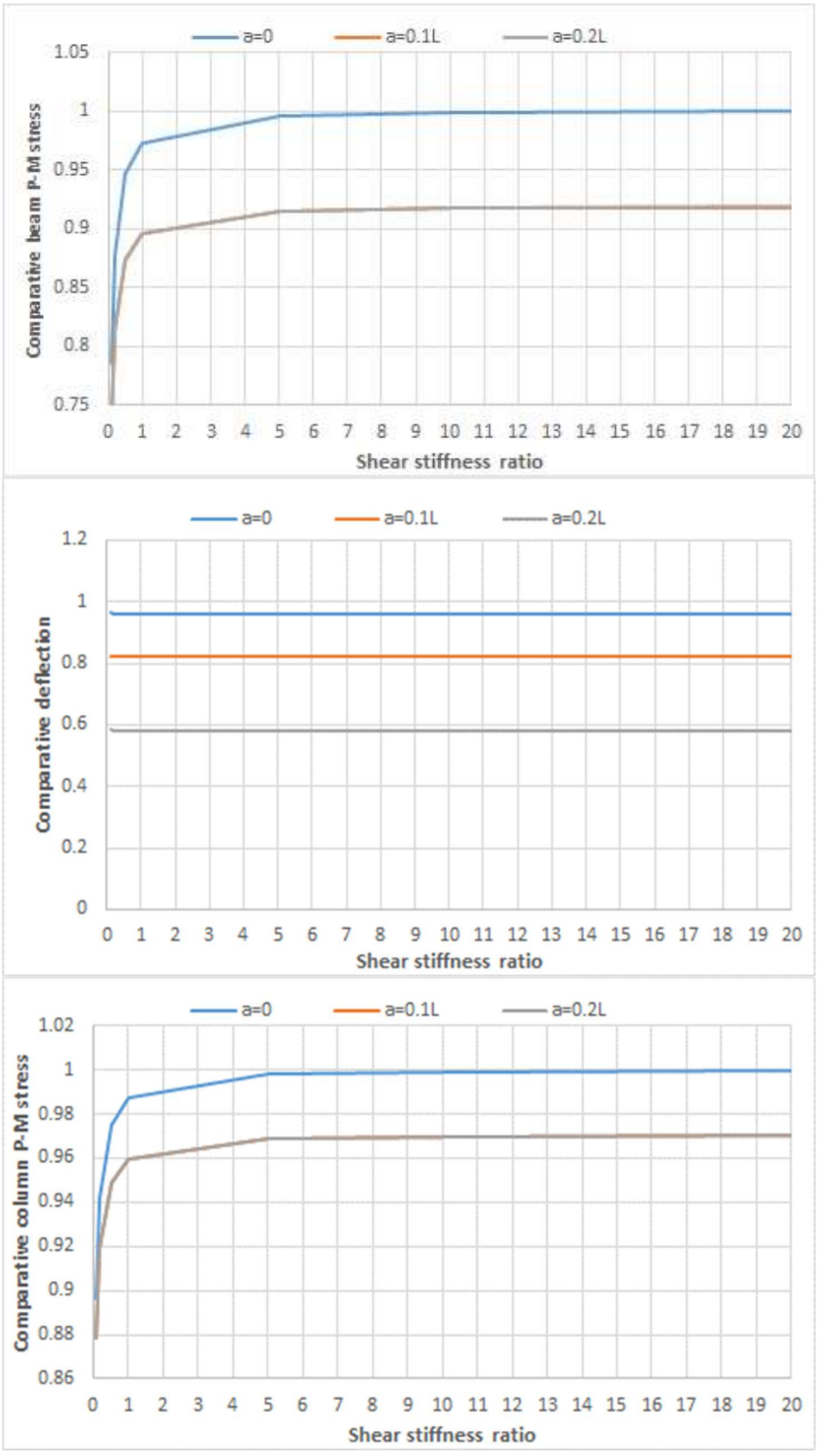

Fig. A 4: Effects of change in shear stiffness on the Frame (a) responses

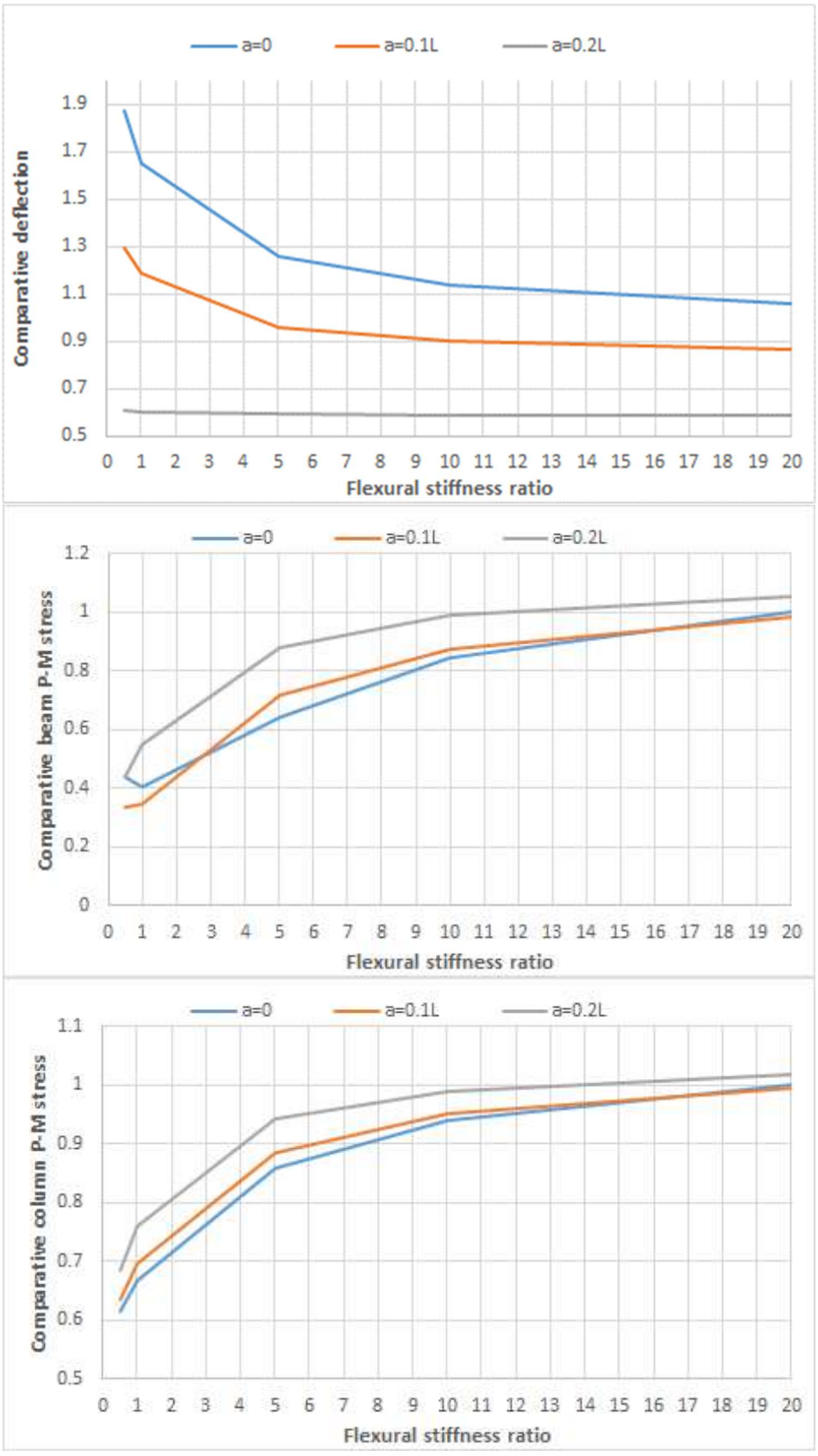

Fig. A 5: Effects of change in flexural stiffness on the Frame (a) responses

Results of Frame (b)

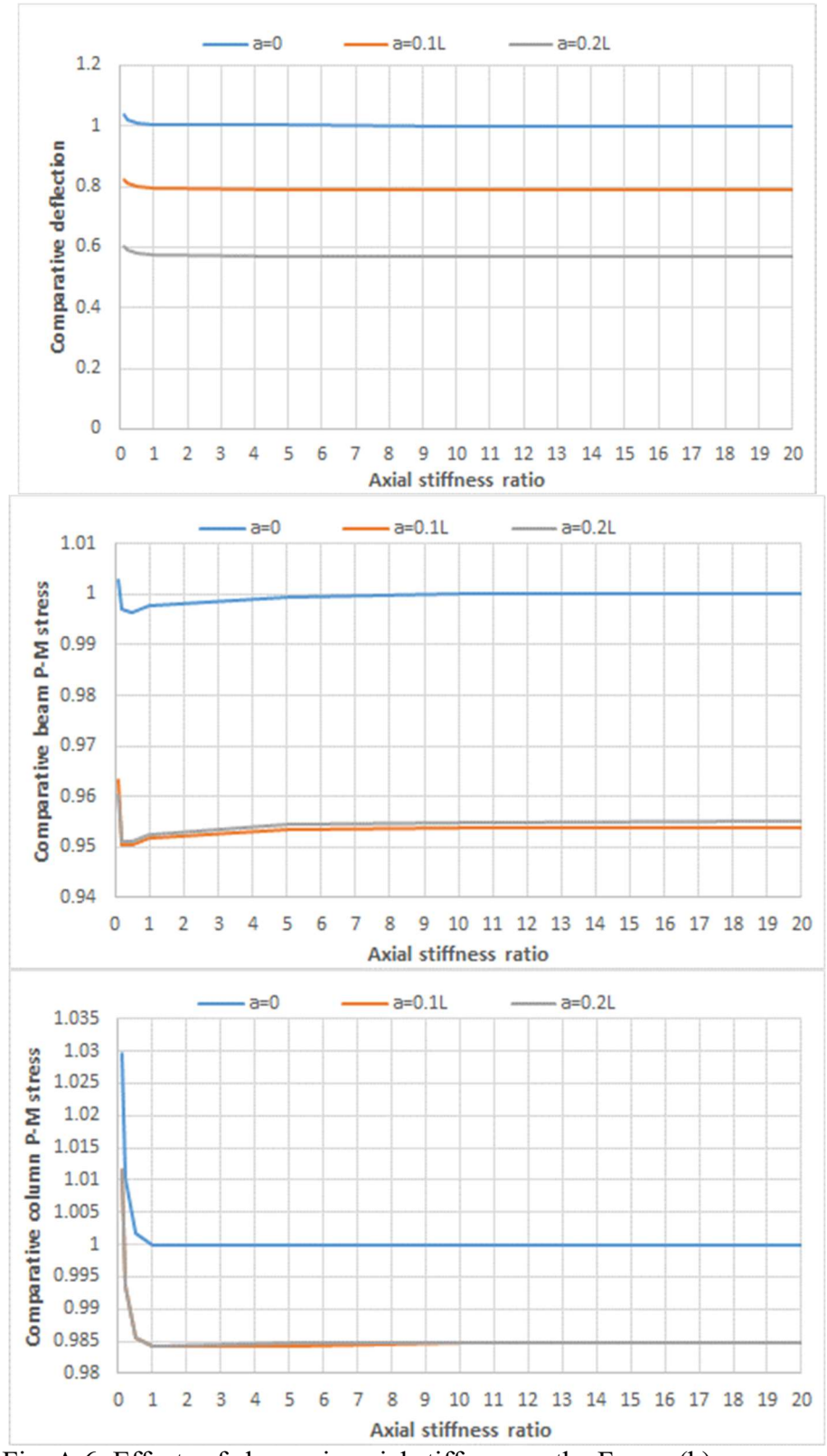

Fig. A 6: Effects of change in axial stiffness on the Frame (b) responses

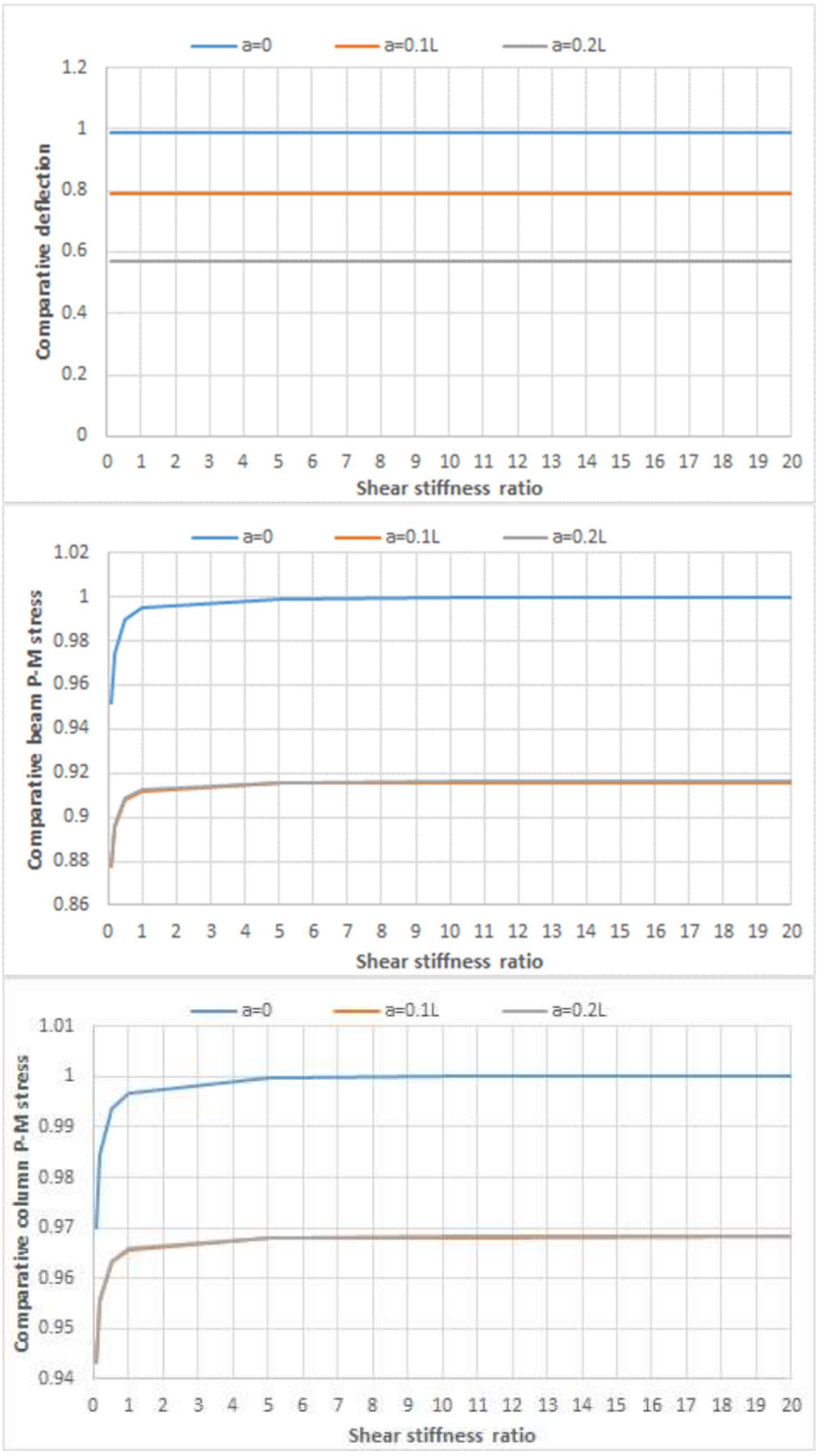

Fig. A 7: Effects of change in shear stiffness on the Frame (b) responses

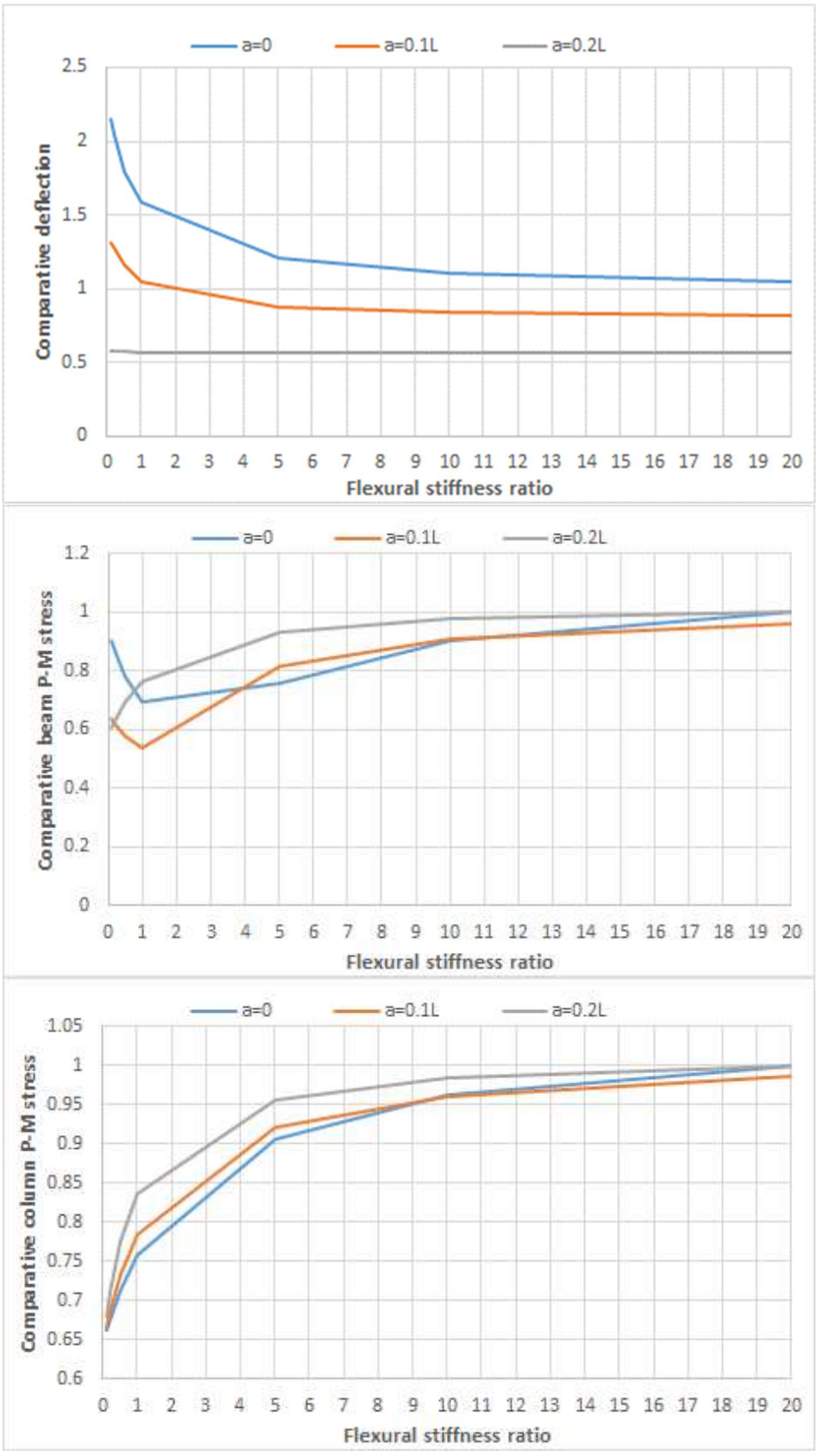

Fig. A 8: Effects of change in flexural stiffness on the Frame (b) responses

Results of Frame (c)

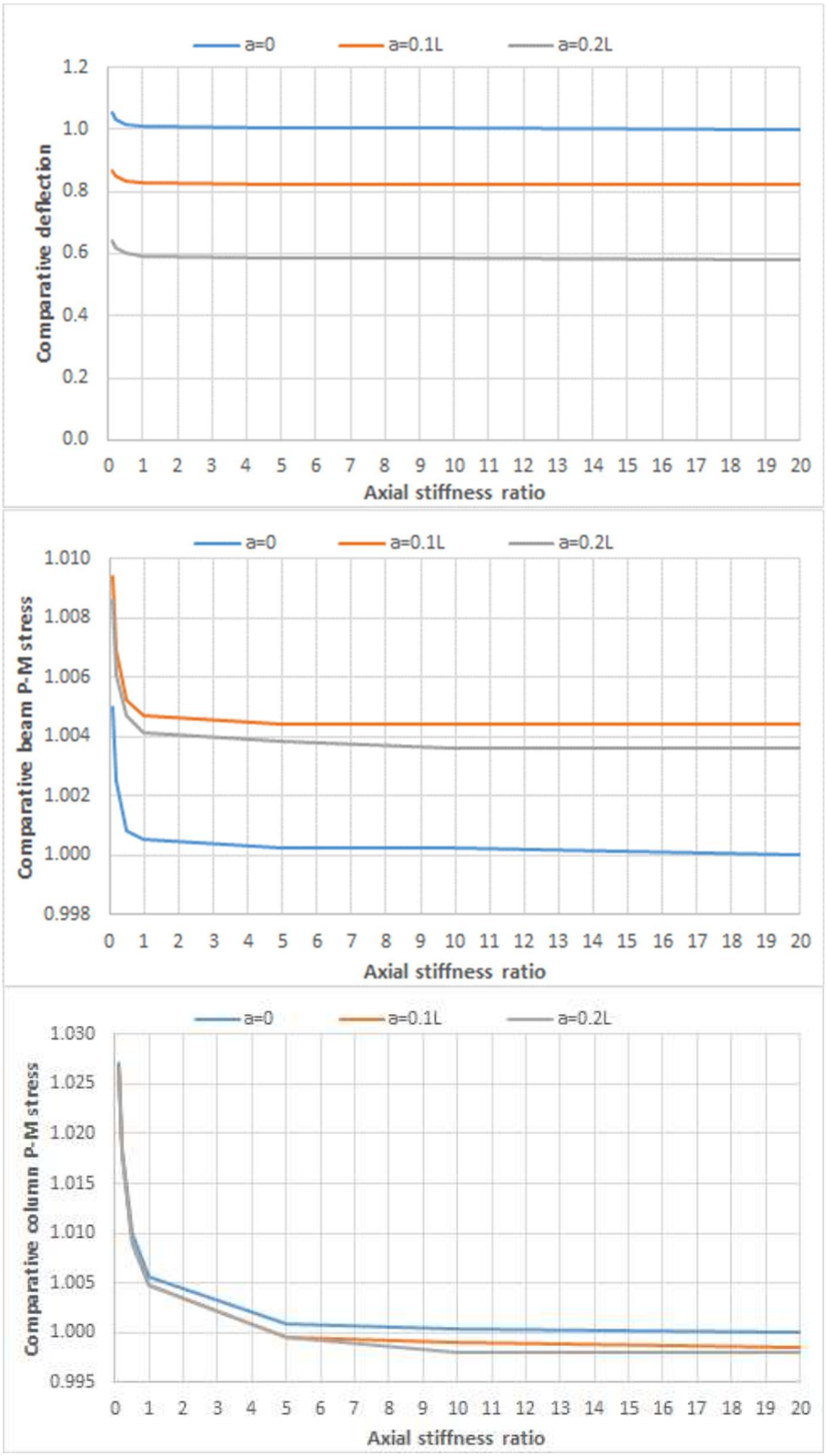

Fig. A 9: Effects of change in axial stiffness on the Frame (c) responses

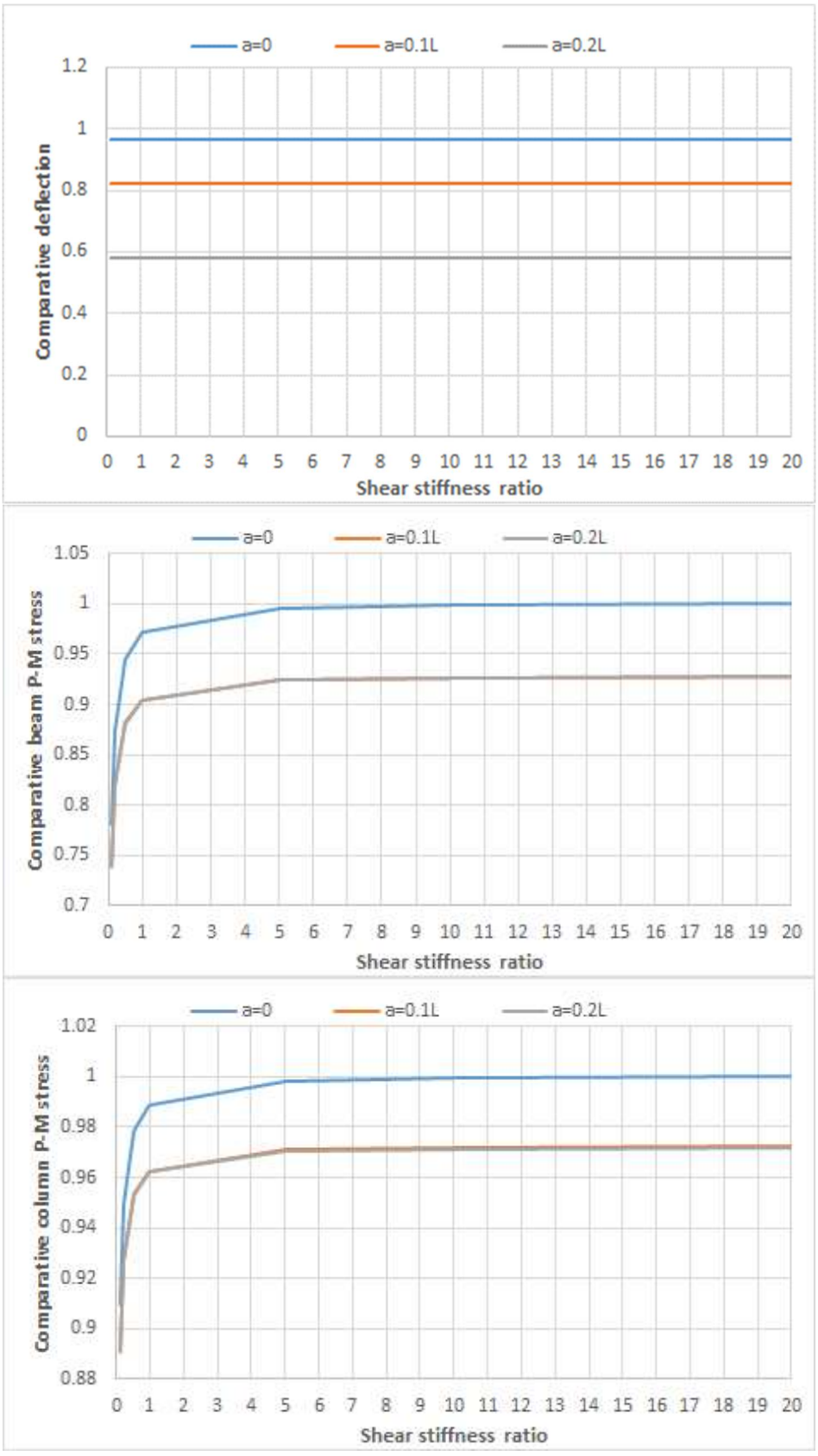

Fig. A 10: Effects of change in shear stiffness on the Frame (c) responses

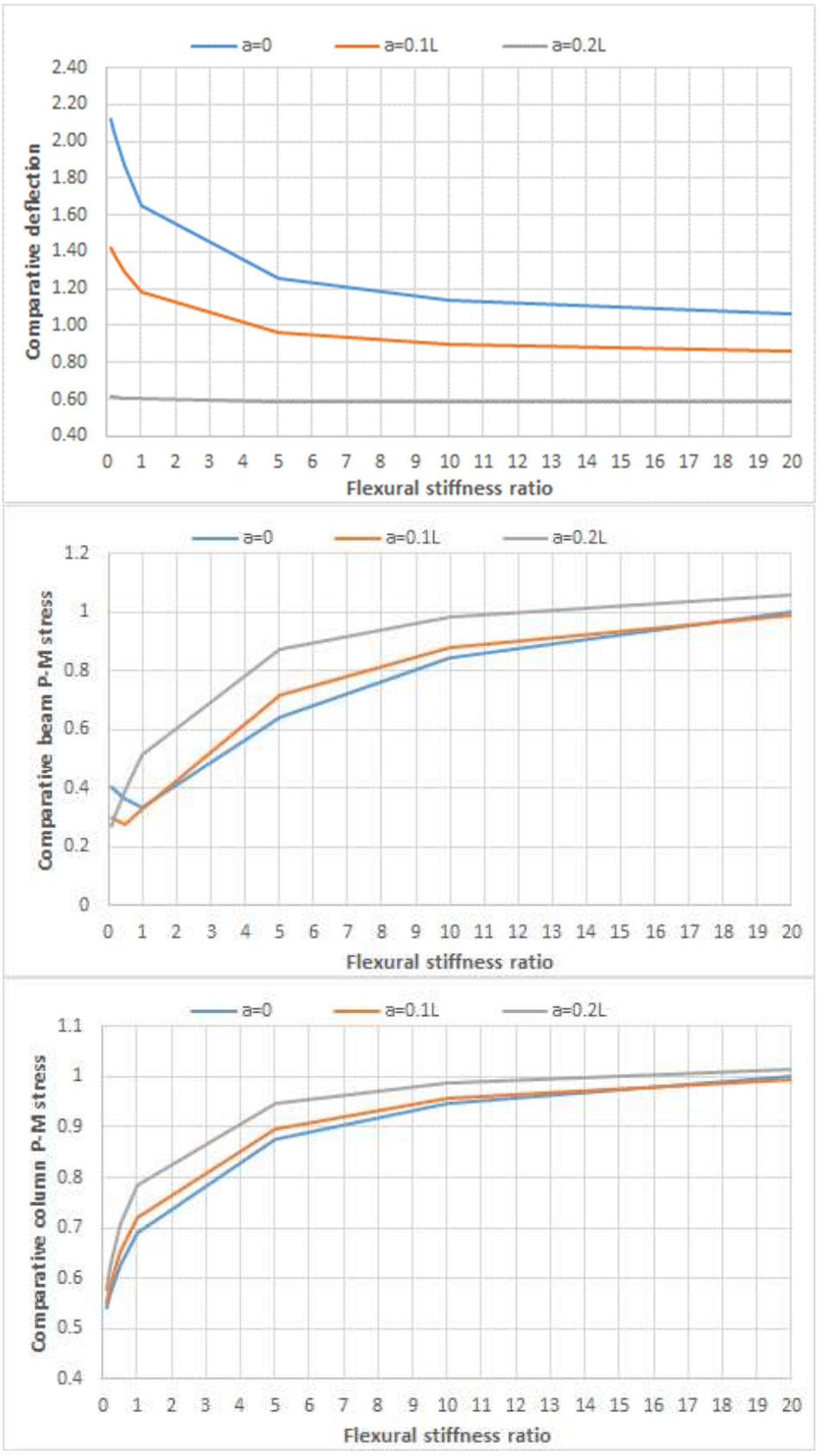

Fig. A 11: Effects of change in flexural stiffness on the Frame (c) responses

Recommendations

1. Combining the results from changing ‘connection stiffness’ and ‘connection position’ leads to an optimum case in which the *P-M* ratio of the beams and columns are minimized, and the deflections are acceptable, while no change in mode shapes is evident in comparison with the original frame.
    - This occurs when intermeshed connections are at *0.1L* & *0.9L* (*L* is the beam length).
    - In this case the axial, shear, and flexural stiffness of the connection is equal to 5, 0.1, and five times of corresponding beam stiffness values, respectively.

2. The optimum case is the most economical case, since it happens when the ‘end moment’ and ‘middle moment’ of the beam are almost equal. This means a more uniform moment distribution along the beam which leads to more efficient usage of the steel material.
    - In this condition, the *P-M* ratio of the beam is approximately 75% of that in the benchmark frame.
    - However, when the ‘end moment’ is significantly larger than the ‘middle moment’ (i.e. moment distribution is not uniform), as an economical approach it can be recommended to strengthen the stub beams locally.

Appendix B: Capacity-Based Shear Plate Strength Requirement

Shear strength requirement for the shear plates based on the targeted flexural capacity of the intermeshed connection is defined. The shear requirement for the shear plates V_{sp} is determined from the uniformly distributed beam load w_{cap} that generates the targeted flexural capacity M_c of the connection at the center of the connection. The beam is assumed to have a moment at the left end from continuity. Note the following definitions:

L = center-to-center span length $\left(\text{between support centerlines}\right)$ of the beam
L_c = distance from the left support to the center of the connection
M_L = moment at the left support
R_L = reaction at the left support

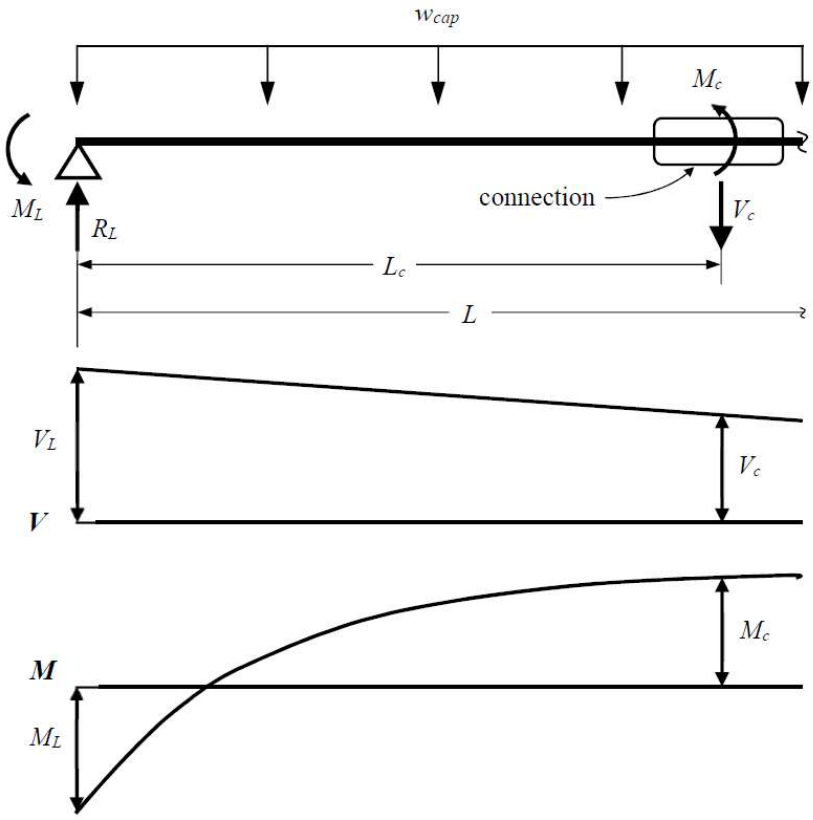

Fig. B 1: Free-body diagram and shear and moment distributions in a beam with intermeshed connection

The moment at the connection M_c is calculated as:

$$M_c = R_L L_c - M_L - w_{cap} L_c \left(\frac{L_c}{2} \right)$$

The reaction R_L is approximated using the expression that is applicable for simply supported beams or beams with equal end moments:

$$R_L = w_{cap} \frac{L}{2}$$

From which the load capacity w_{cap} to generate the connection moment M_c is:

$$w_{cap} = 2 \frac{\left(M_c + M_L \right)}{L_c \left(L - L_c \right)}$$

The shear at the shear plate V_{SP} (i.e. at the center of the connection) is obtained from the shear at the left support V_L.

$$V_{SP} = V_L = R_L - w_{cap} L_c = w_{cap} \left(\frac{L}{2} - L_c \right) = 2 \frac{\left(\alpha M_p + M_L \right)}{L_c \left(L - L_c \right)} \left(\frac{L}{2} - L_c \right)$$

where the connection moment is replaced with the design target αM_p. in terms of the plastic moment capacity M_p. In the tests conducted at the University of Minnesota, the following parameters are relevant:

$$M_L = 0$$
$$\alpha = \tfrac{1}{3}$$
$$L = 12'$$
$$L_c = 2'$$
$$M_p = Z_p F_y$$
$$F_y = 36 \text{ ksi (nominal specified value for Grade 36 steel)}$$
$$Z_p = \left\{ \begin{array}{c} 90.7 \text{ in}^3 \text{ for W18} \times 46 \\ 129 \text{ in}^3 \text{ for W21} \times 57 \end{array} \right\}$$

Thus, the shear requirement for the plate is:

$$V_{SP} = \left\{ \begin{array}{c} 50.4 \text{ kips for W18} \times 46 \\ 71.7 \text{ kips for W21} \times 57 \end{array} \right\}$$

The nominal capacity of the shear plates, assuming plates on either side of the beam web is:

$$V_{SP} = \phi_v \left(0.6 F_y A_p \right) = \left(1 \right) 0.6 F_y d_p \left(2 t_p \right)$$

For the new connection design, revised plate depths d_p were selected as follows:

$$d_p = \left\{ \begin{array}{c} 9" \text{ for W18} \times 46 \\ 12" \text{ for W21} \times 57 \end{array} \right\}$$

from which the plate thickness t_p is obtained:

$$t_p = \left\{ \begin{array}{c} 0.130" \text{ for W18} \times 46 \\ 0.138" \text{ for W21} \times 57 \end{array} \right\}$$

Note, if the actual connection moment, M_c, is much larger than αM_p, then the shear plates will need to be thicker. This suggests that an overstrength factor may be appropriate for the target connection moment.

Appendix C: Effective Lateral Translational Stiffness of the Braces

The effective lateral translational stiffness of the braces K_{brace} is defined as:

$$K_{brace} = \frac{P}{\Delta_t}$$

where

$$\Delta_t = \theta_b H + \delta_f$$

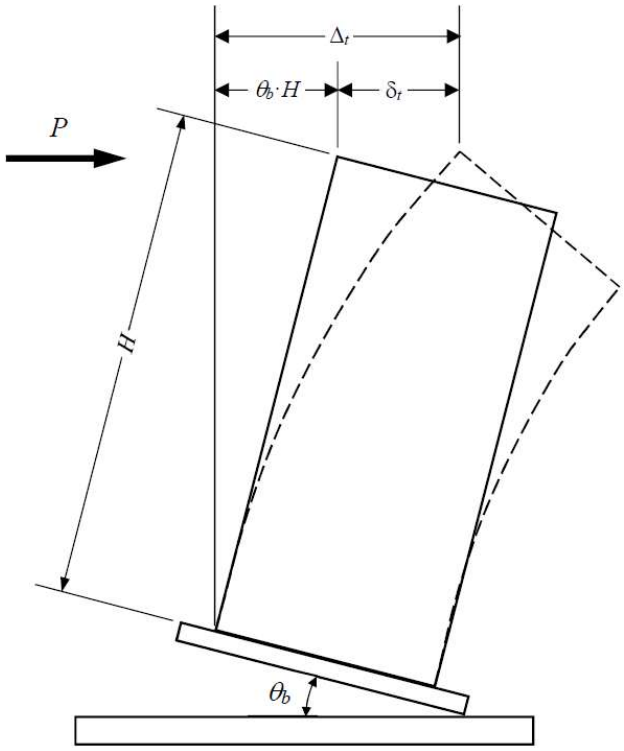

Fig. C 1: Deformation of a typical lateral brace

The rotation of the base of the brace θ_b is generated by elongation of the bolts and the brace base plate simply rocks about the compression corner. No deformation of the compression of the plate is considered.

The deformation of the brace column δ_f is obtained assuming linear, elastic deformation of the brace column acting as a cantilever about its base plate:

$$\delta_f = \frac{PH^3}{3E_s I_{col}}$$

The brace stiffness K_{brace} is expressed as

$$K_{brace} = \frac{P}{\Delta_t} = \frac{P}{\theta_b H + \delta_f} = \frac{P}{\theta_b H + \left(\frac{PH^3}{3E_s I_{col}}\right)} = \frac{1}{\left(\frac{\theta_b H}{P}\right) + \left(\frac{H^3}{3E_s I_{col}}\right)}$$

where the terms in the denominator are identified as the lateral flexibilities f_{base} and f_{col}, respectively, of the base plate and column. These flexibilities are defined as:

$$f_{base} = \frac{\theta_b H}{P}$$

$$f_{col} = \frac{H^3}{3E_s I_{col}}$$

They are associated with the lateral translation contribution at the top of the brace for each component. The brace stiffness becomes:

$$K_{brace} = \frac{1}{f_{base} + f_{col}}$$

and the flexibilities are obtained independently. Column flexibility is obtained from the steel modulus of elasticity E_s, the column height H from the top of the base plate, and the moment of inertia I_{col} of the column section. The base plate flexibility requires the base plate rotation θ_b.

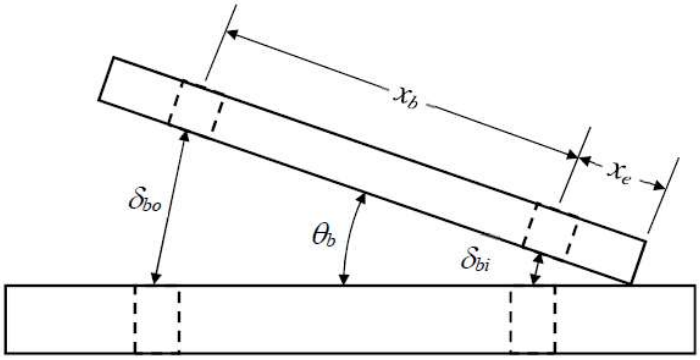

Fig. C 2: Rotation of the base

To calculate base plate rotation, first obtain bolt forces, F_{bo} for the outer bolt (largest tension) and F_{bi} for the inner bolt (smallest tension). Bolt forces are assumed to remain linear, elastic, so that force is proportional to strain in the bolts (ε_{bo} and ε_{bi}), and strains are proportional to the elongations (δ_{bo} and δ_{bi}).

$$\delta_{bi} = \theta_b x_e$$
$$\delta_{bo} = \theta_b \left(x_e + x_b \right)$$

The corresponding strains are obtained using the length l_b flexible portion of the bolt or threaded rod length that is subjected to tension.

$$\varepsilon_{bo} = \frac{\delta_{bo}}{l_b} = \frac{\theta_b}{l_b}\left(x_e + x_b \right)$$
$$\varepsilon_{bi} = \frac{\delta_{bi}}{l_b} = \frac{\theta_b}{l_b} x_e$$

where

$$l_b = t_{nut} + t_{tp} + t_{bp}$$

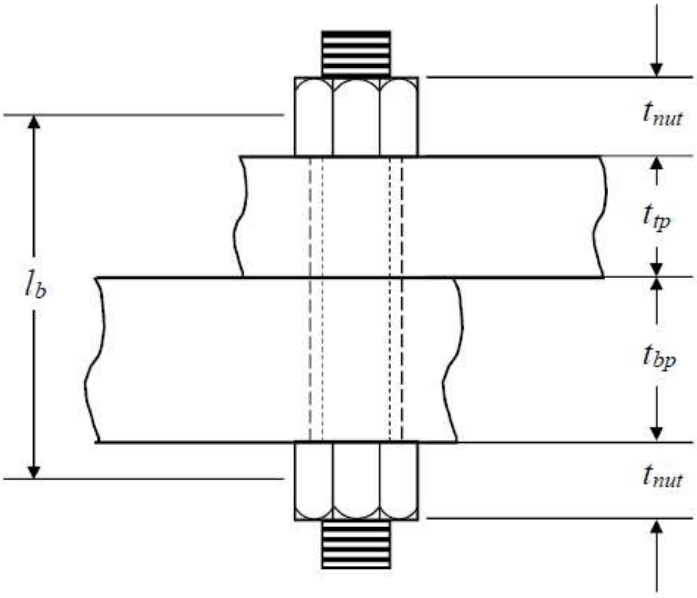

Fig. C 3: Threaded rod detail in the brace

Assuming linear elasticity, the forces in the bolts are:

$$F_{bo} = A_b E_s \varepsilon_{bo} = A_b E_s \frac{\theta_b}{l_b}\left(x_e + x_b\right)$$

$$F_{bi} = A_b E_s \varepsilon_{bi} = A_b E_s \frac{\theta_b}{l_b} x_e$$

where A_b is the net cross-sectional area of the bolts. Note that F_{bi} can be rewritten as:

$$F_{bi} = A_b E_s \frac{\theta_b}{l_b} x_e \left(\frac{x_e + x_b}{x_e + x_b}\right) = A_b E_s \frac{\theta_b}{l_b}\left(x_e + x_b\right)\left(\frac{x_e}{x_e + x_b}\right) = F_{bo}\left(\frac{x_e}{x_e + x_b}\right)$$

The external moment applied to the base connection M_{ext}, which is produced by the brace load P at the top of the column, is resisted by the internal moment M_{int}, which is produced by the bolt tension forces F_{bo} and F_{bi} and the compression reaction at the contact corner in the base plate.

$$M_{ext} = M_{\text{int}}$$

where

$$M_{ext} = P \cdot H$$

$$M_{\text{int}} = F_{bo}\left(x_e + x_b\right) + F_{bi}x_e$$

The internal moment M_{int} can be rewritten as:

$$M_{\text{int}} = F_{bo}\left(x_e + x_b\right) + F_{bo}\left(\frac{x_e}{x_e + x_b}\right)x_e = F_{bo}\left(x_e + x_b + \frac{x_e^2}{x_e + x_b}\right) = F_{bo}\left[\frac{\left(x_e + x_b\right)^2 + x_e^2}{x_e + x_b}\right]$$

Substituting the outer bolt force F_{bo} expression into the internal moment M_{int} gives

$$M_{\text{int}} = A_b E_s \frac{\theta_b}{l_b}\left(x_e + x_b\right)\left[\frac{\left(x_e + x_b\right)^2 + x_e^2}{x_e + x_b}\right] = A_b E_s \frac{\theta_b}{l_b}\left[\left(x_e + x_b\right)^2 + x_e^2\right]$$

Equate the internal and external moments and obtain the base plate flexibility f_{base}

$$P \cdot H = A_b E_s \frac{\theta_b}{l_b}\left[\left(x_e + x_b\right)^2 + x_e^2\right]$$

$$f_{base} = \frac{\theta_b H}{P} = \frac{\left(\frac{H^2 l_b}{A_b E_s}\right)}{\left[\left(x_e + x_b\right)^2 + x_e^2\right]}$$

If the load P is delivered by a threaded rod with length l_{rod} and cross-sectional area A_{rod}, then an additional flexibility f_{rod} is introduced:

$$f_{rod} = \frac{\delta_{rod}}{P} = \frac{1}{P}\left(\frac{Pl_{rod}}{A_{rod}E_s}\right) = \frac{l_{rod}}{A_{rod}E_s}$$

And the effective lateral translational stiffness of the brace is

$$K_{brace} = \frac{P}{\Delta_t} = \frac{1}{f_{base} + f_{col} + f_{rod}}$$

Sample Estimate:

$I_{col} = 285 \text{ in}^4$ for a W 12×35 steel section

$A_b = 0.462 \text{ in}^2$ for a 7/8" anchor bolt

$E_s = 30,000 \text{ ksi}$

$H = 32"$

$x_e \sim 2"$ and $x_b \sim 8"$ (estimated from the experiments)

$t_{nut} \sim 1.5"$ (including an allowance for washers)

$t_{tp} \sim 1"$ (estimated from the experiments)

$t_{bp} \sim 6"$ (includes the depth of the EFCO base - assuming that the anchor bolt/rod extended through the base.)

$A_{rod} = 0.462 \text{ in}^2$ for a 7/8" rod (@ the brace point)

$l_{rod} \sim 24"$ (estimated from the experiments)

$$f_{col} = \frac{H^3}{3E_s I_{col}} = \frac{(32")^3}{3(30,000 \text{ ksi})(285 \text{ in}^4)} = 0.001278 \text{ in/kip} = \frac{1}{782.8 \text{ kip/in}}$$

$$f_{base} = \frac{H^2 l_b}{E_s A_b}\left[\frac{1}{(x_e + x_b)^2 + x_e^2}\right] = \frac{(32")^2 (6")}{(30,000 \text{ ksi})(0.462 \text{ in}^2)}\left[\frac{1}{(2"+8")^2 + (2")^2}\right]$$

$$f_{base} = \frac{0.4433 \text{ in}^3/\text{kip}}{104 \text{ in}^2} = 0.004262 \text{ in/kip} = \frac{1}{234.6 \text{ kip/in}}$$

$$f_{rod} = \frac{l_{rod}}{E_s A_{rod}} = \frac{24"}{(30,000 \text{ ksi})(0.462 \text{ in}^2)} = 0.001732 \text{ in/kip} = \frac{1}{577.5 \text{ kip/in}}$$

$$K_{brace} = \frac{1}{f_{col} + f_{base} + f_{rod}} = \frac{1}{(1/782.8 \text{ kip/in}) + (1/234.6 \text{ kip/in}) + (1/577.5 \text{ kip/in})}$$

$K_{brace} = 137.5 \text{ kip/in}$

Appendix D: Notation

E	Steel Young's modulus
F_{max}	Maximum actuator load in the experiment
I	Moment of inertia of the cross section
L	Beam span length
M	Bending moment
$M_{B,\ max}$	Maximum beam moment in the experiment
$M_{B,\ plastic}$	Beam plastic moment
$M_{C,\ design}$	Connection design moment
$M_{C,\ max}$	Maximum connection moment in the experiment
R	Rosette
SG	Strain Gage
$V_{C,\ design}$	Connection design shear
$V_{C,\ max}$	Maximum connection shear in the experiment
δ_{max}	Maximum beam deflection in the experiment
$\varepsilon_{A,\ max}$	Maximum strain in tensile angle in the experiment
$\varepsilon_{F,\ max}$	Maximum strain in tensile flange in the experiment
ε_u	Ultimate strain
κ	Curvature
σ_u	Ultimate stress
σ_y	Yield stress
Ω_{bb}	Beam bearing contribution factor
Ω_{mo}	Material overstrength contribution factor
Ω_{sh}	Strain hardening contribution factor
Ω_{sp}	Shear plates contribution factor